# Quantification of positron emission tomography brain imaging using $^{18}$F-Fallypride: a simulation

Mohlapoli Stadium Mohlapholi




Thesis presented in partial fulfilment of the requirements for the Degree of *Master of Science in Medical Physics in the Faculty Medicine and Health Sciences* at Stellenbosch University

Supervisor: Mr. Christoph Trauernicht

Co-supervisors: Prof. James Warwick

Mrs. Monique Du Toit

April 2019

# Table of Contents

## Declaration of authenticity

By submitting this thesis electronically, I Mohlapoli Stadium MOHLAPHOLI declare that the entirety of the work contained therein is my own, original work, that I am the sole author thereof, that reproduction and publication thereof by Stellenbosch University will not infringe any third party rights and that I have not previously in its entirety or in part submitted it for obtaining any qualification.

Date: April 2019

# Abstract

$^{18}$F-fallypride is of interest in neurological and psychiatric diseases to visualise dopamine $D_2/D_3$ receptors in striatal and extrastriatal regions.

Several simplified methods of quantifying positron emission tomography (PET) brain imaging using $^{18}$F-fallypride have been described and used on real data using non-invasive methods, but a systematic analysis of their effect on quantification has not been performed.

In this study, mathematical simulations were used to study this effect on quantification using different models to quantify $^{18}$F-fallypride PET in the human brain. The specific uptake areas of interest used in this study for a human brain are the putamen (high receptor density region), thalamus (moderate receptor density region) and temporal cortex (low receptor density region).

Materials and methods

All simulations were performed using Matlab (version R2013a (8.1.0.604) win 64-bit software; MathWorks, Inc.).
Simulations of realistic measurements were performed by modelling varying frame duration, decay of the tracer, and varying noise levels, starting from ideal tissue curves. A modelled input function was used for the generation of ideal tissue curves.
Quantification was carried out with arterial blood sampling models: a 2T4k (two-tissue (or three-compartment) reversible model was used and a Logan graphical analysis was applied.
Using the cerebellum as the reference region, we studied the following reference region models: Logan graphical analysis ($Logan_{ref}$) using a reference region, the reference tissue model (RTM) and the simplified reference tissue model (SRTM). Finally, the standard uptake value ratio (SUVR) was studied as the simplest method.
For the assessment, the results were analysed using a correlation analysis and a Bland-Altman analysis and the relative error (%) and the 5$^{th}$ and 95$^{th}$ percentiles in high/moderate/low receptor density region of the brain were determined. Validation of each method was done in terms of bias and variance.

## Results

The study showed that in all cases the ground truth method and the graphical method using an arterial input function were nearly identical.
The overall accuracy and variability of various methods were determined successfully. $Logan_{ref}$ was the most accurate, with the highest precision as the replacement of the invasive arterial blood sampling in low/moderate receptor density regions. While SRTM gave high precision in high receptor density region, SUVR calculations produced relatively large errors in all receptor density regions used in this study.

The effect of SNR (signal to noise ratio) on quantification was clearly observed since the bias in all reference region methods increased with increasing noise. When the noise level is too high, bias may become too large.

Investigating the effect of the models' performance under a continuous sampling scheme showed the stability in the kinetics of $^{18}$F-fallypride using non-invasive reference region methods when the scan length (continuous sampling scheme) was > 150 min and > 120 min in high and in low/moderate receptor density regions respectively.

To achieve a good compromise between accuracy and patient comfort, breaks can be introduced at pre-determined intervals. Best results were achieved when the total scan time was 90 min and the total break time was 150 min (i.e. 30 min scan + 30 min break + 30 min scan + 120 min break + 30 min scan).

## Conclusion

Simplified models can be used to provide useful estimates of dopamine transporters that are comparable to methods using arterial blood sampling. However, these models should be used with great care as they can be affected by the noise in the data, the length of the scan duration and the length and position of the breaks in the imaging sequence.

# Opsomming

$^{18}$F-Fallypride is van waarde in neurologiese en psigiatriese siekte om dopamien $D_2/D_3$ reseptore in striatale en ekstrastriatale areas te visualiseer.

Verskeie vereenvoudigde metodes vir kwantifisering van $^{18}$F-fallypride positron emissie tomografie (PET) breinbeelding, is deur middel van nie-ingrypende metodes op ware data beskryf en gebruik. Systemiese analise van die effek van hierdie metodes op kwantifisering is nog nie uitgevoer nie.

In die huidige studie, is wiskundige simulasies gebruik om hierdie invloed op die kwantifisering te bestudeer, deur van verskillende metodes gebruik te maak om $^{18}$F-Fallypride PET in die menslike brein te kwantifiseer. Die spesifike areas van opname in hierdie studie, is die putamen (hoë reseptor digtheidsarea), talamus (matige reseptor digtheidsarea) en temporale korteks (lae digtheidsarea).

Materiaal en metodes

Alle simulasies is op Matlab (weergawe R2013a (8.1.0.604) win 64-bit sagteware; MathWorks, Inc.) uitgevoer.

Die werklike metings is gesimuleer deur modellering met wisselende raamduur, verval van spoorelemente en wisselende geraasvlakke, gebasseer op ideale weefselkurwes. ‘n Gemodelleerde insetfunksie is gebruik vir die konstruksie van ideale weefselkurwes. Kwantifisering is uitgevoer met arteriële bloedmonster-modelle: ‘n 2T4k (twee-weefsel of drie-kompartement) omkeerbare model en ‘n Logan grafiese analise. Die serebellum is as verwysingsgebied gebruik, om die volgende modelle te bestudeer: ‘n Logan grafiese analise ($Logan_{ref}$), ‘n verwysingsweefsel-model (VWM) en die vereenvoudigde verwysingsweefsel-model (VVWM). Laastens is die standard-opname verhoudingswaarde as die eenvoudigste metode gebruik.

Die resultate is geanaliseer deur van ‘n korrelasie-analise en ‘n Blandt-Altman analise gebruik te maak. Die relatiewe fout (%), sowel as die 5$^{de}$ en 95$^{ste}$ persentiel in hoë/middelmatige/lae reseptor digtheidsarea van die brein, is bepaal. Die geldigheid van elke metode is geëvalueer in terme van vooroordeel en variasie.

## Resultate

Die studie het in alle gevalle getoon dat die grondwaarheidsmetode en die grafiese metode, wat van die arteriële insetfunksie gebruik maak, byna identies is. Die algehele akkuraatheid en die veranderlike van die verskillende metodes, was suksesvol. $Logan_{ref}$ analise was die akkuraatste in die lae/middelmatige reseptor-digtheidsareas in plaas van die gebruik van die ingrypende arteriële bloedmonster metode.

Die vereenvoudigde verwysingsweefsel-model (VVWM) was die akkuraatste in die hoë reseptor digtheidsarea, daarenteen het die standard-opname verhoudingswaarde relatief groot foute getoon.

Die effek van sein tot geraasverhouding op kwatifisering was duidelik, aangesien die vooroordeel van alle verwysingsgebied-metodes met toenemende geraas verhoog het. Wanneer die geraasvlak egter te hoog is, word die vooroordeel ook te groot.

'n Ondersoek na die effek van modelverrigting onder die aaneenlopende monsterprogram, toon stabiliteit in die kinetika van $^{18}$F-fallypride. Hierdie effek vind plaas met die gebruik van 'n minder ingrypende verwysingsmetode wanneer die beeldingstyd > 150 minute en > 120 minute in onderskeidelik hoë en in lae/middelmatige reseptor- digtheidsareas is.

Die beeldingtydsduur met tussensposes was gebruik om 'n ooreenkoms tussen akkuraatheid en pasiëntgemak te bereik. Die beste kwantitatiewe resultate is verkry met die volgende program: 30 minute beelding, 30 minute tussenpose, gevolg deur 30 minute beelding met 'n 120 minute onderbreking en laastens weer 'n 30 minute beelding.

## Gevolgtrekking

Vereenvoudigde modelle kan gebruik word om nuttige voorspellings van dopamien-draers, te verkry, wat vergelykbaar is met metodes waar arteriële bloedmonsters gebruik word. Die modelle moet egter met groot sorg gebruik word, aangesien dit deur datageraas, die duur van die beelding, die tipe onderbrekings of die onderbreking van die monsterprogram, beïnvloed kan word.

# Acknowledgements

A journey of thousands miles begins with small steps. The work presented in this thesis required dedicated help of several individuals.

First, I am deeply grateful to my mentor, Prof.dr. Patrick Dupont (KU Leuven, Belgium, Laboratory for Cognitive Neurology, Department of Neurosciences), who taught me various neuroimaging analysis skills and programming and shown me the value of scientific enthusiasm. You have been extremely supportive throughout the start of this project and always had answers to my questions and made everything sound easier than it was. Your kind guidance has always been of high intellectual standard. I value the time and the effort you put in this project. Thank you for providing me with countless opportunities for which I am enormously grateful.

The head of Medical Physics Division and my supervisor Mr. Chris Trauernicht and co-supervisor Ms. Monique du Toit for their outstanding constant support and positive contribution towards the journey of completing this project.

Importantly, this work was also done in close collaboration with my co-supervisor Prof. James Warwick, who made this project possible through immense scientific knowledge and also initiated my scientific visit to Belgium.

Dr Michael Mix (University Medical Center Freiburg, Germany) for his initial input in the project. The head of Radiation Oncology Division Prof. Hannah Simonds, and the Head of Nuclear Medicine division Prof. Annare Ellmann for encouragement.

Special thanks to:

The International Atomic Energy Agency (IAEA) for funding my fellowship to Leuven, Belgium.
University Hospital Gasthuisberg - University of Leuven (K.U. LEUVEN) and Laboratory for cognitive neurology for hosting me.
My colleagues Mr. TCG Moalosi and Mr. TD Mkhize for their in-house support.
The staff of the Medical Physics, Radiation Oncology and Nuclear Medicine Divisions

Finally, to the people of Belgium, thank you for treating me with love and respect during my visit, may God continue to bless your great nation!!!

# Dedications

Forever now in the greatness of my Saviour (GOD), all this time You were there. Without any uncertainty this work is dedicated to You.

To my loving wife (Siyamthanda) and my son (Tshenolo), you deserve an Academy award. I thank you both for introducing me to the game of fatherhood and forever thankful for your prestigious support through many nights away from home.

To my late parents, Mamatela Anna Mohlapholi and January Maphodi Mapuru, you gave birth to humanity. I remember your brave faces. Your memory of spreading love became our treasure and has kept us from falling apart. Today we firmly stand our ground, armed with courage, faith and hope. To the lives you have touched and the happiness you brought, all of this will live on forever in the hearts of many.

To my family of eight (Mohlapholi's) and all the sons of the second generation, Bakubung ba tshehlana. We all share a common story. The battle is not against who we have been, it is the war against who we are becoming. I'm forever grateful for your support by giving me every opportunity to pursue the path I choose. I became the man I am today because you believed in me wholeheartedly.

*"My father, my mother,*

*If these were the days of our ancestors,*
*I would ask you for a cows and goats,*
*Now I ask you to send me to school.*
*My father, my mother,*
*Yesterday's heroes called for spears to defend the nation,*
*Today's heroes demand pen and slate to save the nation,*
*That's why I ask you to send me to school".*

Ngũgĩ wa Thiong'o
"*Birth of a Dream Weaver*"

# List of Figures

# List of Tables

# List of Formulas

# List of Abbreviations

| | |
|---|---|
| $^{18}$F-fallypride | {{((S)-N[1-allyl-2-pyrrolidinyl)methyl]-5-(3[$^{18}$F] fluoropropyl-2,3-dimethoxybenzamide)} |
| 2T4k | two tissue (or three-compartment) model |
| 2TC | two-tissue compartment modelling |
| $B_{max}$ | binding site density |
| BP | binding potential |
| $BP_{ND}$ | the ratio of the concentration of specifically bound tracer in tissue to the concentration of non-displaceable tracer in tissue, $BP_{ND} = \frac{V_T - V_{ND}}{V_{ND}} = \frac{V_T}{V_{ND}} - 1$ |
| $C_B$ | concentration of Fallypride bound to D2/D3 receptors |
| $C_{F+NS}$ | concentration of free and non-specifically bound fallypride |
| $C_P$ | concentration of Fallypride in the arterial plasma |
| $C_T$ | total concentration of fallypride in tissue |
| D 2/3 | dopamine receptors |
| DA | dopamine |
| DV | distribution volume, also defined as $V_{ND}$ |
| DVR | distribution volume ratio in brain tissue in the non-displaceable compartment, $\frac{V_T}{V_{ND}}$ |
| $K_1$ to k4 | fallypride rate constants |
| LRSC | linear regression and spatial constraint |
| PET | positron emission tomography |
| RTM | reference tissue model |
| SNR | signal to noise ratio |
| SPECT | single-photon emission computed tomography |

| | |
|---|---|
| SRTM | simplified reference tissue model |
| SUV | standard uptake value |
| SUVR | standardized uptake value ratios |
| TAC | time-activity curve |
| $V_{ND}$ | distribution volume, $V_{ND} = \frac{K_1}{k_2}$ also defined as DV |
| $V_T$ | total distribution volume, $V_T = \frac{K_1}{k_2}(1 + \frac{k_3}{k_4})$ |

# Chapter 1: Introduction to the context of the study

## 1.1 Background

### 1.1.1 Functional neuroimaging

Over the years, understanding the development of the brain has led to the cognitive neuroscience and the rise of functional neuroimaging (Morita et al., 2016).

Functional neuroimaging is a research tool which uses technology to measure the activity of the brain function (specific mental functions) in real time and captures images of the different brain anatomy structures. This provides an in vivo window into the human brain network by finding the relationship between the brain function and its anatomy (Meier et al., 2016).

Humans are prone to physical and mental changes throughout their lifespan (Morita et al., 2016). Functional neuroimaging of the brain plays an important role in neuroscience for the study of neurological and psychiatric disorders to measure these changes, as well as for early stage drug development. Even though the neurological (disorders of the brain) and psychiatric disease (disorders of the mind) are considered “disorders of the nervous system”, both of them express two different kinds of disorders from a perspective of neuroimaging (Crossley et al., 2015). Psychiatric disorders are different than neurological disorders, changes in the neuroimaging study can not be seen with the naked eye when assessing psychiatric disorders (Masdeu et al., 2011).

The most commonly used functional neuroimaging techniques are electro-encephalography (EEG) and magneto-encephalography (MEG) to measure the electric activity of cell groups in the brain; functional magnetic resonance imaging (fMRI), near-infrared spectroscopy (NIRS), single-photon emission computerised tomography (SPECT) and positron emission tomography (PET) to measure the change in blood flow associated with brain activity (Morita et al., 2016; Lystad et al., 2009).

### 1.1.2 Positron Emission Tomography (PET)

PET is a non-invasive medical technique used to generate high-resolution images and enables in vivo examination of human and animal brain functions including physiological functions focusing on cerebral blood flow and metabolism, including neurotransmitters, receptor binding and radiolabelled drugs (Tai et al., 2005).

It involves an intravenous administration of a radioactive tracer into the human body, usually labelled positron emitting isotopes such as $^{15}O$ (oxygen-15), $^{18}F$ (fluorine-18), $^{11}C$ (carbon-11), or $^{13}N$ (nitrogen-13).

These unstable positron emitting isotopes are prepared with a particle accelerator (cyclotron), and they have relatively short half-lives. They reach stability when they decay into a neutron, a positron, and a neutrino. The emitted positron travels only a few millimetres and meets an electron inside the patient's body. When the electron and positron meet (annihilation), two gamma rays are produced and released at 180 degrees with the energy of 511keV each moving in opposite directions.

When these gamma rays are detected at the same time, high spatial resolution image is produced by PET.

PET plays a role by measuring in vivo neurotransmitter and receptor activity in the brain in healthy and diseased states (Sossi at al., 2003; Patel et al., 2010).

### 1.1.3 Neurotransmitters

Neurotransmitters are endogenous chemicals which allow the transport of signals between neurons across synapses.

They are clustered in synaptic vesicles. When released, they bind to the receptors of the synapse.

Different types of neurotransmitters include amino acids, monoamines and other biogenic amines.

Amino acids include glutamate, aspartate, D-serine, γ-aminobutyric acid (GABA), glycine while monoamines and other biogenic amines include dopamine (DA), norepinephrine, epinephrine, histamine, serotonin (5-HT). Other neurotransmitters are acetylcholine (ACh), adenosine, anandamide and nitric oxide.

### 1.1.4 Dopamine (DA)

DA neurons reside in the substantia nigra and some in ventral tegmental area of the brain.

DA plays a major contribution in a range of neurological and psychiatric disorders including Parkinson's disease, schizophrenia and drug addiction (Zald et al., 2010).

It is a neurotransmitter in the brain that plays an important role in the control of motor function, reward, and emotional expression including neuroendocrine release and behavioural homeostasis in the central and peripheral nervous system (D'Souza et al., 2010).

### 1.1.5 Dopamine $D_2/D_3$ receptors

A receptor is a protein that resides on the membrane of the neuronal synapse. Neurotransmitters bind to receptors using a lock and key mechanism, where the key in this case is a neurotransmitter and the lock a receptor.

Neuroreceptor imaging gives researchers an opportunity to gain access to quantitative information based on the distribution of the receptors in the human brain.

The involvement of DA system has been found in different neurological and neuropsychiatric processes (Hurd and Hall et al., 2005; Christian et al., 2009). Dopamine $D_2/D_3$ receptors are an important target in understanding and treating neurological and psychiatric disorders.

It has been pointed out that the highest concentration of $D_2$ receptors is found in striatum, while $D_3$ receptors can be found in low concentrations in the extrastriatal brain (Volkow et al., 1996). The $D_3$ receptor is mainly linked to the limbic system (Cave et al., 2009). Dopamine $D_2/D_3$ receptors play a major role in cognitive and behavioural output and disruption (Vandehey et al., 2010).

### 1.1.6 The properties of $^{18}$F-fallypride and its importance for quantification of $D_2/D_3$ receptors

To quantify striatal and extrastriatal $D_2/D_3$ receptors in PET imaging, $^{18}$F-fallypride is a radiotracer of interest (Gründer et al., 2008; Vernaleken et al., 2011). It binds to DA

$D_2$ and $D_3$ receptors and gets distributed in the brain in striatal and extrastriatal regions but shows insignificant binding to other common neuroreceptors.

The fluorine-18 label of $^{18}$F-fallypride provides the benefits of a longer physical half-life (109.8 minutes) in comparison to the carbon-11 label of $^{11}$C-raclopride. $^{18}$F-fallypride is thus a tracer of choice as a PET radiopharmaceutical for the study of both striatal and extrastriatal DA receptors in a single PET scan. An advantage of $^{18}$F-fallypride is that it does not form metabolites in the brain. Metabolites created outside the brain region do not pass over the blood brain barrier.

The quantification of neuroreceptor imaging information based on PET can be derived accurately taking into account the concentration of free and non-specifically bound tracer, and the concentration of the tracer bound to the brain receptors. Additional quantification includes the delivery, uptake, binding, clearance or washout of the radiotracer and its transport across the blood brain barrier.

Using models for the behaviour of the tracer in vivo and with measurements of the tracer distribution over time using PET, relevant parameters (e.g. binding potential ($BP_{ND}$), volume of distribution (DV)) can be derived using kinetic modelling (Heiss and Herholz 2006).

Quantification of brain PET imaging using $^{18}$F-fallypride has been performed using different kinetic modelling methods, each based on the different assumptions regarding the complex pathways these tracers follow in brain tissue (Cropley et al., 2008; Matsubara et al., 2011).

## 1.2 Reconstruction of $^{18}$F-fallypride two tissue (or three-compartment) model (2T4k)

It is important to know the amount of tracer that will be trapped at metabolism site or the tracer bound to the brain receptors.

The complex pathways of the tracer's molecule in the brain can be divided into segments known as compartments. For example, the molecules that are bound to the brain receptors can constitute one compartment.

The idea is to move from a highly complex physiological system to a simplified compartmental model. Compartmental model is used to analyse dynamic PET data. The principle of the compartmental model is to eliminate invasive procedures with highly predictive power to provide mathematical solution.

In simple terms, the compartmental models describe the kinetics of a tracer injected into a physiological system which is the brain in this case.

In pharmacokinetic modelling, the behaviour of the tracer in tissue is assumed to be separated into multiple “compartments”. This means the tracer can be specifically bound, nonspecifically bound or move freely in tissue. The compartments in figure 1.1 are chemical species in a physical place and they are represented by boxes while the connections between these compartments are represented by arrows (known as fallypride exchange rate constants).

Every compartment has several exchange rate constants leading to the region of interest (inflows) and several exchange rate constants leading from the region of interest (outflows).

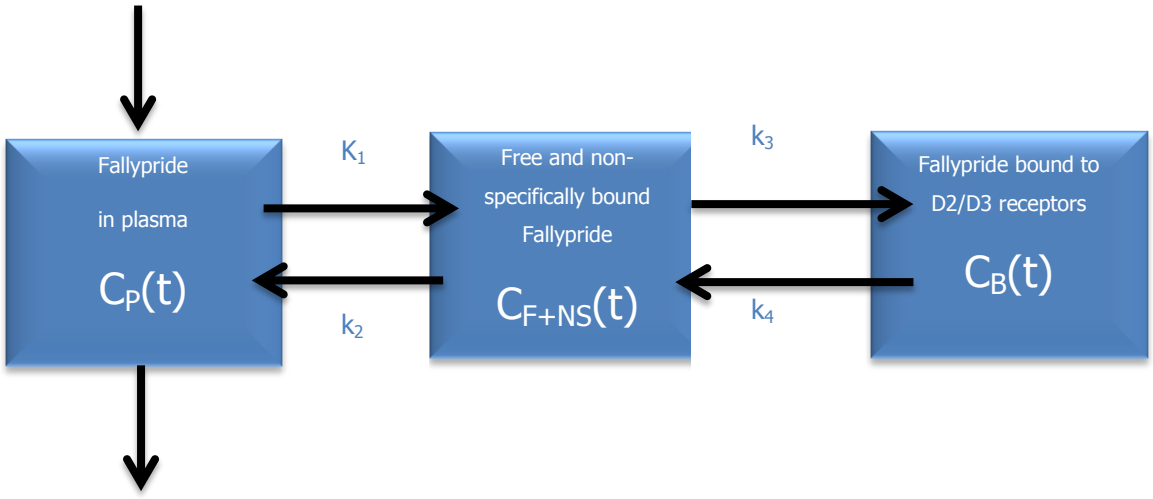


*Figure 1.1: Two tissue (or three-compartment) model or (2T4k) of $^{18}$F-fallypride*

Figure 1.1 provides the general 2T4k model of $^{18}$F-fallypride and an overview of the various paths that fallypride may follow after delivery by intravenous injection. This model consists of components of plasma, free and non-specifically bound ligand in tissue and ligand bound to $D_2/D_3$ receptors in tissue.

The tracer inside a compartment is assumed to be well mixed, kinetically homogeneous and distributed uniformly, meaning all the molecules of the tracer in a particular compartment have equal chance to exchange into other compartments.

This assumption simplifies the mathematics of compartmental modelling but also produces limitations of the compartment models to accurately describe some biological structures. Carson (2005, p. 132)

First compartment is used for the input function, it represents the concentration of tracer in arterial blood plasma as a function of time $C_P(t)$, therefore, the concentration of the tracer in the plasma is referred to as input function.

There is no need to define this compartment with an equation because the arterial blood plasma curve is measured.

From arterial blood, the radioligand is transported into the second compartment, free and non-specifically bound compartment. In the compartment, the free tracer in tissue can diffuse back into the blood or bound non-specifically to other cells than the target. This is represented by the concentration $C_{F+NS}(t)$ of $^{18}$F-fallypride in tissue.

The main interest is in the third compartment. In this compartment, the tracer in the tissue has been bound to D2/D3 receptors site. The concentration in this compartment is represented by $C_B(t)$.

The relationship between the different compartments is described by four rate constants ($K_1$–$k_4$). The rate constant in the compartmental model represents the amount of the total tracer leaving that compartment per unit time (fractional clearance). The unit of the rate constant is the inverse of time i.e., the fraction of tracer molecules required to travel in another compartment in one minute.

$K_1$ has a perfusion-dependent entity, this is indicated by capital letter (K). Perfusion is the volume of blood delivered through certain mass (or volume) of tissue per unit time. Blood flow is usually given in units ($ml.g^{-1}.min^{-1}$) or ($ml.ml^{-1}.min^{-1}$) or ($ml.cm^{-3}.min^{-1}$). Since the units of volume cancel out, therefore $K_1$ has the units of per minute ($min^{-1}$).

In this study, for the transport and binding rates of the tracer, $K_1$, $k_2$, $k_3$, and $k_4$ have units of per minute ($min^{-1}$), indicating the fraction of mass or volume transferred per unit time.

### 1.2.1 Mathematical description of 2T4k model and the estimation of the model parameters

The dynamics of the tracer molecule are governed using the mathematical models to analyse PET data.

The concentration in each compartment is time dependent, and these concentrations are therefore related through sets of ordinary differential equations (ODEs) which can be solved simultaneously to determine the quantities of interest.

From figure 1.1, only the second $C_{F+NS}(t)$ and the third compartment $C_B(t)$ can be defined with mathematical equations. The first compartment $C_P(t)$ is regarded as the input function where the arterial blood curve is measured, for this reason it not necessary to define it using the ordinary differential equations.

Table 1.1 shows how ODEs were reconstructed to define the mathematical description of the 2T4k model in the second compartment and Table 1.2 shows these ODEs in the third compartment.

In general, the rate of change of the amount of the fallypride in any compartment is equal to the sum of the rates of fallypride transfer into the compartment minus the sum of the rates of fallypride transfer out of the compartment.

*Table 1.1 Reconstruction of ODEs for 2T4k model in the second compartment*

| Compartments layout and the direction of exchange rate constant flow | The rate of change | The sign of flow | Rate constant | Ordinary differentials equations (ODEs) | |
|---|---|---|---|---|---|
| From $C_P(t)$ to $C_{F+NS}(t)$ 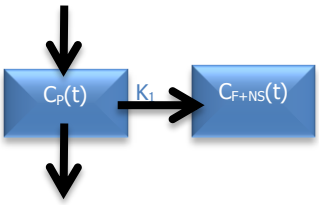  | $\frac{dC_{F+NS}(t)}{dt}$ | Inflow = positive (+) | $K_1$ | $\frac{dC_{F+NS}(t)}{dt} = K_1 C_P(t)$ | (1) |
| From $C_{F+NS}(t)$ to $C_P(t)$ 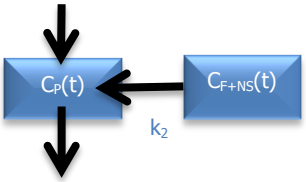  | $\frac{dC_{F+NS}(t)}{dt}$ | Outflow = negative (-) | $k_2$ | $\frac{dC_{F+NS}(t)}{dt} = -k_2 C_{F+NS}(t)$ | (2) |
| From $C_{F+NS}(t)$ to $C_B(t)$   | $\frac{dC_{F+NS}(t)}{dt}$ | Outflow = negative (-) | $k_3$ | $\frac{dC_{F+NS}(t)}{dt} = -k_3 C_{F+NS}(t)$ | (3) |
| From $C_B(t)$ to $C_{F+NS}(t)$ 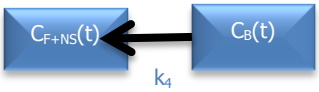  | $\frac{dC_{F+NS}(t)}{dt}$ | Inflow = positive (+) | $k_4$ | $\frac{dC_{F+NS}(t)}{dt} = k_4 C_B(t)$ | (4) |

*Note: The rate of transfer carries a positive (+) sign if it points into the compartment and a negative (-) sign if it points out of the compartment.*

The rate of change $\frac{dC_{F+NS}(t)}{dt}$ of the amount of the fallypride moving in and out of the second compartment ($C_{F+NS}(t)$), is equivalent to the sum of equations (1) to (4), which is described by the following differential equation.

$$\frac{dC_{F+NS}(t)}{dt} = K_1 C_P(t) - k_2 C_{F+NS}(t) - k_3 C_{F+NS}(t) + k_4 C_B(t) \quad (5)$$

Rearranging equation (5) gives the following ODE:

$$\frac{dC_{F+NS}(t)}{dt} = K_1 C_P(t) - (k_2 + k_3) C_{F+NS}(t) + k_4 C_B(t) \quad (5.1)$$

*Table 1.1 Reconstruction of ODEs for 2T4k model in the third compartment*

| Compartments layout and the direction of exchange rate constant flow | The rate of change | The sign of flow | Rate constant | Ordinary differentials equations (ODEs) |
|---|---|---|---|---|
| **From $C_{F+NS}(t)$ to $C_B(t)$** 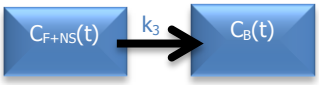  | $\frac{dC_B(t)}{dt}$ | Inflow = positive (+) | $k_3$ | $\frac{dC_B(t)}{dt} = k_3 C_{F+NS}(t)$ (6) |
| **From $C_B(t)$ to $C_{F+NS}(t)$** 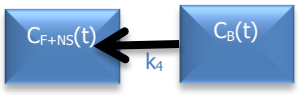  | $\frac{dC_B(t)}{dt}$ | Outflow = negative (-) | $k_4$ | $\frac{dC_B(t)}{dt} = -k_4 C_B(t)$ (7) |

*Note: The rate of transfer carries a positive (+) sign if it points into the compartment and a negative (-) sign if it points out of the compartment.*

Similarly rate of change $\frac{dC_B(t)}{dt}$ of the amount of the fallypride moving in and out of the third compartment ($C_B(t)$), is the sum of equations (6) and (7), which is described by the following differential equation.

$$\frac{dC_B(t)}{dt} = k_3 C_{F+NS}(t) - k_4 C_B(t) \quad (8)$$

The transport and binding rates of the tracer are assumed to be linearly related to the concentration differences between two compartments, and thus equation (5.1) and equation (9) first-order differential equations describe the model of figure 1.1 at time t [min] (Heiss and Herholz 2006).

The compartment activities given in equation (5.1) and (8) are not individually accessible from imaging measurements but their sum given in equation (9) below can be measured.

$$C_T(t) = C_{F+NS}(t) + C_B(t) \tag{9}$$

where,

$C_{F+NS}(t)$ = Concentration of free and non-specifically bound fallypride in brain tissue in [kBq/ml]

$C_P$ = Concentration of fallypride in the arterial plasma in [kBq/ml]

$C_B$ = Concentration of fallypride bound to $D_2/D_3$ receptors in [kBq/ml]

$C_T$ = Total concentration of fallypride in tissue in [kBq/ml]

$K_1$ to $k_4$ = Fallypride exchange rate constants associated with delivery, uptake, binding, and clearance.

where:

$K_1$ [$min^{-1}$] = net influx or the delivery of the tracer to the brain

$k_2$ [$min^{-1}$] = washout of the tracer from the brain

$k_3$ [$min^{-1}$] = forward receptor-ligand reaction, the delivery of the tracer to $D_2/D_3$ receptors in tissue

$k_4$ [$min^{-1}$] = reverse receptor-ligand reaction, the clearance or washout of the tracer from $D_2/D_3$ receptors in tissue

The ground truth compartmental model described in figure 1.1 can be converted into mathematical form giving a rise to a solution obtained by solving the ordinary differential equations and by estimating the rate constants given an arterial input function $C_P(t)$ and given the PET measurement $C_T$ over tissue.

The total concentration of fallypride in tissue represented by equation (9) can be expanded further by solving the differential equations (5.1) and (8).

Therefore, the solution of the ground truth model (Nelissen N, Warwick J & Dupont P at al., 2012) described in figure 1.1 is given by:

$$C_T(t) = C_{F+NS}(t) + C_B(t) \ = (\emptyset_1 e^{-\theta_1 t} + \emptyset_2 e^{-\theta_2 t}) \otimes C_P(t) \tag{10}$$

where:

$$\emptyset_1 = \frac{K_1(\theta_1 - k_3 - k_4)}{\Delta}$$

$$\emptyset_2 = \frac{K_1(\theta_2 - k_3 - k_4)}{-\Delta}$$

$$\theta_1 = \frac{k_2 + k_3 + k_4 + \Delta}{2}$$

$$\theta_2 = \frac{k_2 + k_3 + k_4 - \Delta}{2}$$

$$\Delta = \sqrt{(k_2 + k_3 + k_4)^2 - 4k_2k_4}$$

This estimation is typically performed using a non-linear least square fitting approach.

The quantity of interest is the binding potential $BP_{ND}$, which is the ratio of the concentration of specifically bound tracer in tissue to the concentration of non-displaceable tracer in tissue. A commonly used quantitative approach is to define tracer binding in terms of distribution volume (DV) or $V_{ND}$ (Kimura et al., 2007).

$V_{ND}$ is the distribution volume with no specific binding regions. $V_T$ is the total distribution volume. The relationship between $BP_{ND}$ and the volumes of distribution is given by:

$$BP_{ND} = \frac{V_T - V_{ND}}{V_{ND}} = \frac{V_T}{V_{ND}} - 1 = DVR - 1 \quad (11)$$

where the term, $\frac{V_T}{V_{ND}} = DVR$ = distribution volume ratio. (11.1)

For two-tissue compartment models, volumes of distribution can be derived from rate constants. The relationship of compartmental rate constants to the total volume of distributions given by:

$V_T = \frac{K_1}{k_2}(1 + \frac{k_3}{k_4})$ (unit-less) in a region containing the receptors of interest (12)

and

$V_{ND} = \frac{K_1}{k_2}$ (unit-less) in a reference region void of these receptors. (13)

## 1.3 The description of the various models used in $^{18}$F-fallypride receptor-ligand quantification

In this work, five models were compared, using a sixth model (2T4k) as the ground truth: (1) the Logan graphical analysis (LGA) with arterial blood sampling, (2) the Logan graphical analysis using a reference region (cerebellum) ($Logan_{ref}$), (3) the reference tissue model (RTM) using the cerebellum as reference region, (4) the simplified reference tissue model (SRTM) and (5) standardized uptake value ratios (SUVR) measured as the ratio of the activity in a region of interest and the activity in the cerebellum.

The arterial blood sampling is used to determine the transport of the radioactive tracers' washout and metabolism in PET studies (Sijbesma et al., 2016). The arterial blood sampling models, 2T4k and LGA are regarded as invasive methods.

The receptor kinetics can be modelled without the need to measure the arterial input function using the reference region models. This means the arterial blood sampling and metabolite measurements can be avoided, making the reference region models non-invasive methods. If the reference model (non-invasive) compares well to the arterial blood sampling model (invasive), then the arterial blood sampling model can be replaced by the non-invasive procedure. The reference region models, $Logan_{ref}$, RTM, SRTM and SUVR are regarded as non-invasive methods.

### 1.3.1 LGA with arterial blood sampling

LGA (Logan et al., 1990) is used for tracers that have reversible binding to the receptors of interest and when a steady state is reached. Logan graphical analysis requires an arterial plasma input function of the intact tracer as a function of time, which can be obtained by arterial blood sampling.

Intact tracer represents the unchanged or free fraction of authentic parent tracer in plasma which is not bound to plasma proteins. It is assumed to equal to 1 at the time of injection (t=0), this means there is 100% of the input concentration of the unchanged tracer with no metabolites present.

Under the conditions above, it is possible to find a linear relationship between two new variables $\frac{\int_0^t C_T(\tau)d\tau}{C_T(t)}$ and $\frac{\int_0^t C_P(\tau)d\tau}{C_T(t)}$ depending on $C_p$ and $C_T$ and the slope of this relationship is the total volume of distribution ($V_T$):

The following steps show how the mathematical equations for LGA with arterial blood sampling can be derived by integrating the first-order differential equations. As discussed before, these first-order differential equations are used to describe the behaviour of an administered $^{18}$F-fallypride in target tissues using three-compartment model of $^{18}$F-fallypride in figure 1.1.

To find the solution for LGA with arterial blood sampling:

The sum of Eq. (5.1) and Eq. (8) can be arranged to give $C_{F+NS}(t)$ in Eq. (14) and Eq. (8) to give $C_B(t)$ in Eq. (15)

$$C_{F+NS}(t) = \frac{K_1}{k_2}C_P(t) - \frac{1}{k_2}\left(\frac{dC_{F+NS}(t)}{dt} + \frac{dC_B(t)}{dt}\right) \quad (14)$$

$$C_B(t) = \left(\frac{1}{k_4}\right)\frac{dC_{F+NS}(t)}{dt} - \frac{K_1}{k_2}C_P(t) + \left(\frac{k_2+k_3}{k_4}\right)C_{F+NS}(t) \quad (15)$$

Substituting Eq. (14) into Eq. (9), the output is:

$$C_T(t) = \left(1 + \frac{k_2+k_3}{k_4}\right)C_{F+NS}(t) + \left(\frac{1}{k_4}\right)\frac{dC_{F+NS}(t)}{dt} - \frac{K_1}{k_4}C_P(t) \quad (16)$$

Further substitution with Eq. (14) and rearrangements gives:

$$C_T(t) = \frac{K_1}{k_2}\left(1 + \frac{k_3}{k_4}\right)C_P(t) - \frac{1}{k_2}\left(1 + \frac{k_3}{k_4}\right)\left[\frac{dC_{F+NS}(t)}{dt} + \frac{dC_B(t)}{dt}\right] - \frac{1}{k_4}\frac{dC_B(t)}{dt} \quad (17)$$

The integrated form of this equation is:

$$\int_0^T C_T(t) = \frac{K_1}{k_2}\left(1 + \frac{k_3}{k_4}\right)\int_0^T C_P(t) - \frac{1}{k_2}\left(1 + \frac{k_3}{k_4}\right)[C_{F+NS}(t) + C_B(t)] - \frac{1}{k_4}C_B(t) \quad (18)$$

Dividing Eq. (16) by $C_T(t)$ gives:

$$\frac{\int_0^T C_T(t)}{C_T(t)} = \left(\frac{K_1}{k_2}\left(1 + \frac{k_3}{k_4}\right)\right)\frac{\int_0^T C_P(t)}{C_T(t)} - \frac{1}{k_2}\left(1 + \frac{k_3}{k_4}\right)\frac{[C_{F+NS}(t)+C_B(t)]}{C_T(t)} - \left(\frac{1}{k_4}\right)\frac{C_B(t)}{C_T(t)} \quad (19)$$

Rearrangement of Eq. (19) gives:

$$\frac{\int_0^T C_T(t)}{C_T(t)} = \left(\frac{K_1}{k_2}\left(1+\frac{k_3}{k_4}\right)\right)\frac{\int_0^T C_P(t)}{C_T(t)} - \frac{1}{k_2}\left(1+\frac{k_3}{k_4}\right) - \left(\frac{1}{k_4}\right)\frac{C_B(t)}{C_{F+NS}(t)+C_B(t)} \quad (20)$$

The condition for linearity of Eq. (20) is that the intercept $-\frac{1}{k_2}\left(1+\frac{k_3}{k_4}\right) - \left(\frac{1}{k_4}\right)\frac{C_B(t)}{C_{F+NS}(t)+C_B(t)}$ is constant. After some time t>t*, the compartment concentrations follow the plasma concentration so that $\frac{C_{F+NS}(t)+C_B(t)}{C_P(t)}$ and $\frac{C_B(t)}{C_P(t)}$ are constant, which ensures that the intercept is constant since $C_P(t)$ cancels. In many cases the intercept becomes constant even before $\frac{C_{F+NS}(t)+C_B(t)}{C_P(t)}$ becomes constant so that the graphical method can be applied before the steady-state condition becomes valid.

If distribution volume, $V_T = DV = \frac{K_1}{k_2}\left(1+\frac{k_3}{k_4}\right)$, and the intercept is marked with A, the

Logan plot can be represented as:

$$\frac{\int_0^t C_T(\tau)d\tau}{C_T(t)} = V_T\frac{\int_0^t C_P(\tau)d\tau}{C_T(t)} + A \quad (21)$$

where A is regarded as a constant if $\frac{C_T}{C_P}$ remains constant after a certain time t*. By calculating this relationship for all time frames after time t*, $V_T$ can be determined by linear regression.

### 1.3.2 Logan$_{ref}$ using a reference region (cerebellum)

If the metabolite corrected plasma curve is not available, but instead a reference region can be found which is void of the receptors of interest, Logan graphical analysis using a reference region can be applied under the same conditions as the classical Logan graphical analysis (Logan et al., 1996):

$$\frac{\int_0^t C_T(\tau)d\tau}{C_T(t)} = DVR\frac{\int_0^t C_{ref}(\tau)d\tau}{C_T(t)} + B \quad (22)$$

where the distribution volume ratio (DVR) is the ratio of the volume of distribution in the region of interest and the reference region. B is regarded as a constant if $\frac{C_T}{C_{ref}}$ remains constant after some time t* (Wong et al., 2012). The relation between DVR and $BP_{ND}$ can be found by re-arranging equation (11):

$$DVR = 1+BP_{ND} \quad (23)$$

For $^{18}$F-fallypride the cerebellum was used as reference region for all models that require this. The cerebellum is a structure in the brain with very low $D_2\backslash D_3$ receptor density (Christian et al., 2006).

### 1.3.3 Reference tissue model

The RTM in (figure 2.1) assumes that:

1) The regions of interest and the reference region share the same arterial input function (Lammertsma et al., 1996; Watabe et al., 2006);
2) A reference region which is void of the receptors of interest can be found;
3) The DV of free ligand in tissue in the region of interest and the reference region is the same i.e. in the target region and in the reference region the relation following relationship holds.

$$DV = V_{ND} = \frac{K_1}{k_2} = \frac{K_1^{ref}}{k_2^{ref}} \quad (24)$$

When these assumptions are met, the model does not require an arterial input function. This means the reference region is then used as an indirect input function to the total target region.

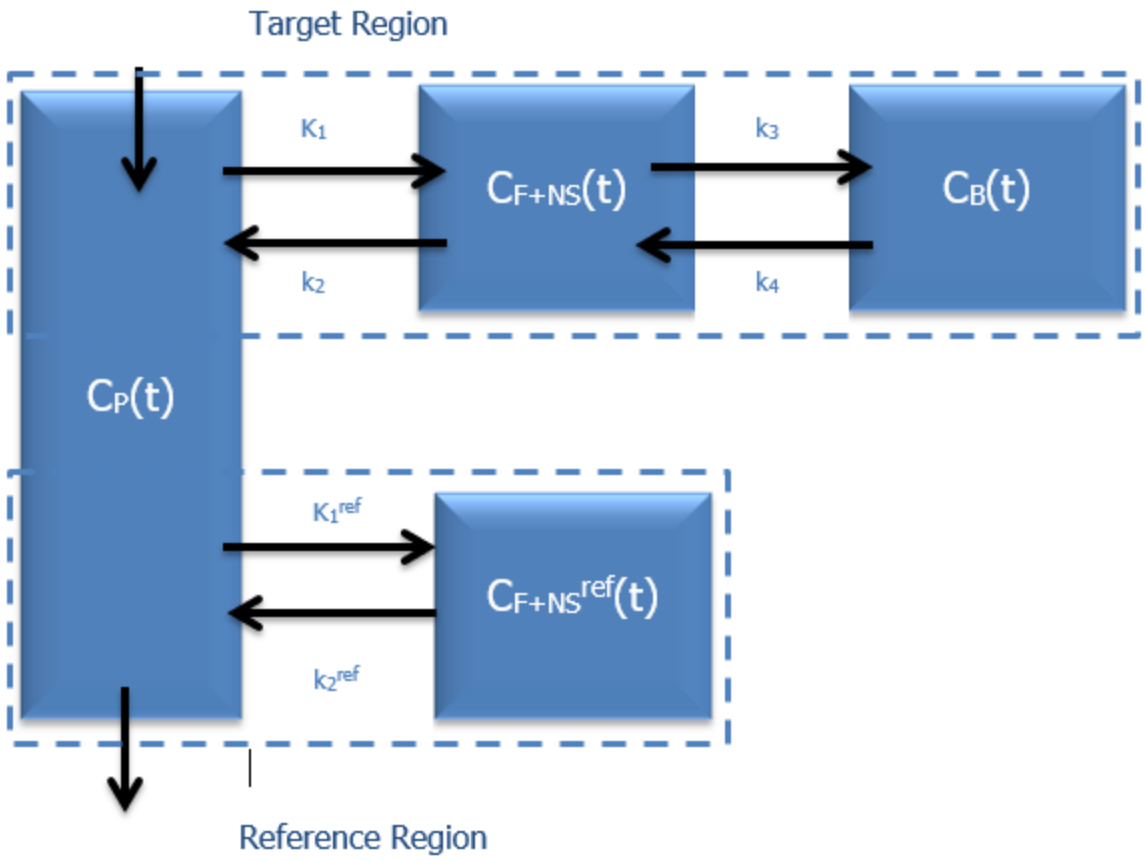


*Figure 2.1: Reference tissue model*

The operational equation of the reference tissue model (Lammertsma, 1996) is:

$$C_t(t) = R_1[C_{ref}(t) + (ae^{-ct} + be^{-dt}) \otimes C_{ref}(t)] \quad (25)$$

Where

$$R_1 = \frac{K_1}{K_1^{ref}}$$

$$a = \frac{(k_3 + k_4 - c)(c - r)}{p}$$

$$b = \frac{(d - k_3 - k_4 - c)(d - r)}{p}$$

$$c = \frac{(k_2 + k_3 + k_4 + p)}{2}$$

$$d = \frac{(k_2 + k_3 + k_4 - p)}{2}$$

$$p = \sqrt{(k_2 + k_3 + k_4)^2 - 4k_2k_4}$$

$$r = \frac{k_2}{R_1}$$

$\otimes$ = *convolution*

Using non-linear fitting the equation can be used to obtain four parameters namely ($R_1$, $k_2$, $k_3$, and $k_4$), and $BP_{ND}$ can be calculated as:

$$BP_{ND} = \frac{k_3}{k_4}. \tag{26}$$

For $^{18}$F-fallypride, the cerebellum will be used as reference region (Christian et al., 2006).

### 1.3.4 Simplified reference tissue model

The SRTM is a further simplification of the RTM by assuming that in the receptor-rich tissue of interest, it is not easy to differentiate between specific and the free/non-specific compartment and as result of this, it can be described by a single tissue compartment. The other assumptions of the RTM are required as well.

When the SRTM is appropriate, it produces more stable results and smaller standard errors compared to the RTM, because it reduces the number of parameters to be estimated from four to three.

The operational equation of the simplified reference tissue model (Lammertsma and Hume, 1996) is:

$$C_T(t) = R_1 C_{ref}(t) + k_2 (1 - \frac{R_1}{1 + BP_{ND}}) C_{ref}(t) \otimes e^{-\frac{k_2 t}{1 + BP_{ND}}} \tag{27}$$

where $C_T(t)$ represents the time activity curve (TAC) in the region of interest and $C_{ref}(t)$ is the TAC in the reference region (in our case the cerebellum).

The three parameters ($R_1$, $k_2$, $BP_{ND}$) in the equation above can be fitted using standard nonlinear estimation techniques.

### 1.3.5 Standard uptake value ratio

SUVR is measured as the ratio of the activity in a region of interest and the activity in the reference region, which is the cerebellum in our study. SUVR is a dimensionless quantity which is easy to calculate and which does not depend on scaling factors related to the scanner or the patient (van den Hoff et al., 2013; McNamee et al., 2009).

As explained by McNamee et al (2009), the equation of the SUVR can be written as follows.

$$SUVR = \frac{SUV_{ROI}}{SUV_{REF}} = \frac{\int_{t_1}^{t_2} C_{ROI}(t)dt}{\int_{t_1}^{t_2} C_{REF}(t)dt} \tag{28}$$

Where $C_{ROI}$ and $C_{REF}$ are the activities in the region of interest and cerebellum respectively between the time $t_1$ and $t_2$. $SUV_{ROI}$ and $SUV_{REF}$ are the SUV values (Pavlopoulos et al., 2007), (Kinahan et al., 2010). SUVR will be measured in different time intervals (McNamee et al., 2009).

## 1.4 The use of simulations in kinetic modelling

Modeling and simulation provide more detailed depth of theoretical and experimental analysis on the issues that are impractical to solve. They supplement theory and experimentation, improving the scientific method.
The number of researchers employing simulations to analyze data is increasing. It is, however, very important that this kind of simulations are fully understood.

Kinetic modelling simulation involves the following basic steps as stated by Resat et al., (2009): Identification of the kinetic modelling problem which involves the determination of the input and output variables as well as the intermediates, model formulation, choosing a method, simulation, and studying the sensitivity to parameter variations.

## 1.5 The use of the graphical and simplified methods in $^{18}$F-fallypride quantification and their importance in kinetic modelling

Graphical and/or simplified methods are used for quantifying brain PET data because they are quantitatively accurate, thus producing fast and simplified calculation methods or less invasive procedures. Even though the arterial blood sampling is used to determine the transport of the radioactive tracers' washout and metabolism in PET studies (Sijbesma et al., 2016), the main advantage of using the simplified methods is to eliminate the need to perform arterial blood sampling. Quantitative accuracy can be achieved while maximizing patient comfort. (Salinas et al., (2015). In case of $^{18}$F-fallypride, the cerebellum can be used as a reference region due to its low density of $D_2$ and $D_3$ receptors (Christian et al., 2006). The main advantage of graphical methods is that they are easy to use, simple to implement and fast and therefore ideally suited for parametric imaging in which we perform voxel based kinetic modelling (Kimura et al., 2007).

## 1.6 Problem Statement and research impact

Several simplified methods of quantifying $^{18}$F-fallypride have been described and used on real data, but a systematic analysis of their effect on quantification has not been performed.

While performing simplified methods of quantification of $^{18}$F-fallypride, simulations are useful for the tracer in question, because they allow the study of different models and approaches under fully controlled conditions and also provide a ground truth. Simulation involves the calculation of solving the equations for the 'ground truth' model (figure 1.1) given a perfect input function $C_p(t)$ with a given set of parameters. This leads to the ground truth parameters of interest.

Simulating the dynamic PET data plays an important role in the validation of model analysis and the software development.

The general idea is that with known "flawless" input data, a model and a set of model parameters, a flawless tissue curve can be calculated. This can be done for any time point (within the time interval of the input function).

A real PET experiment will consist of a dynamic measurement using a number of frames with defined duration. This means that the tissue curve is sampled according to the frame definition. Furthermore, PET data contains noise, which depends on the amount of tracer in the region of interest, the duration of the frame and the decay of the tracer.

The parameters of interest of each simplified model were calculated using realistically simulated PET data as the measurement and were compared with the ground truth results.

## 1.7 Aim and Objectives of the study

The aim of this study is to investigate simplified methods to quantify $^{18}$F-fallypride, and to study the impact of different acquisition protocols on this quantification by using simulations.

Specific objectives of the study:

1. To evaluate the accuracy/reliability of various models in $^{18}$F-fallypride quantification.
2. To investigate the effect of models performance under varying noise-level/signal to noise ratio (SNR) in brain regions with high, moderate, and low receptor density
3. To investigate the effect of models performance under varying conditions in brain regions with high, moderate, and low receptor density such as:
    a) Total scan duration (continuous sampling scheme)
    b) Scan duration with breaks (interrupted sampling scheme)

# Chapter 2: Literature Review

## 2.1 Introduction

The search and selection strategy of the literature review was based on a search using comprehensive search keywords (Fallypride, simulation, kinetic modelling, positron emission tomography OR PET, $D_2/D_3$ receptors, binding potential). The database on PubMed and other internet resources (from 1970 to 2018) were used in this study. Only those publications in peer-reviewed journals in English language were considered.

Abstracts were collected based on how relevant they are to our study.

## 2.2 The use of fallypride PET in neurological and psychiatric diseases

Extrastriatal DA plays a very important role in human cognition/behavior which is implicated in a number of neurological and psychiatric diseases, including Parkinson's disease, Huntington's chorea, schizophrenia, and psychostimulant dependence syndromes to name few. Several radiopharmaceuticals have been targeted to different areas in the brain in order to study the nature of these various diseases.

As described by Riccardi et al (2006), there are several radioligands used to measure DA $D_2$ receptor levels in the striatum, such as $^{11}$C-raclopride, and $^{123}$I-IBZM.

High-affinity radioligands, such as $^{11}$C-FLB 457, $^{123}$I-epidepride, and $^{18}$F-fallypride are used to visualize DA $D_2/D_3$ receptors in striatal and extrastriatal regions. However, $^{11}$C-FLB 457 and $^{123}$I-epidepride have prolonged striatal uptake, which makes it difficult to estimate striatal DA $D_2/D_3$ receptor levels. $^{18}$F-fallypride, on the other hand, has relatively slow kinetics and more rapid washout from striatum, which makes it easy to estimate striatal DA $D_2/D_3$ receptor levels (Riccardi et al., 2006; Zald et al., 2010; Ceccarini et al., 2012). This makes it suitable to use in neurological and psychiatric diseases.

The affinity of $^{18}$F-fallypride to DA $D_2$ and $D_3$ receptors is comparable to that of [$^{11}$C]-FLB457, and some 10-fold higher than the affinities of $^{11}$C-raclopride or $^{11}$C- (1)-PHNO (Cumming et al., 2013).

There is an interest in fallypride PET for various reasons. Some of these reasons include its use and application in neurological and psychiatric diseases, which has accelerated over the years.

### 2.2.1 The choice of reference tissue models in $^{18}$F-fallypride human experiments studies

Work relevant to our research has already been performed by Salinas et al., (2015), Ishibashi et al., (2013) and Slifstein et al., (2010) using simplified models with fallypride tested on humans.

Below is what has been done and concluded, applying these models using optimizing protocols, while taking into consideration the selection or the best model for quantification of fallypride.

#### 2.2.1.1 Simplified reference tissue model

Reference tissue models (less invasive procedures) have been used in last the two decades as the methods of choice for the quantification of brain PET (Salinas et al 2015). They can be used to eliminate arterial blood sampling, which requires blood measurements and metabolite concentrations for input function generation.

SRTM assumes that tracer activity exchange between tissue compartments can be described by a 1-tissue compartment model. This reduces the number of parameters to three, hence allowing precise accuracy in mapping ($BP_{ND}$).

The three parameters produce more accurate fitting of kinetic data, resulting in stable parameter estimation. Due to its simplicity the model can produce a good fit, which can affect the estimates of the binding potential ($BP_{ND}$) (Salinas et al., 2015).

In their study Salinas et al., (2015) used computer simulation to study the bias introduced in $BP_{ND}$ estimates by violating the model assumptions. Their study showed that violating the model assumptions led to bias in $BP_{ND}$ (both over and underestimation).

Their conclusion was that the bias found in SRTM $BP_{ND}$ should be carefully assessed when using new radiotracers (Salinas et al 2015).

Using the simplified reference tissue model, Ishibashi et al., (2013) investigated the influence of reference region choice on the striatal binding potential of a high-affinity DA $D_2/D_3$ receptor radioligand ($^{18}$F-fallypride). Comparison was made between the use of the visual cortex and a white matter to the cerebellum (used as reference region). In comparison to cerebellum, visual cortex gave greater sample variance in BP relative to $BP_{ND}$. The results showed that $BP_{ND}$ values in white matter produced similar results as the $BP_{ND}$ values cerebellum.

The study suggests white matter to be used as an alternative to the cerebellum due to similar kinetic properties (Ishibashi et al., 2013).

$^{18}$F-fallypride $BP_{ND}$ was calculated by Siessmeier et al., (2005) using a 2-tissue compartment model, Logan method using metabolite-corrected arterial inputs, Logan reference tissue method, conventional simplified reference tissue method (SRTM), and SRTM with linear regression and spatial constraint (LRSC). It was found that the ratio of BP in the striatum to that in the thalamus was much higher for $^{18}$F-fallypride (Siessmeier et al., 2005).

The BP's coefficient of variation was found to be less favourable for $^{18}$F-fallypride in the striatum (dopamine receptor rich region). Siessmeier et al., (2005) reported that the very slow approach when it comes to $^{18}$F-fallypride equilibrium binding may affect the accuracy in estimating striatum BP, even for long 4 hour scans.

Slifstein et al., (2010) used $^{18}$F-fallypride to measure the effects of amphetamine on $D_2/D_3$ ligand binding in striatum and extra-striatal brain regions in one scan session.

The two tissue compartment model (2T4k) with arterial plasma input and simplified reference tissue model (SRTM) were used to analyze PET data.

It was found that the estimated amount of the decreases in $BP_{ND}$ amphetamine effect tend to be greater with 2T4k than SRTM method.

It was concluded that $^{18}$F-fallypride is a suitable for measuring the effect of amphetamine in striatum and limbic regions, but in cortical regions (Slifstein et al., 2010).

#### 2.2.1.2 Application of SRTM focusing on total scan duration

The available antagonist radioligands for quantitation of extrastriatal DA $D_2/D_3$ receptors all have strengths and limitations. $^{18}$F-fallypride can be used to estimate DA $D_2/D_3$ receptor levels in both striatal and extrastriatal regions but requires about 3–3.5 hours of scanning (Vernaleken et al., 2011; Riccardi et al., 2006, 2011).

Vernaleken, et al., (2011) investigated the applicability of a simplified reference tissue model (SRTM) when the scan duration was changed in a large sample of PET scans. Subjects were scanned using fallypride for 180 min scan duration. SRTM was used to calculate the binding potential ($BP_{ND}$) for putamen, thalamus, and temporal cortex.

Shortening the scan time duration caused $BP_{ND}$ underestimation to escalate from 0.58% in 10 min to 5.76% in 1 hour (Vernaleken, et al., 2011). For $^{18}$F-fallypride, it was found out that 180 min scan duration reached equilibrium even in $D_2/D_3$ receptor rich regions.

Moderate reductions in fallypride scan durations only caused small changes to SRTM results even in receptor rich regions. Their results correlated with the data published by Riccardi et al., (2006, 2011), stating that $^{18}$F-Fallypride requires about 3 – 3.5 hours of scanning.

Furthermore, in their study, Constantinescu et al., (2011), used the maximum scan time of up to 2.5 hours for $^{18}$F-fallypride studies. The results revealed the stability in $^{18}$F-fallypride kinetics at 2.5 hours, which can be an advantage to human studies. Such reduced acquisition times and imaging protocols aim to balance quantitative accuracy between patient comfort and image artefacts due to possibility of patient motion during acquisition.

Honer et al., (2004) estimated $BP_{ND}$ as a function of scan duration using $^{18}$F-fallypride with 2.5 hours scanning time. Tantawy et al., (2009) used the total scan duration of 2 hours estimated $BP_{ND.}$

Ishibashi et al., (2013) stated that $^{18}$F-fallypride has relatively slow kinetics, thus requiring a prolonged scanning time of at least 2 to 3 hours.

#### 2.2.1.3 Logan reference tissue model

$Logan_{ref}$ yields a parameter (DVR) that is proportional to specific binding. The method assumes the existence of a reference region which is incorporated rather than the arterial blood radioligand concentration (Logan et al., 1996; Mukherjee et al., 2001).

#### 2.2.1.4 RTM

RTM can be used as an alternative method to eliminate the use of invasive arterial blood sampling (Ishibashi et al., 2013).
To our knowledge, the reference tissue model (RTM) using the cerebellum as the reference region is not yet studied for fallypride, but has been for other tracers.

#### 2.2.1.5 SUVR

Arterial blood sampling, dynamic imaging and kinetic modeling are regarded as the 'gold standard' for quantification of PET measurements. Kinetic modeling techniques play an important role in replacing the blood data with the data from a reference region, thus further simplifications such as calculation of standard uptake value ratios (SUVR) act as a replacement for kinetic modeling (Gunn et al., 2015) which reflects the relative contribution of specific and non-specific binding as represented by the reference region and it does not require arterial blood sampling or long scanning durations (Heurling et al., 2017).

However, to determine whether SUVR truly reflects true quantification, it has to be validated against the quantitative gold standard (Gunn et al., 2015; Heurling et al., 2017). SUVR has thus far been the most widely used with different tracers ([$^{18}$F]-AV45 PET, [$^{11}$C]-PiB PET, T807 (tau) (20), florbetapir (Aβ), [$^{18}$F]THK-5117) other than fallypride (Blautzik et al., 2017; Brier et al., 2016; Ishiki et al., 2015).

## 2.3 Simulations in kinetic modelling

The uptake and washout of a tracer in a tissue region depends on physiological and biochemical parameters which can be quantified by analyzing TACs obtained from dynamic PET.

Kinetic modelling simulation is used to study the kinetics of tracers. It can be used to determine the input and output functions, model formulation, choosing a method, simulation, and studying the sensitivity to parameter variations (Resat et al., 2009)

### 2.3.1 Simulation of the input function

The simulation of the input function includes methods like linear interpolation between the measured points, spline fitting and mathematical function fitting using the sum of exponential functions, a Thompson and Golish bolus input function (Thompson et al., 1964; Golish et al., 2001) or a Gamma variate (Davenport et al., 1984; Madsen, 1992).

Several studies have simulated the input function using the sum of exponential functions.

Ito et al., (1998) used $^{11}$C-raclopride with a three-compartment model, and simulated the input function as an interpolation of a sum of two exponential functions with time interval of 3.5 to 60 minutes (0 to 3.5 minutes, linear interpolation). Since the kinetic method requires determination of an arterial input function, it was concluded that the transient equilibrium method and the interval method used in the study are suitable for routine clinical research, because they do not require determination of an arterial input function.

A direct comparison of $^{18}$F-fallypride and $^{11}$C-FLB457 using the multiple-injection protocol was performed by Vandehey et al., (2010). TACs were fitted with the sum of three exponents to describe the decline of the radiotracer. The rate of clearance between $^{11}$C-FLB457 and $^{18}$F-fallypride were compared.

### 2.3.2 Simulation of the Time Activity curves

Ceccarini et al., (2012) used $^{18}$F-fallypride PET to detect striatal and extrastriatal dopamine release using human and simulation studies. PET data was analyzed using the linearized simplified reference region model. The noiseless TACs of $^{18}$F-fallypride were generated using simulations. The simulations were performed using extended standard compartmental model commonly used in tracer kinetic PET analysis (Ceccarini et al., 2012).

The concentration of the plasma input function was modeled by biexponential decay function. Time–activity curves were simulated using the rate constants of $^{18}$F-fallypride based on Christian et al., (2004). It was found that the effect of striatal

dopamine release could be detected if the activation starts between 190 to 200 minutes after injection using the linearized simplified reference region model.

# Chapter 3: Methods

## 3.1 Research design and material used

The study was conducted at Tygerberg Academic Hospital in the department of Medical Imaging and Clinical Oncology (MICO) of Stellenbosch University.

In this study $^{18}$F-fallypride kinetics in the human brain were investigated using simulations. All simulations were performed using Matlab (version R2013a (8.1.0.604) win 64-bit software; MathWorks, Inc.) and the software developed at KU Leuven (Belgium).

The Matlab scripts were further adapted for the current study.

Simulations of realistic measurements were performed by:

1). Simulation/modelling of a representative input function
2). Modelling the fraction of intact tracer
3). Simulation of the theoretical output function (TAC) in brain regions with high, moderate and low receptor density
4). Simulation of the measurement noise by Gaussian noise model

Different analysis methods (LGA, Logan$_{ref}$, RTM, SRTM and SUVR) were tested with the simulated tissue data. The ability of each method to reproduce the model parameters, or distribution (the parameter associated with the physiological drug uptake) was then assessed.

## 3.2 Research methodology

### 3.2.1 Simulation/modelling of a representative input function

A representative curve of arterial blood plasma input function after a bolus $^{18}$F-fallypride administration (figure 3.1) was taken from the literature (Mukherjee et al., 2002).

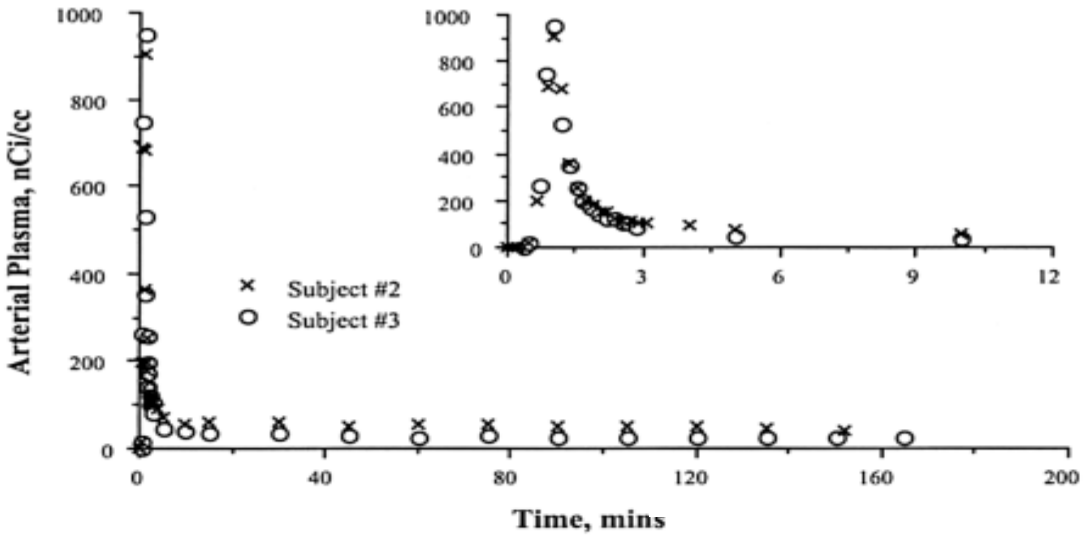


*Figure 3.1: A representative curve of arterial blood plasma levels of fluorine-18 radioactivity after a bolus $^{18}$F-fallypride administration. The inset shows the peak in the first 12 minutes. Reprinted with permisson from Mukherjee, J., Christian, BT, Dunigan KA., Shi, B, Narayanan, TK, Satter, M, & Mantil, et al. Brain imaging of $^{18}$F-fallypride in normal volunteers: Blood analysis, distribution, test-retest studies, and preliminary assessment of sensitivity to aging effects on dopamine D-2/D-3 receptors. Synapse, 2002;46(3), 170–188. Copyright 2002, John Wiley & Sons Inc.*

*A representative input function curve in figure 3.1 was used to reproduce a simulated input function using Matlab (refer to figure 3.2 (A) and (B)).*

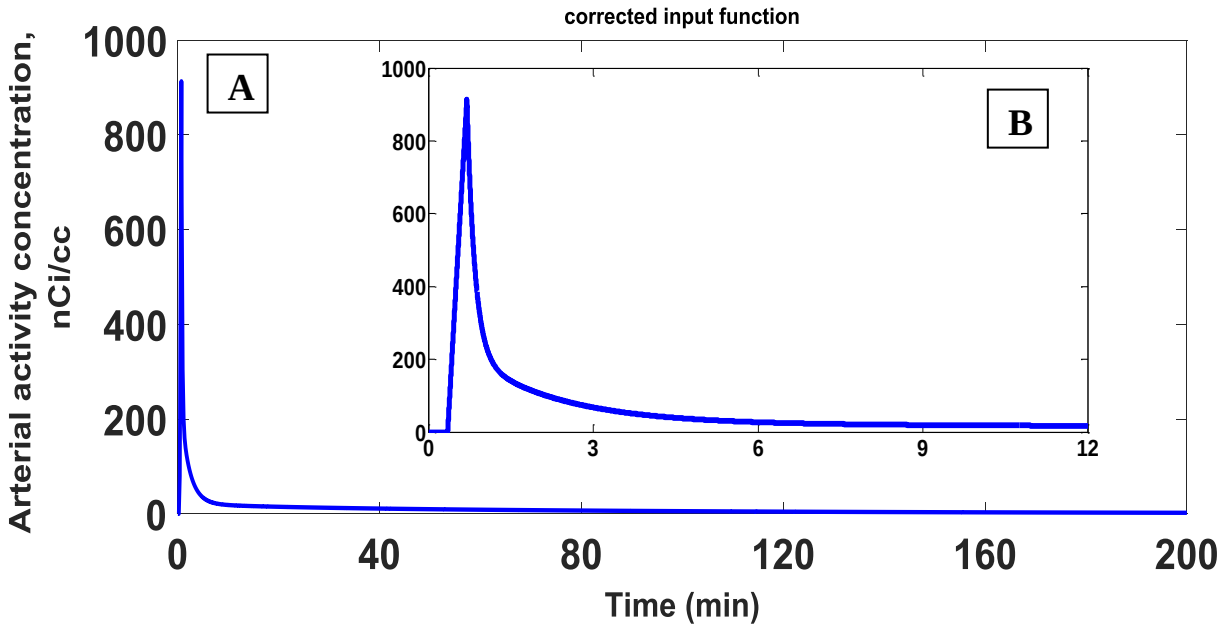


*Figure 3.2: (A) A simulated curve of arterial blood plasma activity concentration of fluorine-18 radioactivity after a bolus $^{18}$F-fallypride administration. (B) The inset shows the peak in the early section of the of the arterial blood plasma curve in the first 12 minutes. (Note: the concentration peaked before 3 min).*

A typical arterial plasma input function after a bolus injection will have a short interval after the start of the injection (at t = 0) where no activity has reached the brain, followed by a sharp rise to a peak (arrival of the bolus in the brain) and then a rapid decline and levelling off of the arterial plasma concentration. Therefore, the input function (figure 3.2) was modelled as follows:

$$C_a(t) = \begin{cases} 0 & if \quad t \le t_s \\ \dfrac{\sum_{i=1}^{3} A_i}{t_p - t_s}(t - t_s) & if \quad t_s \le t \le t_p \\ \sum_{i=1}^{3} A_i e^{-\frac{\ln(2)(t-t_p)}{\beta_i}} & if \quad t_p \le t \end{cases} \tag{29}$$

where $C_a(t)$ is the arterial plasma activity concentration, $t_s$ is the time when the bolus reaches the brain and $t_p$ is the time of the peak concentration of the bolus in the brain. After a short delay $t_s$, the increase in concentration is modelled as a linear increase until reaching the peak value, followed by behaviour which is modelled as a sum of 3 exponentials with different biological decay constants $\beta_i$ and amplitudes $A_i$.

The parameters of this model were chosen in such a way that the simulated input function (figure 3.2) resembles a true input function (figure 3.1).

When selecting the parameters $t_s$ = 0.35 min, $t_p$ = 0.7 min, A = [27.50 7.50 0.925] kBq/ml, β = [0.1 1.2 100] min, an input function is obtained which is similar to that in figure 3.1, as seen in figure 3.2. Note that the parameter A, expressed in kBq/ml was converted to nCi/cc to enable comparison of figures 3.1 and 3.2. The unit kBq/ml is otherwise used in this thesis.

The input function defined by selecting the parameters above, represents the concentration of $^{18}F$ (fraction of the intact tracer and metabolites) in plasma as a function of time.

The fraction of the intact tracer represents the unchanged or free fraction of authentic parent tracer in plasma which is not bound to plasma proteins. It is assumed to equal to 1 at the time of injection (t=0), this means there is 100% of the input concentration of the unchanged tracer with no metabolites present.

Metabolites refer to a specific series of reactions that the trace will undergo once injected in the body. The tracer will be broken down or metabolised into a different substances which leads to the logical changes to a parent compound.

Note that the input function is decay corrected to the time of injection.

### 3.2.2 Modelling the fraction of the intact tracer

The fraction of metabolites of $^{18}$F-fallypride in arterial plasma, based on experimental data is plotted as a percentage of the intact fraction in figure 3.3 (Mukherjee et al., 2002). The fraction of intact tracer starts with a value of 1 at the time of injection which means that no metabolites are present initially. It gradually decreases as metabolites accumulate.

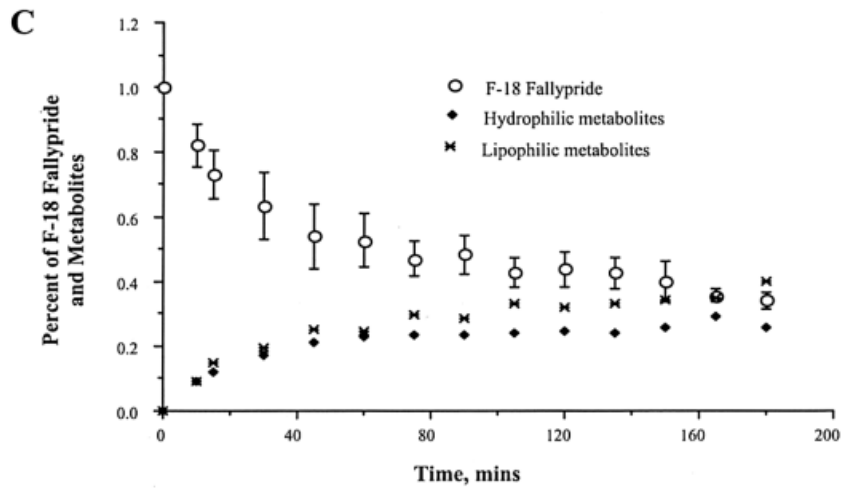


*Figure 3.3: Fraction of intact $^{18}$F-fallypride tracer in arterial plasma as function of time after injection Reprinted with permisson from Mukherjee, J., Christian, BT, Dunigan KA., Shi, B, Narayanan, TK, Satter, M, & Mantil, et al. Brain imaging of $^{18}$F-fallypride in normal volunteers: Blood analysis, distribution, test-retest studies, and preliminary assessment of sensitivity to aging effects on dopamine D-2/D-3 receptors. Synapse, 2002;46(3), 170–188. Copyright 2002, John Wiley & Sons Inc.*

The fraction of intact $^{18}$F-fallypride tracer in arterial plasma (figure 3.3) was used to create a simulated fraction of intact tracer (figure 3.4).

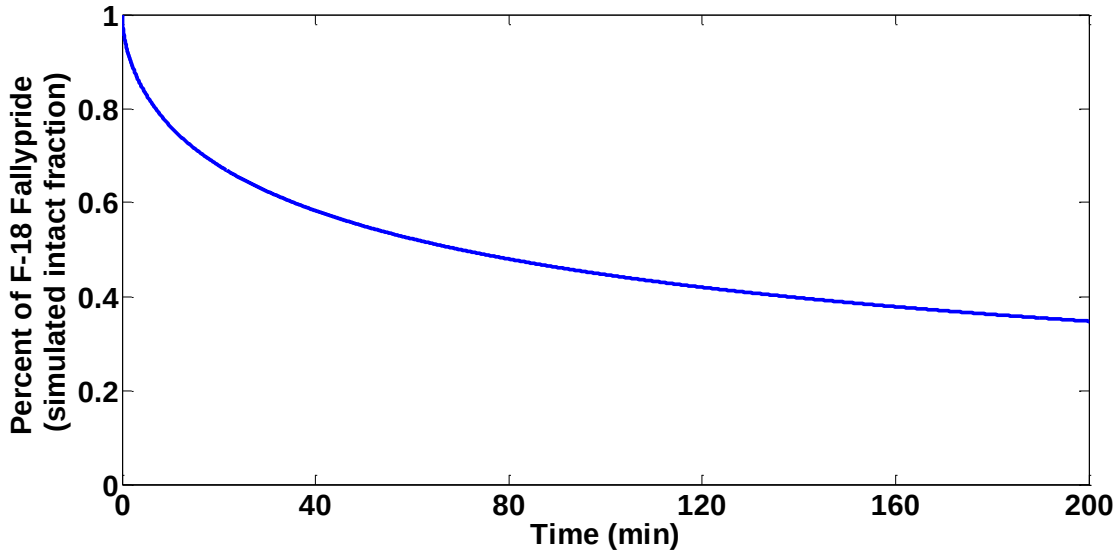


*Figure 3.4: Simulated fraction of intact $^{18}$F-fallypride tracer in arterial plasma as function of time after injection.*

To model the intact fraction of the tracer, the following function was used:

$$F(t) = \frac{b}{1+\left(\frac{a}{t}\right)^{n}} \tag{30}$$

The parameter “b” was set to b = 1, assuming that at time 0 the input concentration consists of 100% intact tracer. The parameter n determines the steepness of the slope and should be negative, and “a” is the time when the function reaches half of its maximum (b/2).

In figure 3.4, the simulated intact fraction of tracer is based on Eq. 31 using b = 1, a =70 min, n = -0.6.

Metabolites of fallypride that are created outside the brain were assumed to not cross the blood-brain-barrier, in which case the input function (Eq. 29) needs to be multiplied by the intact fraction (Eq. 30) which gives:

$$C_a(t)_{corr} = F(t) * C_a(t) \tag{31}$$

where $C_a(t)_{corr}$ is the input function corrected for the intact fraction, $F(t)$ is the intact fraction and $C_a(t)$ is the input corrected for decay to the time of injection from Eq. 29.

### 3.2.3 Simulation of the theoretical output function (TAC) in brain regions with high, moderate and low receptor density

The 2T4k model of $^{18}$F-fallypride was considered as the ground truth model (refer to figure 1.1).

Four different VOI's in the brain with different kinetic behaviour were used: putamen, thalamus, temporal cortex and cerebellum. For each VOI, ground truth values were taken from the literature (Christian et al., 2004). Values were not available for the human brain and therefore values were selected from non-human primate brain data for the simulations. Note that the data from Mukherjee et al., (2002) obtained from human data, was only used as the representative curve of arterial blood plasma input function.

A similar strategy is used in other human brain imaging studies (Vandehey et al., 2010; Morris et al., 2007).

*Table 3.1 Four rate constants for different VOIs taken from Christian et al., 2004.*

| Rate constant | Putamen | Thalamus | Temporal cortex | Cerebellum |
|---|---|---|---|---|
| $K_1$ ($min^{-1}$) | 0.17 | 0.14 | 0.24 | 0.33 |
| $k_2$ ($min^{-1}$) | 0.21 | 0.26 | 0.24 | 0.42 |
| $k_3$ ($min^{-1}$) | 0.108 | 0.187 | 0.026 | 0.0097 |
| $k_4$ ($min^{-1}$) | 0.043 | 0.056 | 0.043 | 0.043 |

Based on the parameters selected and using 2T4k model, ideal concentration-time curves were generated for the four different VOI's using a modelled input function corrected for decay and intact tracer. These are shown in figures 3.5 (A – D).

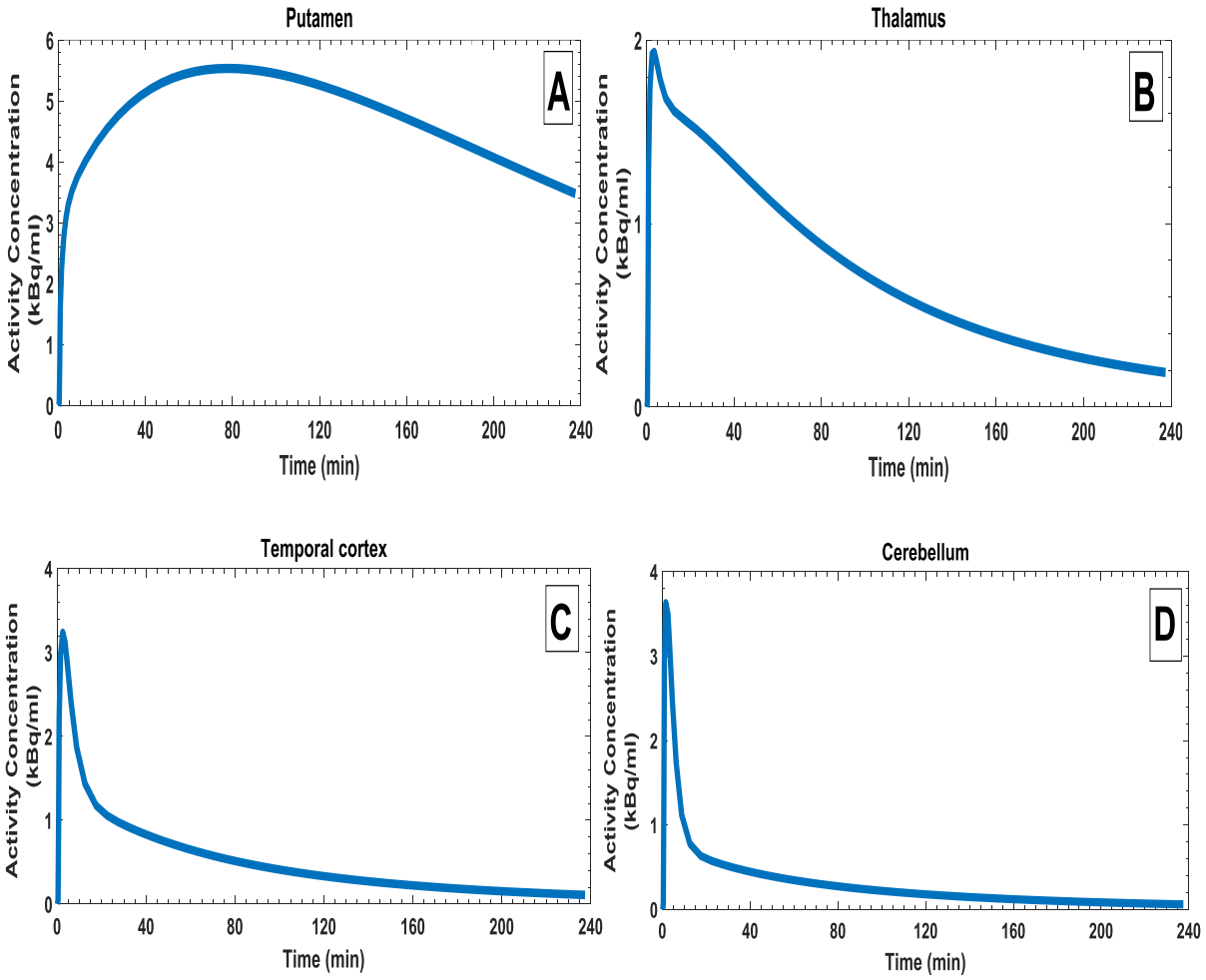


*Figure 3.5: Ideal output function for the putamen (A), thalamus (B), temporal cortex (C) and cerebellum (D)*

### 3.2.4 Simulation of the measurement noise by Gaussian model

Noise was added to the sampled PET output to obtain realistic simulations. To add noise, the physical decay of the isotope was first modelled and noise was then added to this value using a Gaussian noise model with zero mean (μ = 0) and standard deviation (σ).

$$\sigma = f\sqrt{\frac{C_{uncor}(i)}{\Delta t_i}} \quad \text{(Logan et al., 2001)} \qquad (32)$$

$C_{uncor}(i)$ is the average counts in a VOI during frame i before decay correction and $\Delta t_i$ is the duration of frame i. The parameter f controls the amount of noise. To investigate the effect of signal to noise we have used f = 0.05, 0.15 and 0.25 representing low, moderate and high noise respectively

In our study we took a more realistic approach and looked at the effect of noise based on the acquisition described by Dunn et al., (2013) which corresponds to sampling scheme (i) in this study (refer to section 3.2.5). We tested if the simplified models perform well enough and if they can be used to avoid arterial blood sampling. This depends on the amount of noise applied. We specified the noise model by varying the fraction of noise level using f = 0.05, 0.15 and 0.25.

### 3.2.5 Specifying the scan duration with continuous and interrupted sampling schemes

In reality, a fallypride scanning session can last 3 hours or more. The advantage of a simulation is that it can go up to even longer scanning times without artefacts being created by patient movement.

In this work two different sampling schemes ((i) continuous sampling scheme (ii) interrupted sampling scheme) with different total scan duration were simulated. Both sampling schemes consisted of a common part which covers the first 30 minutes, measured using the following frame definition: 4 x 15s; 4 x 60s; 2 x 150s; 4 x 300s to capture the rapid changes in concentration as a result of the bolus injection to match real-world sampling constraints. The continuous sampling scheme consisted of this common part followed by additional frames of 5 minutes until the end of the scan. The total scan duration was varied between 30 minutes and 240 minutes as follows: 30 minutes, 1 hour, 1.5 hours, 2 hours, 2.5 hours, 3 hours, 3.5 hours, and 4 hours.

An interrupted sampling scheme (containing breaks) during which the patient can be taken out of the scanner was simulated using a series of 10 different interrupted sampling schemes tabulated in (Table 3.2 and Table 3.3). These interrupted sampling schemes consisted of the common part (first 30 minutes) followed by 5 minutes frames until 240 minutes post injection but with inclusion of breaks of 60, 120 or 180 minutes or by including two breaks.

*Table 3.2 Different interrupted sampling schemes (1hour break)*

| Sampling number | Interrupted sampling scheme | Total scan time |
|---|---|---|
| 1 | 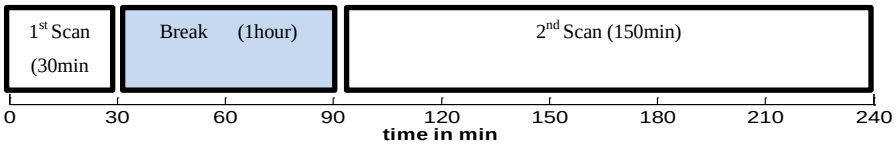 | 180 minutes |
| 2 | 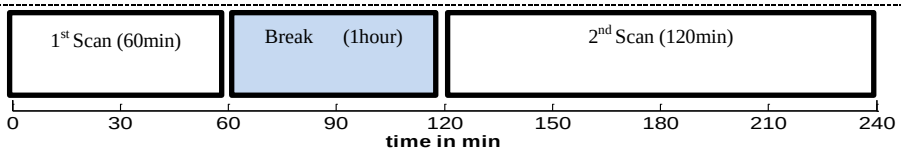 | 180 minutes |
| 3 | 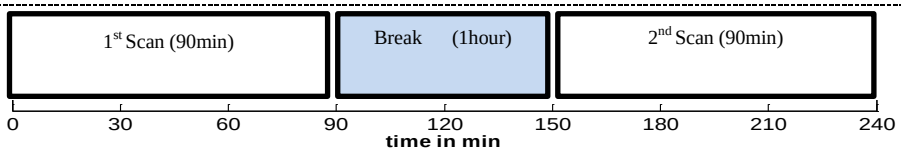 | 180 minutes |
| 4 | 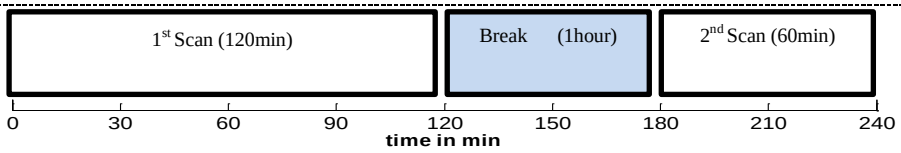 | 180 minutes |
| 5 | 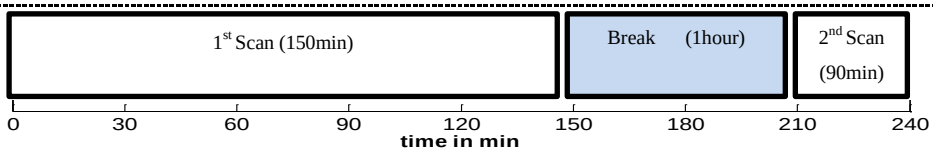 | 180 minutes |

*Table 3.3 Different interrupted sampling schemes (2 to 3 hours break)*

| Sampling number | Interrupted sampling scheme | Total scan time |
|---|---|---|
| 6 | 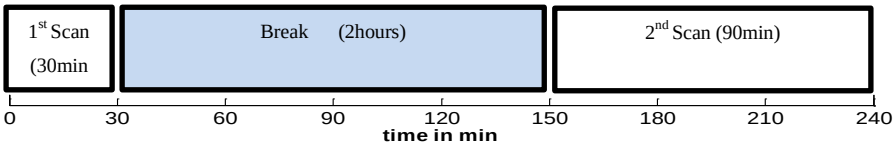 | 120 minutes |
| 7 | 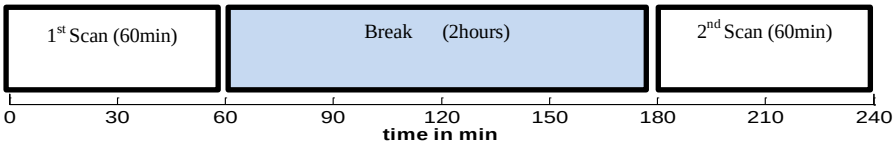 | 120 minutes |
| 8 | 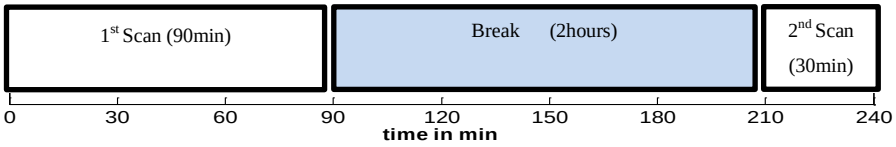 | 120 minutes |
| 9 | 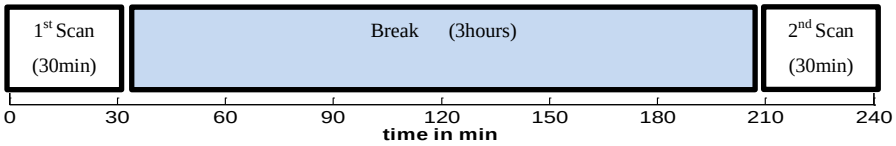 | 60 minutes |
| 10 | 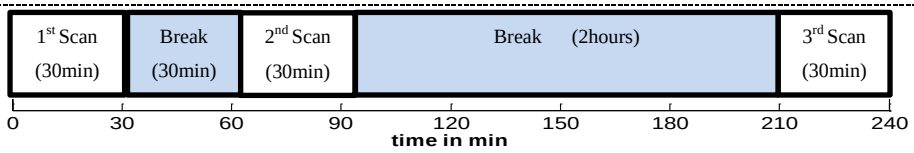 | 90 minutes |

To obtain integrals of the time activity curves, simple trapezoidal integration with a step size of 0.001 min was used.

The final sampled PET output is the theoretical output function measured at the midscan time of each frame as is usually done in dynamic PET measurements, with the addition of noise.

Modelled data including sampling and noise for the four different VOIs at three different noise levels for the full 240 minutes are shown in figures 3.6 to 3.9.

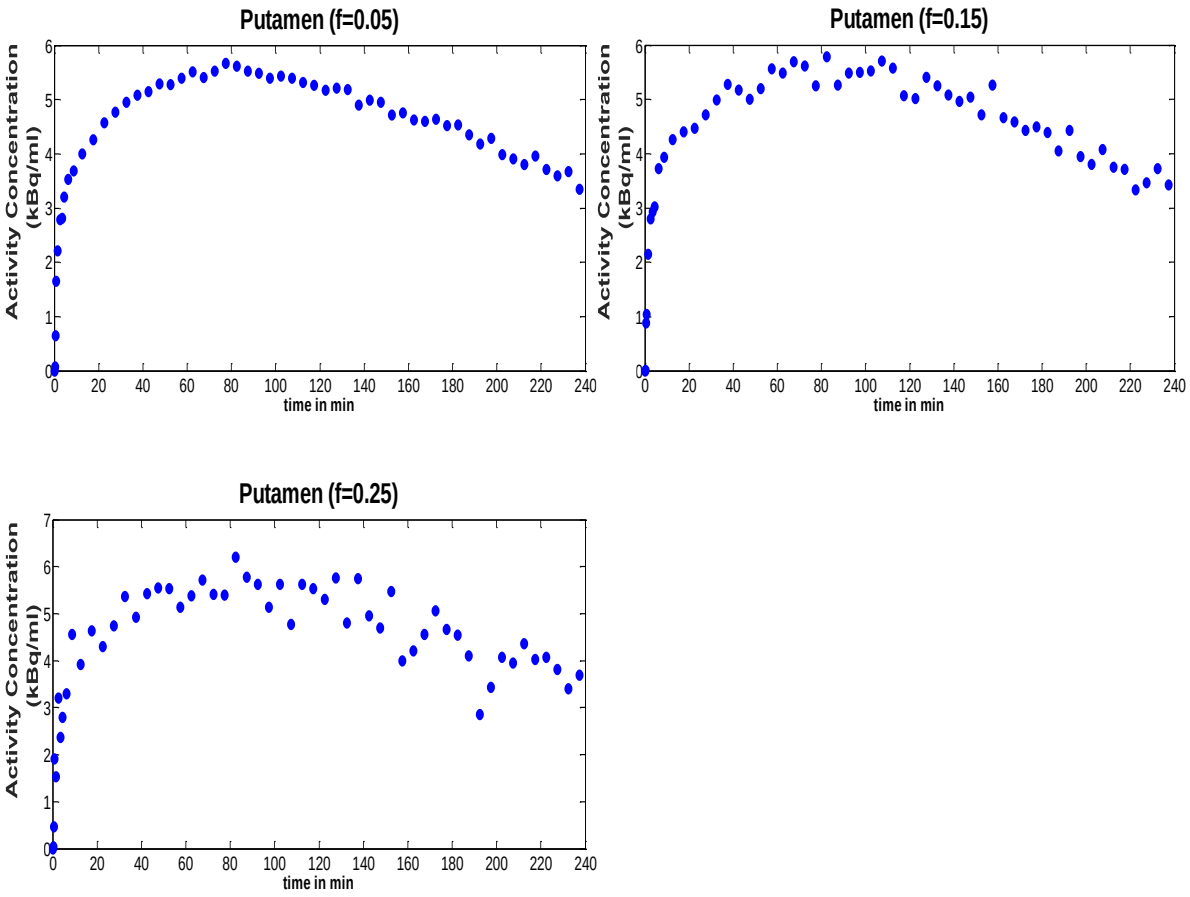


*Figure 3.6: Modelled data for the putamen at three noise levels using continuous sampling scheme with scan duration of 240 minutes.*

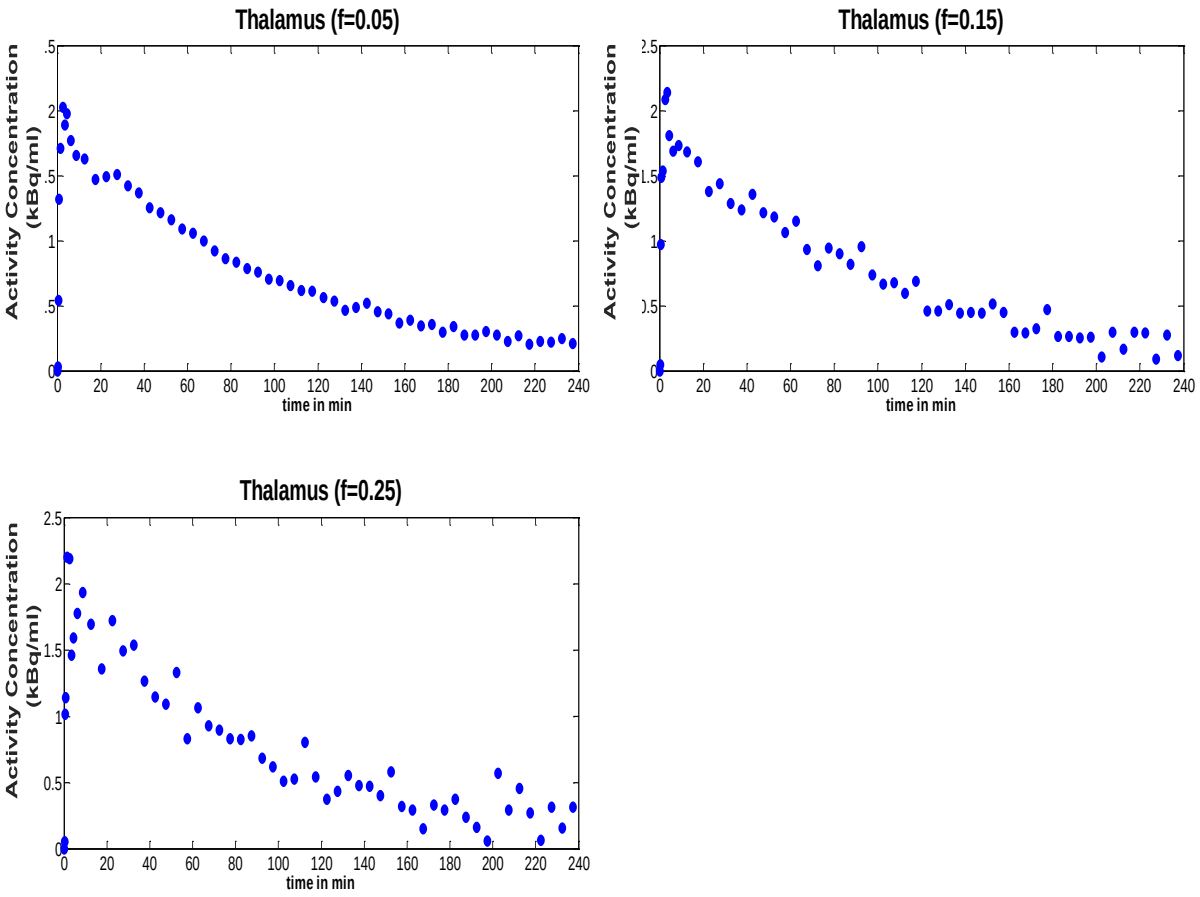


*Figure 3.7: Modelled data for the thalamus at three noise levels continuous sampling scheme with scan duration of 240 minutes.*

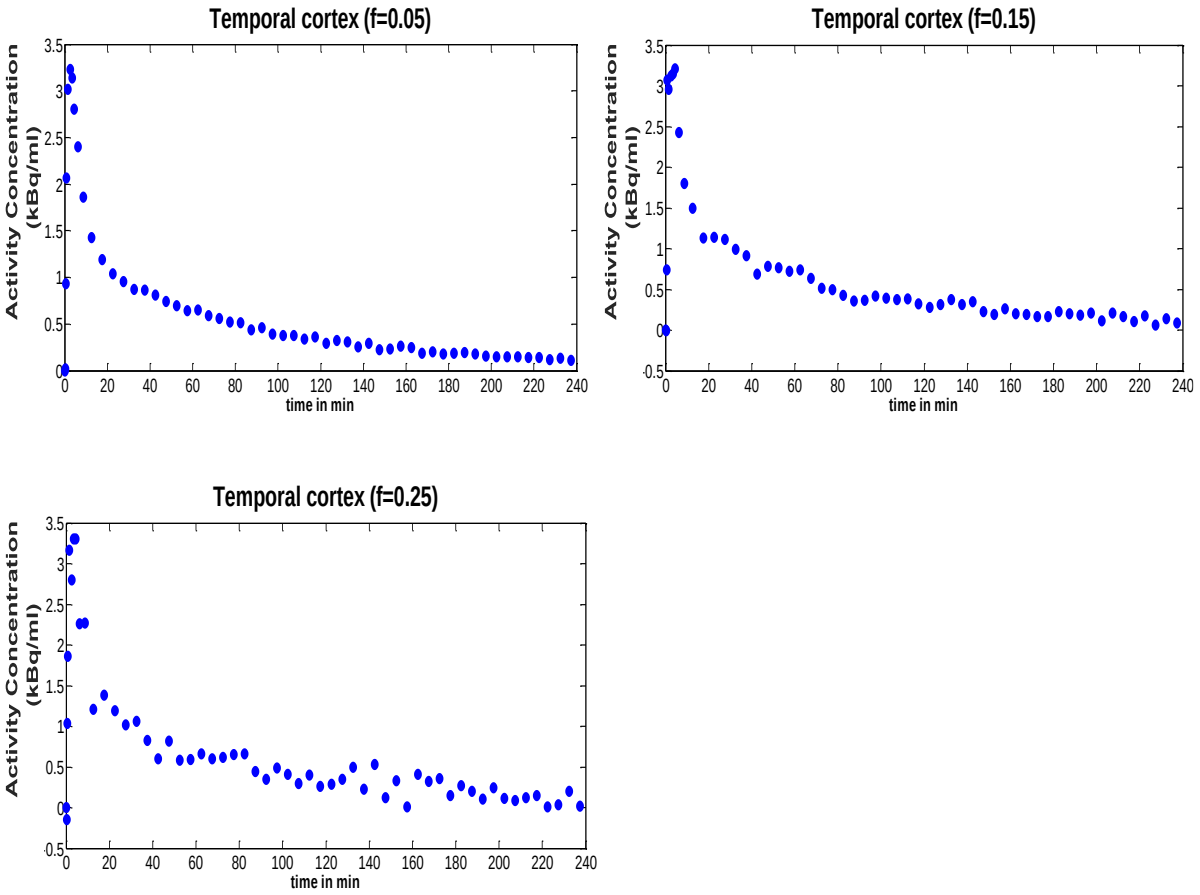


*Figure 3.8: Modelled data for the temporal at three noise levels using continuous sampling scheme with scan duration of 240 minutes.*

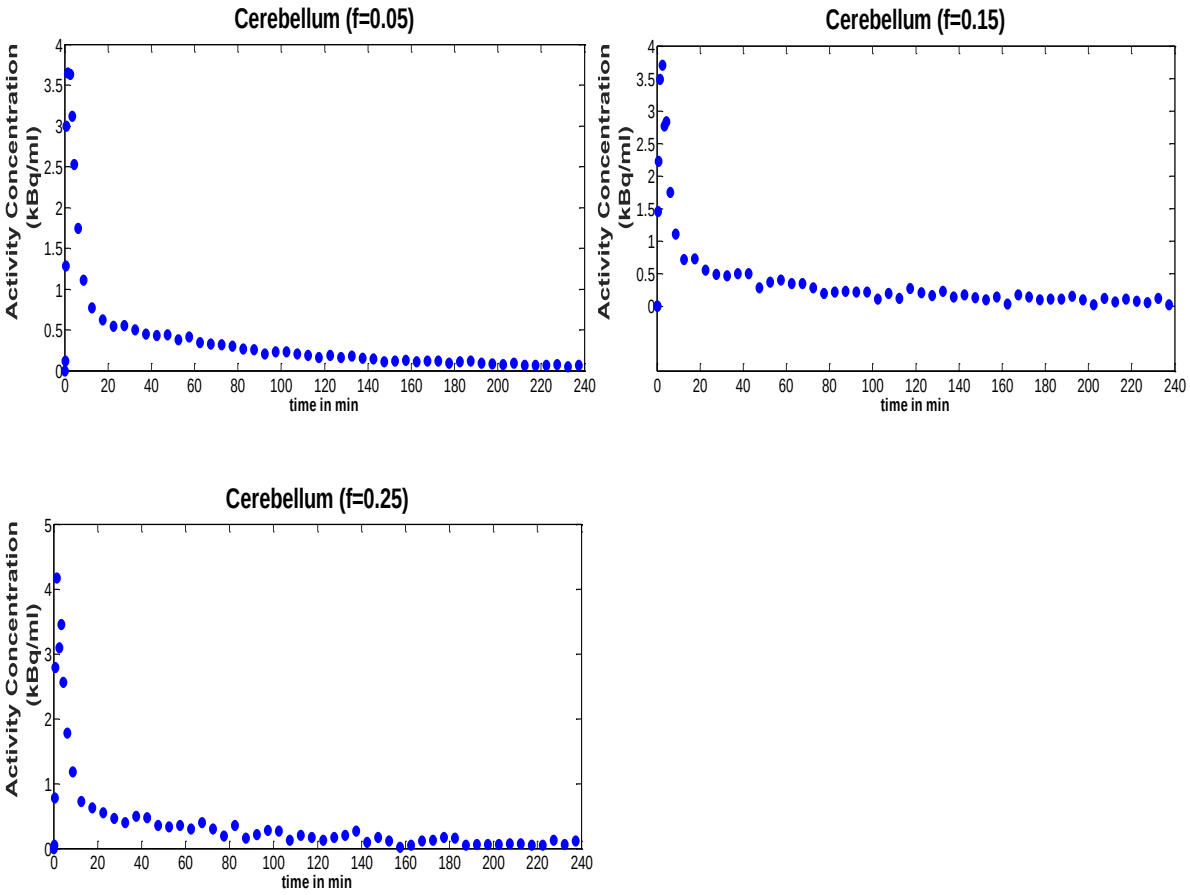


*Figure 3.9: Modelled data for the cerebellum at three noise levels using continuous sampling scheme with scan duration of 240 minutes.*

### 3.2.6 Volume of distribution

The parameters of interest include the total volume of distribution ($V_T$) and the volume of distribution ratio (DVR) taking the cerebellum as the reference. These values can be calculated from the ground-truth rate-constants. Based on these theoretical values, the following values were obtained which were used as a ground truth: $V_T$ (putamen) = 21.09; $V_T$ (thalamus) = 2.37; $V_T$ (temporal cortex) = 1.71; $V_T$ (cerebellum) = 0.97; DVR (putamen) = 21.71; DVR (thalamus) = 2.44; DVR (temporal cortex) = 1.76. In order to evaluate the different simplified models under investigation, a figure of merit was defined as the absolute error of the estimated $V_T$ or DVR with respect to the ground truth values, for the different settings under investigation.

### 3.3 The accuracy/reliability of various models in $^{18}$F-fallypride quantification

$^{18}$F-fallypride binds to DA $D_2$ and $D_3$ receptors and is distributed in the brain in striatal and extrastriatal regions. These regions in the brain can be divided into “high”, “moderate” and “low” uptake regions depending on the receptor occupancy and the binding of $^{18}$F-fallypride in the brain as depicted in table 3.3.

Putamen is classified as the “high” uptake region because of its high receptor occupancy, thus making $^{18}$F-fallypride easy to bind to DA $D_2/D_3$ receptors.

Thalamus and temporal cortex can be classified as “moderate” and “low” uptake regions respectively, depending on the amount of DA $D_2/D_3$ receptors.

The knowledge of the rate constants helps in optimizing the protocols for measuring small changes in DA D2/D3 receptor occupancy, Christian et al (2004)

The process of measurements can alter the results. How far apart can measurements be without causing difficulties, is a question of judgment.

To study the accuracy/reliability of various models, a range of possibilities was explored by varying the set rate constant values for putamen, temporal cortex and thalamus around those proposed by Christian et al (2004).

This method introduces the probability of how far apart can rate constants be without deviating completely form the original values. It takes into account the small uncertainties in variation of rate constants.

The fourth main VOI (cerebellum) served as the reference region (Slifstein et al., 2004, Constantinescu et al., 2011, Christian et al., 2006, Ishibashi et al., 2013, Werhahn et al,. 2006).

Simulations were performed up to 4 hours scan duration and the noise level for the reference region was set to f = 0.05.

*Table 3.4 Different rate constants corresponding to VOIs with "high", "moderate" or "low" uptake regions*

| High uptake region (putamen) | | | | | | | | | |
|---|---|---|---|---|---|---|---|---|---|
| **Rate constant set** | **$K_1$ ($min^{-1}$)** | **$k_2$ ($min^{-1}$)** | **$k_3$ ($min^{-1}$)** | **$k_4$ ($min^{-1}$)** | **Rate constant set** | **$K_1$ ($min^{-1}$)** | **$k_2$ ($min^{-1}$)** | **$k_3$ ($min^{-1}$)** | **$k_4$ ($min^{-1}$)** |
| **1** | 0.15 | 0.21 | 1.08 | 0.043 | **11** | 0.17 | 0.21 | 1.00 | 0.043 |
| **2** | 0.16 | 0.21 | 1.08 | 0.043 | **12** | 0.17 | 0.21 | 1.04 | 0.043 |
| **3** | 0.17 | 0.21 | 1.08 | 0.043 | **13** | 0.17 | 0.21 | 1.08 | 0.043 |
| **4** | 0.18 | 0.21 | 1.08 | 0.043 | **14** | 0.17 | 0.21 | 1.12 | 0.043 |
| **5** | 0.19 | 0.21 | 1.08 | 0.043 | **15** | 0.17 | 0.21 | 1.16 | 0.043 |
| **6** | 0.17 | 0.19 | 1.08 | 0.043 | **16** | 0.17 | 0.21 | 1.08 | 0.037 |
| **7** | 0.17 | 0.20 | 1.08 | 0.043 | **17** | 0.17 | 0.21 | 1.08 | 0.040 |
| **8** | 0.17 | 0.21 | 1.08 | 0.043 | **18** | 0.17 | 0.21 | 1.08 | 0.043 |
| **9** | 0.17 | 0.22 | 1.08 | 0.043 | **19** | 0.17 | 0.21 | 1.08 | 0.046 |
| **10** | 0.17 | 0.23 | 1.08 | 0.043 | **20** | 0.17 | 0.21 | 1.08 | 0.049 |
| Moderate/low uptake region (thalamus and temporal cortex) | | | | | | | | | |
| **Rate constant set** | **$K_1$ ($min^{-1}$)** | **$k_2$ ($min^{-1}$)** | **$k_3$ ($min^{-1}$)** | **$k_4$ ($min^{-1}$)** | **Rate constant set** | **$K_1$ ($min^{-1}$)** | **$k_2$ ($min^{-1}$)** | **$k_3$ ($min^{-1}$)** | **$k_4$ ($min^{-1}$)** |
| **1** | 0.12 | 0.26 | 0.187 | 0.056 | **21** | 0.22 | 0.24 | 0.026 | 0.043 |
| **2** | 0.13 | 0.26 | 0.187 | 0.056 | **22** | 0.23 | 0.24 | 0.026 | 0.043 |
| **3** | 0.14 | 0.26 | 0.187 | 0.056 | **23** | 0.24 | 0.24 | 0.026 | 0.043 |
| **4** | 0.15 | 0.26 | 0.187 | 0.056 | **24** | 0.25 | 0.24 | 0.026 | 0.043 |
| **5** | 0.16 | 0.26 | 0.187 | 0.056 | **25** | 0.26 | 0.24 | 0.026 | 0.043 |
| **6** | 0.14 | 0.24 | 0.187 | 0.056 | **26** | 0.24 | 0.22 | 0.026 | 0.043 |
| **7** | 0.14 | 0.25 | 0.187 | 0.056 | **27** | 0.24 | 0.23 | 0.026 | 0.043 |
| **8** | 0.14 | 0.26 | 0.187 | 0.056 | **28** | 0.24 | 0.24 | 0.026 | 0.043 |
| **9** | 0.14 | 0.27 | 0.187 | 0.056 | **29** | 0.24 | 0.25 | 0.026 | 0.043 |
| **10** | 0.14 | 0.28 | 0.187 | 0.056 | **30** | 0.24 | 0.26 | 0.026 | 0.043 |
| **11** | 0.14 | 0.26 | 0.147 | 0.056 | **31** | 0.24 | 0.24 | 0.018 | 0.043 |
| **12** | 0.14 | 0.26 | 0.167 | 0.056 | **32** | 0.24 | 0.24 | 0.022 | 0.043 |
| **13** | 0.14 | 0.26 | 0.187 | 0.056 | **33** | 0.24 | 0.24 | 0.026 | 0.043 |
| **14** | 0.14 | 0.26 | 0.207 | 0.056 | **34** | 0.24 | 0.24 | 0.030 | 0.043 |
| **15** | 0.14 | 0.26 | 0.227 | 0.056 | **35** | 0.24 | 0.24 | 0.034 | 0.043 |
| **16** | 0.14 | 0.26 | 0.187 | 0.050 | **36** | 0.24 | 0.24 | 0.026 | 0.037 |
| **17** | 0.14 | 0.26 | 0.187 | 0.053 | **37** | 0.24 | 0.24 | 0.026 | 0.040 |
| **18** | 0.14 | 0.26 | 0.187 | 0.056 | **38** | 0.24 | 0.24 | 0.026 | 0.043 |
| **19** | 0.14 | 0.26 | 0.187 | 0.059 | **39** | 0.24 | 0.24 | 0.026 | 0.046 |
| **20** | 0.14 | 0.26 | 0.187 | 0.062 | **40** | 0.24 | 0.24 | 0.026 | 0.049 |

*Note: Compartmental model rate constant denotes the fraction of the total tracer that will leave the compartment per unit time (fractional clearance). It has the unit of inverse time i.e., the proportion of tracer molecules in a given compartment that will "move" to another compartment in one minute.*

For each VOI corresponding to a set of rate constants, TAC's were generated and the theoretical distribution volumes (DV) and theoretical distribution volume ratios (DVR) were calculated similar as described for the main VOIs in this study. Noise was added as described before. The results of each model and the ground truth

values were compared using 1) a correlation analysis and 2) a Bland-Altman analysis.

## 3.4 Methods of data analysis

### 3.4.1 Regression and Correlation analysis

Regression analysis is the first step to figure out if there is a relationship between two variables.

To determine the accuracy/reliability of various models in $^{18}$F-fallypride quantification, linear regression was then used to find a relationship of different models against the ground-truth values of DV and DVR. The analysis using different models is shown in Appendix.

The correlation coefficient (r) was used as an indicator to obtain agreement between the results of the two variables. Since high correlation does not mean that the two methods agree, Bland-Altman analysis was introduced as an addition to interpret the results.

### 3.4.2 Bland-Altman analysis

The first step of Bland-Altman is to find the significant difference between two measurements i.e. to look if there is a variation from zero of the difference between two measurements. If the measurements differ from zero, the two measurements do not agree.

Bias is calculated as the mean of the difference between the true values and the values measured by the model for DV or DVR i.e. bias = mean (diff). The bias as proposed by (Bland and Altman 1986) helps in finding the degree of agreement between measurements.

The difference is calculated as, diff = X-Y and the average value = (X+Y)/2.

To determine the upper confidence limit, the standard deviation of the difference is multiplied by 1.96 and added to the mean difference. Therefore, the upper limit = [(σ x 1.96) +mean].

To determine the lower confidence limit, the standard deviation of the difference is multiplied by 1.96 and subtracted from the mean difference. Therefore, the lower limit = [mean - (σ x 1.96)].

The constant bias is observed when there is an equal number of data points above and below the mean difference line (bias) on Bland-Altman plot.

The proportional bias is observed if there are a huge number of points above the mean difference line (bias) on Bland-Altman.

### 3.4.3 Relative error

If the true value of the measured quantity is $x$ and the measured value is $x_0$, then the relative error (%) is defined as

$$Relative\ error(\%) = 100 * \left[\frac{x_0 - x}{x}\right] = 100 * \left[\frac{x_0}{x} - 1\right] \quad (33)$$

Where, $x_0$ is represented by $DV_{method}$ or $DVR_{method}$ and $x$ is represented $DV_{True}$ or $DVR_{True}$

## 3.5 Criteria for best method selection

Three conditional criteria or benchmarks were used to determine if the method is appropriate to use.

This is conducted with reference to the question of whether to accept or reject the method. To investigate these possibilities, the following criteria were used as a condition in selection of the best method:

a). The relative bias must be within the predetermined threshold range of ±10%.

b). The relative error must be within the predetermined threshold range of ±10%.

c). Both 5$^{th}$ and 95$^{th}$ percentiles or variability must be within ±10% limits at any given point.

Those methods that perform well according to the above chosen criteria were considered as the methods of choice. These criteria were applied to the remainder of all the research questions or the specific objectives of this study.

# CHAPTER 4: Results

## 4.1 The accuracy/reliability of various methods in $^{18}$F-fallypride quantification

Kinetic data generated with a noise fraction levels of 0.05, 0.15 and 0.25 were processed and analysed. The medium noise data (noise level fraction of 0.15) is presented in this section as data that lies between the low and high noise data.

In this case, the data is presented in terms of correlation and Bland-Altman analysis (refer to the end of chapter 3 for description and appendix for Matlab scripts).

Note that in all the cases, the units for DV and DVR are unit less.

### 4.1.1 Brain region with high receptor density (putamen)

The regression and Bland-Altman plots for the distribution volume (DV) for models which require blood sampling for 2T4k and Logan method are shown in figure 4.1.

In the regression analysis plots, it was observed that most of the points fall on or close to the dotted line (line of identity) in figure 4.1. The true values of DV are therefore well estimated by applying these methods.

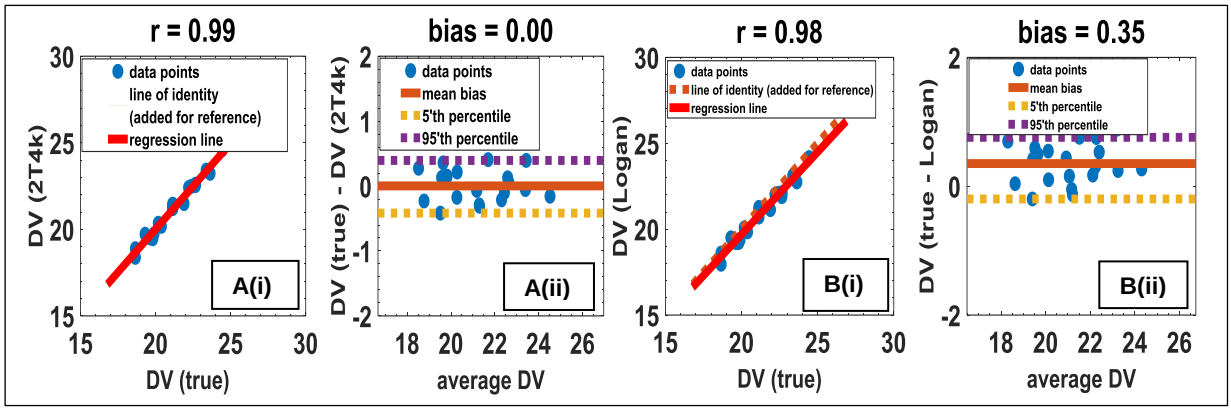


*Figure 4.1: Regression and Bland-Altman plots for the distribution volume (DV) in high uptake regions obtained by the 2T4k model (A(i) and A(ii)) and the Logan model (B(i) and B(ii)) compared to the ground-truth values.*

Both 2T4k and Logan have a constant bias. For a constant bias, the error made on Bland-Altman plot is independent on the value itself.

The relative bias can also be calculated by dividing the bias by the average value of DV.

Compared to the actual values of DV, the bias is small with relative average biases of 0.0% and 1.7% for 2T4k and Logan respectively. Variation is also small with $5^{th}$ to $95^{th}$ percentile ranges of -2.0% to 1.9% for 2T4k, and -0.9% to 3.6% for Logan.

The distribution volume ratio (DVR) is the ratio of the volume of distribution in the region of interest and the reference region. The plots of DVR calculated using invasive arterial blood sampling models ((2T4k, Logan) and non-invasive reference region models (RTM, SRTM, $Logan_{ref}$) are shown in figure 4.2. We also show SUVR calculated in the interval 215 min – 240 min for completeness (Figure 4.2 F (i) and F (ii)).

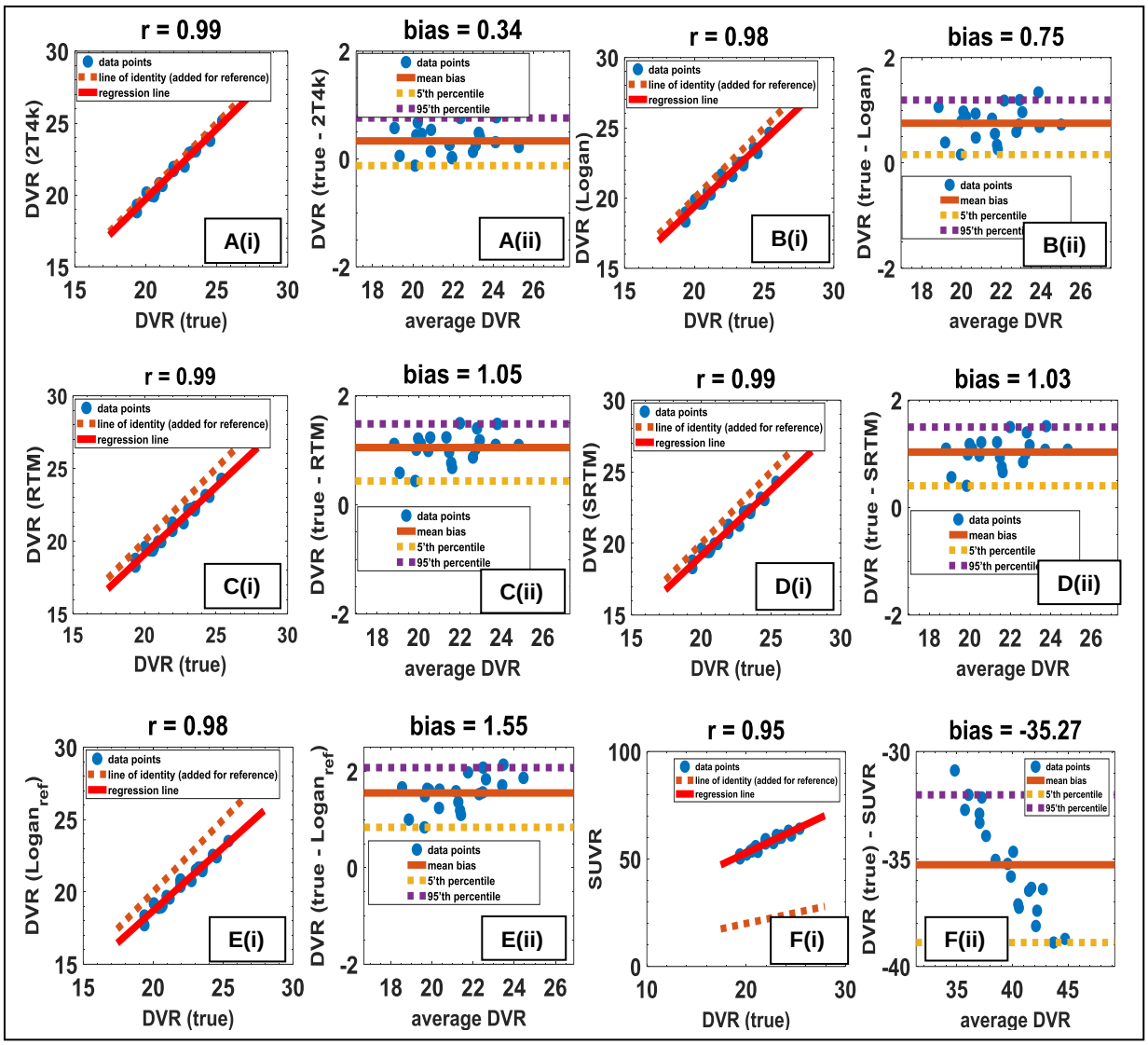


*Figure 4.2: Regression and Bland-Altman plots for the distribution volume ratio (DVR) obtained in high uptake regions by the 2T4k model (A(i) and A(ii)), Logan model (B(i) and B(ii)), RTM (C(i) and C(ii)), SRTM (D(i) and D(ii)), Logan$_{ref}$ (E(i) and E(ii)) and SUVR (F(i) and F(ii)) compared to the ground-truth values.*

In figure 4.2, most of the points fall on or close to the dotted line (line of identity) for different models in regression analysis plots. This implies the true values of DVR are well estimated by applying all the models with an exception to SUVR. SUVR values are much higher than the true values of DVR.

Correlation analysis showed that the DVR values estimated by different models in high uptake regions were positively correlated with the true DVR values. A good correlation was observed with correlation coefficients (r) ≥ 0.98 in all regression analysis plots except for SUVR (r = 0.95).

*Table 4.1: Comparison of arterial blood sampling models (2T4k and Logan) and reference models (Logan$_{ref}$, RTM, SRTM, SUVR) for the description of $^{18}$F-fallypride in high uptake region (putamen)*

| **Arterial blood sampling models (invasive)** | **r** | **bias** | **5-percentile** | **95-percentile** | **average value (unit less)** |
|---|---|---|---|---|---|
| **2T4k DV** | 0.99 | 0.00 | -0.42 | 0.40 | 21.22 |
| **Logan DV** | 0.98 | 0.35 | -0.20 | 0.76 | 21.04 |
| **2T4k DVR** | 0.99 | 0.34 | -0.12 | 0.76 | 21.86 |
| **Logan DVR** | 0.98 | 0.75 | 0.60 | 1.19 | 21.66 |
| **Reference region models (non-invasive)** | **r** | **bias** | **5-percentile** | **95-percentile** | **average value (unit less)** |
| **Logan REF DVR** | 0.98 | 1.55 | 0.84 | 2.08 | 21.26 |
| **RTM DVR** | 0.99 | 1.05 | 0.44 | 1.48 | 21.51 |
| **SRTM DVR** | 0.99 | 1.03 | 0.41 | 1.50 | 21.52 |
| **SUVR** | 0.95 | -35.2 | -38.90 | -32.02 | 39.67 |

*r = correlation coefficient; bias = mean difference; variability represented by (5-precentile = [mean - (σ x 1.96)]; 95-precentile = [(σ x 1.96) +mean]); average value = the average of all the data point in x-axis from Band-Altman plot.*

All methods give a good correlation with correlation coefficients (r) ≥ 0.98 with an exception to SUVR where (r) = 0.95. The reason to include Bland-Altman plots was to see if the bias and variability are constant over the range of values that were used in the plots.

Invasive arterial blood sampling methods (2T4k DVR and Logan DVR) gave biases > 1.0, which were lower than the non-invasive reference region methods where the biases < 1.0. The SUVR was observed to give the bias of -35.2, which is higher than any other method stated in table 4.1.

*Table 4.2: Relative bias (%) and variation (5-percentile and 95-percentile) (%) calculated by arterial blood sampling models (2T4k, Logan) and reference models ($Logan_{ref}$, RTM, SRTM, SUVR) for $^{18}$F-fallypride in high uptake region (putamen)*

| Arterial blood sampling models (invasive) | Relative bias | 5-percentile | 95-percentile |
|---|---|---|---|
| **2T4k DV** | 0.0% | -2.0% | 1.9% |
| **Logan DV** | 1.7% | -0.9% | 3.6% |
| **2T4k DVR** | 1.6% | -0.6% | 3.5% |
| **Logan DVR** | 3.5% | 2.8% | 5.5% |
| **Reference region models (non-invasive)** | **Relative bias** | **5-percentile** | **95-percentile** |
| **Logan REF DVR** | 7.3% | 4.0% | 9.8% |
| **RTM DVR** | 4.9% | 2.0% | 6.9% |
| **SRTM DVR** | 4.8% | 1.9% | 7.0% |
| **SUVR** | -88.8% | -98.1% | -80.7% |

*Relative bias (%) = [(bias/average value) x 100%]; variability represented by (5-precentile (%) = [5-precentile/average value x100%; 95-precentile (%) = [95-precentile/average value x100%)*

Compared to the actual values of DVR, the relative bias and variation of 5$^{th}$ to 95$^{th}$ percentile ranges vary form one method to the other, with SUVR being the highest in (table 4.2). It was observed that the invasive arterial blood sampling methods gave relative biases lower than those observed using non-invasive reference region methods. The lowest relative bias was observed with 2T4k method. This was however not surprising because 2T4k method was regarded as the ground truth method.

The criteria or benchmarks used to determine if the non-invasive reference region methods can be use as the replacement of the invasive arterial blood sampling methods were met. In non-invasive reference region methods, SRTM DVR was found to have the lowest relative bias of 4.8%.

### 4.1.2 Brain regions with moderate (thalamus) and low (temporal cortex) receptor density

The regression and Bland-Altman plots for the distribution volume (DV) for models which require blood sampling for 2T4k and Logan method are shown in figure 4.3.

In the regression analysis plots (refer to figure 4.3), it was observed that most of the points fall on or close to the dotted line (line of identity). The true values of DV are therefore well estimated by applying these methods in low/moderate uptake regions.

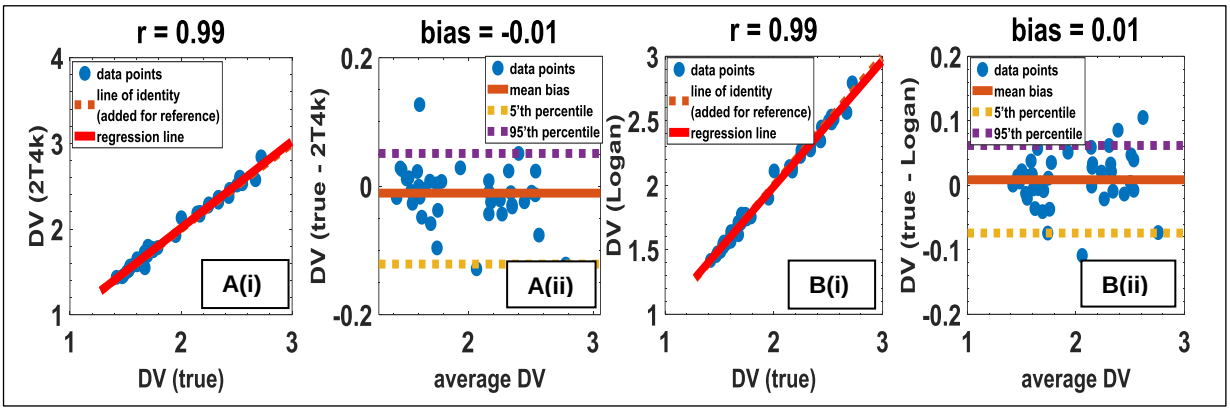


*Figure 4.3: Regression and Bland-Altman plots for the distribution volume (DV) obtained in low/moderate uptake regions by the 2T4k model (A(i) and A(ii)) and the Logan model (B(i) and B(ii)) compared to the ground-truth values.*

Both invasive arterial blood sampling methods (2T4k DV and Logan DV) have a constant bias with a good correlation (r = 0.99) when comparing their DV values with the true DV values.

The constant bias is observed in both methods with the bias of 0.01 and -0.01 for 2T4k and Logan respectively in figure 4.3 (A(ii) and B(ii)) on Bland-Altman plots.

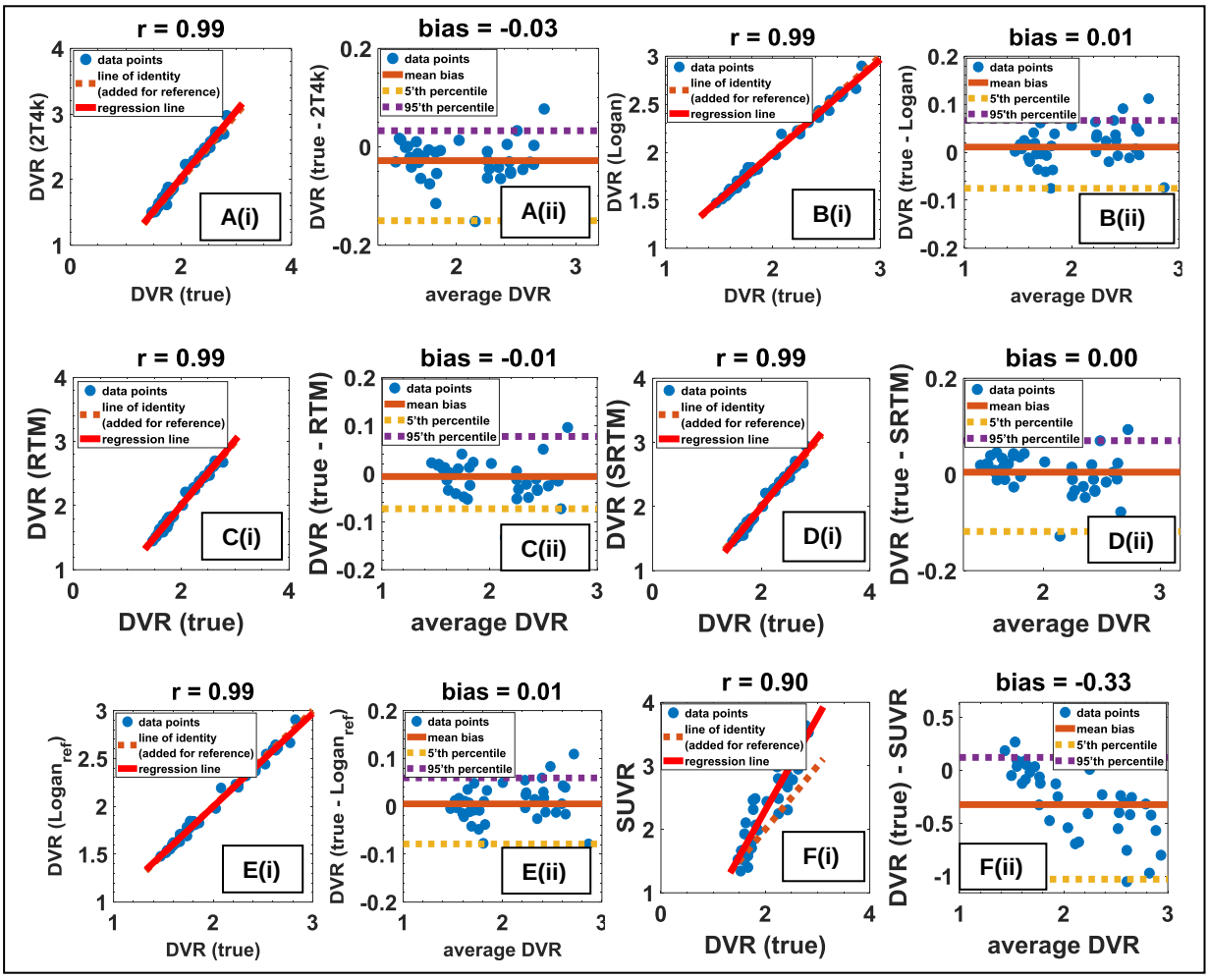


*Figure 4.4: Regression and Bland-Altman plots for the distribution volume ratio (DVR) obtained in low/moderate uptake regions by the 2T4k model (A), Logan model (B), RTM (C), SRTM (D), Logan$_{ref}$ (E) and SUVR (F) compared to the ground-truth values.*

Figure 4.4 shows the distribution volume ratio (DVR) obtained in low/moderate uptake regions. The results of the plots show the regression and Bland-Altman plots for invasive arterial blood sampling models and non-invasive reference region models.

A good correlation coefficient (r) = 0.99 was observed for all invasive and non-invasive methods in the regression plots. This good correlation showed that the DVR values estimated by different models were positively correlated with the true DVR values.

SUVR however, showed a correlation coefficient (r) = 0.90 in figure 4.4 F(i), with further analysis on Bland-Altman plot (figure 4.4 F(ii)) with bias of -0.33. The summary of the results is presented in table 4.3

*Table 4.3: Comparison of arterial blood sampling models (2T4k and Logan) and reference models ($Logan_{ref}$, RTM, SRTM, SUVR) for the description of $^{18}$F-fallypride in low/moderate uptake region (temporal cortex and thalamus)*

| **Arterial blood sampling models (invasive)** | **r** | **bias** | **5-percentile** | **95-percentile** | **average value (unit less)** |
|---|---|---|---|---|---|
| **2T4k DV** | 0.99 | -0.01 | -0.12 | 0.05 | 1.98 |
| **Logan DV** | 0.99 | 0.01 | -0.07 | 0.06 | 1.97 |
| **2T4k DVR** | 0.99 | -0.03 | -0.15 | 0.03 | 2.06 |
| **Logan DVR** | 0.99 | 0.01 | -0.08 | 0.07 | 2.06 |
| **Reference region models (non-invasive)** | **r** | **bias** | **5-percentile** | **95-percentile** | **average value (unit less)** |
| **Logan REF DVR** | 0.99 | 0.01 | -0.08 | 0.06 | 2.05 |
| **RTM DVR** | 0.99 | -0.01 | -0.07 | 0.08 | 2.01 |
| **SRTM DVR** | 0.99 | 0.00 | -0.12 | 0.07 | 2.05 |
| **SUVR** | 0.90 | -0.33 | -1.03 | 0.12 | 2.21 |

*r = correlation coefficient; bias = mean difference; variability represented by (5-precentile = [mean - (σ x 1.96)]; 95-precentile = [(σ x 1.96) +mean]); average value = the average of all the data point in x-axis from Band-Altman plot.*

In table 4.4, the relative bias and variation of 5$^{th}$ to 95$^{th}$ percentile ranges in low/moderate uptake regions are shown.

*Table 4.4: Relative bias (%) and variation (5-percentile and 95-percentile) (%) calculated by arterial blood sampling models (2T4k, Logan) and reference models ($Logan_{ref}$, RTM, SRTM, SUVR) for $^{18}$F-fallypride in low/moderate uptake region (temporal cortex and thalamus)*

| **Arterial blood sampling models (invasive)** | **Relative bias** | **5-percentile** | **95-percentile** |
|---|---|---|---|
| **2T4k DV** | -0.7 | -6.1 | 2.5 |
| **Logan DV** | 0.5 | -3.6 | 3.0 |
| **2T4k DVR** | -1.5 | -7.3 | 1.5 |
| **Logan DVR** | 0.5 | -3.9 | 3.4 |
| **Reference region Models (non-invasive)** | **Relative bias** | **5-percentile** | **95-percentile** |
| **Logan REF DVR** | 0.2 | -3.9 | 2.9 |
| **RTM DVR** | -0.3 | -3.6 | 3.8 |
| **SRTM DVR** | 0.2 | -5.9 | 3.4 |
| **SUVR** | -14.9 | -46.6 | 5.6 |

*Relative bias (%) = [(bias/average value) x 100%]; variability represented by (5-precentile (%) = [5-precentile/average value x100%; 95-precentile (%) = [95-precentile/average value x100%)*

Compared to the actual values of DV, the bias is small with relative average biases of -0.7% and 0.5% for 2T4k and Logan respectively. Variation is also small with 5$^{th}$ to 95$^{th}$ percentile ranges of -6.1% to 2.5% for 2T4k, and -3.6% to 3.0% for Logan in low/moderate uptake areas.

The criteria used to determine if the non-invasive reference region methods can be use as the replacement of the invasive arterial blood sampling methods were met. For non-invasive reference region methods, Logan$_{ref}$ DVR and SRTM DVR were both found to have the lowest relative bias of 0.2% followed by RTM DVR with the relative error of -0.3%. SUVR holds the highest relative error of -14.9%.

SUVR calculations are probably not among the best methods for quantification $^{18}$F-fallypride as they produce relatively large errors. For this specific reason, SUVR was completely excluded in this study for investigating models performance under varying conditions such as total scan duration, noise-level and breaks in sampling scheme for all brain regions.

## 4.2 The effect of noise-level variation/signal to noise ratio (SNR) in brain regions with high, moderate, and low receptor density

### 4.2.1 Brain region with high receptor density (putamen)

The relative error (in %) for DV and DVR is plotted against noise levels (f = 0.05, 0.1, 0.15, 0.20, 0.25 and 0.30) for different VOIs (putamen, temporal cortex and thalamus) using different models. The ground truth values were used as a reference.

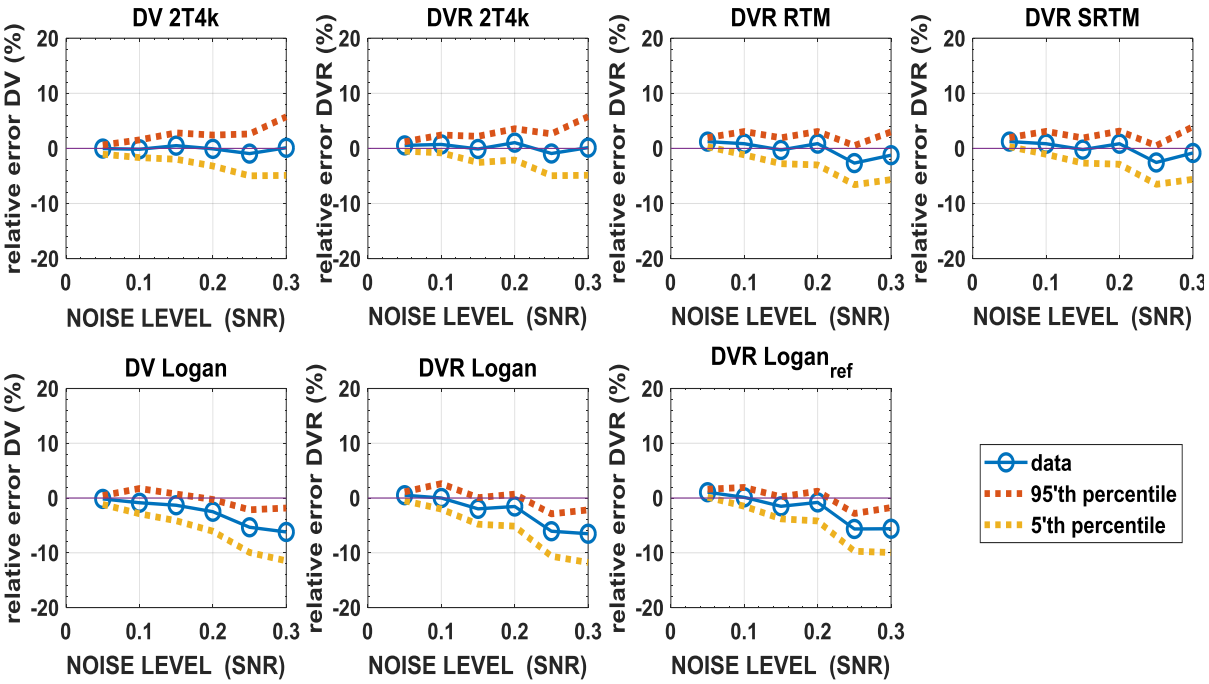


*Figure 4.5: The plots of the relative error (%) against the noise level (SNR) for the distribution volume (DV) and the distribution volume ratio (DVR) in the brain region with high receptor density (putamen). The plots show invasive arterial blood sampling methods (2T4k and Logan) and reference region methods (RTM, SRTM and Logan$_{ref}$).*

From figure 4.5 the variability (5$^{th}$ and 95$^{th}$ percentiles) of all 5 methods increases with increasing noise as expected. The change in the relative error of 2T4k, RTM and SRTM keep the similar trend with the increasing noise with almost constant change in relative error as the noise level increases.

The change in the relative error for Logan and Loganr$_{ef}$ also keep the similar the similar trend with the increasing noise, but the values turn towards negative values with increasing noise levels.

### 4.2.2 Brain region with moderate (thalamus) and low (temporal cortex) receptor density

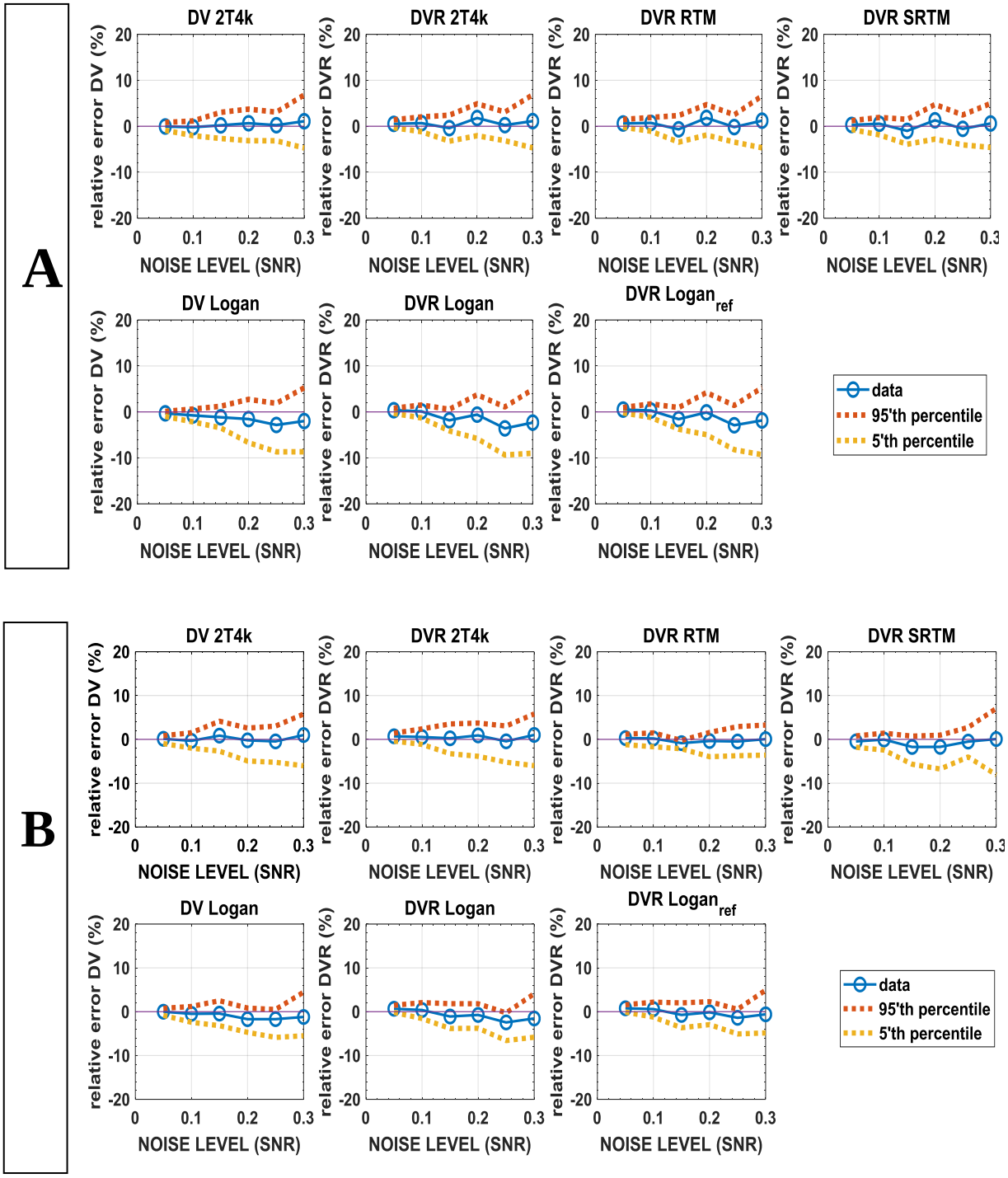


*Figure 4.6: The plots of the relative error (%) against the noise level (SNR) for the distribution volume (DV) and the distribution volume ratio (DVR) in the brain region with moderate and low receptor density (thalamus (A) and temporal cortex (B)). The plots show invasive arterial blood sampling methods (2T4k and Logan) and reference region methods (RTM, SRTM and Logan$_{ref}$).*

In figure 4.6 all the methods used in the brain regions with moderate (thalamus) and low (temporal cortex) receptor density perform similarly, with very little change in the relative error as the noise level increases.

The variability (5$^{th}$ and 95$^{th}$ percentiles) of all 5 methods increases with increasing noise as expected.

In all cases, the relative error and variability were found to be within the range of ±10% at any given data point. This passes the set criteria which conclude that the non-invasive reference region methods can be use as the replacement of the invasive arterial blood sampling.

## 4.3 The effect of total scan duration (continuous sampling scheme) in brain regions with high, moderate, and low receptor density

### 4.3.1 Brain region with high receptor density (putamen)

Figure 4.7 below shows the simulated graphs of the relative error plotted against scan duration (continuous sampling scheme) in the brain region with high receptor density (putamen) using invasive and non-invasive methods.

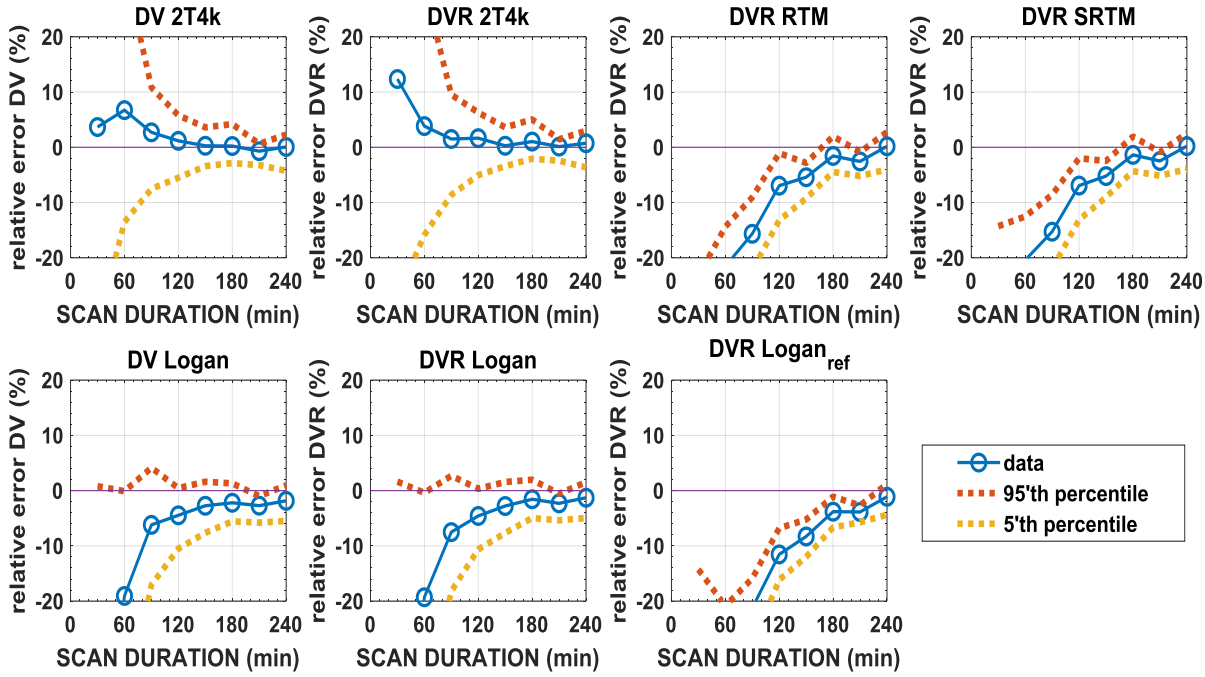


*Figure 4.7: The plots of the relative error (%) against the scan duration (continuous sampling scheme) for the distribution volume (DV) and the distribution volume ratio (DVR) in the brain region with high receptor density (putamen). The plots show invasive arterial blood sampling methods (2T4k and Logan) and reference region methods (RTM, SRTM and Logan$_{ref}$).*

RTM, SRTM and both Logan methods (invasive and non-invasive) all tend to converge from a strongly negative bias for shorter scan duration, towards a less negative bias with increasing scan duration in high uptake areas (figure 4.7). The 2T4k method shows an initially positive bias which decreases when scan duration increases.

The variability decreases with increasing scanning time as expected for the 2T4k and Logan methods. This is only true up to 150 min. However, variability of the RTM, SRTM, and $Logan_{ref}$ models is relatively insensitive to the scan duration.

### 4.3.2 Brain regions with moderate (thalamus) and low (temporal cortex) receptor density

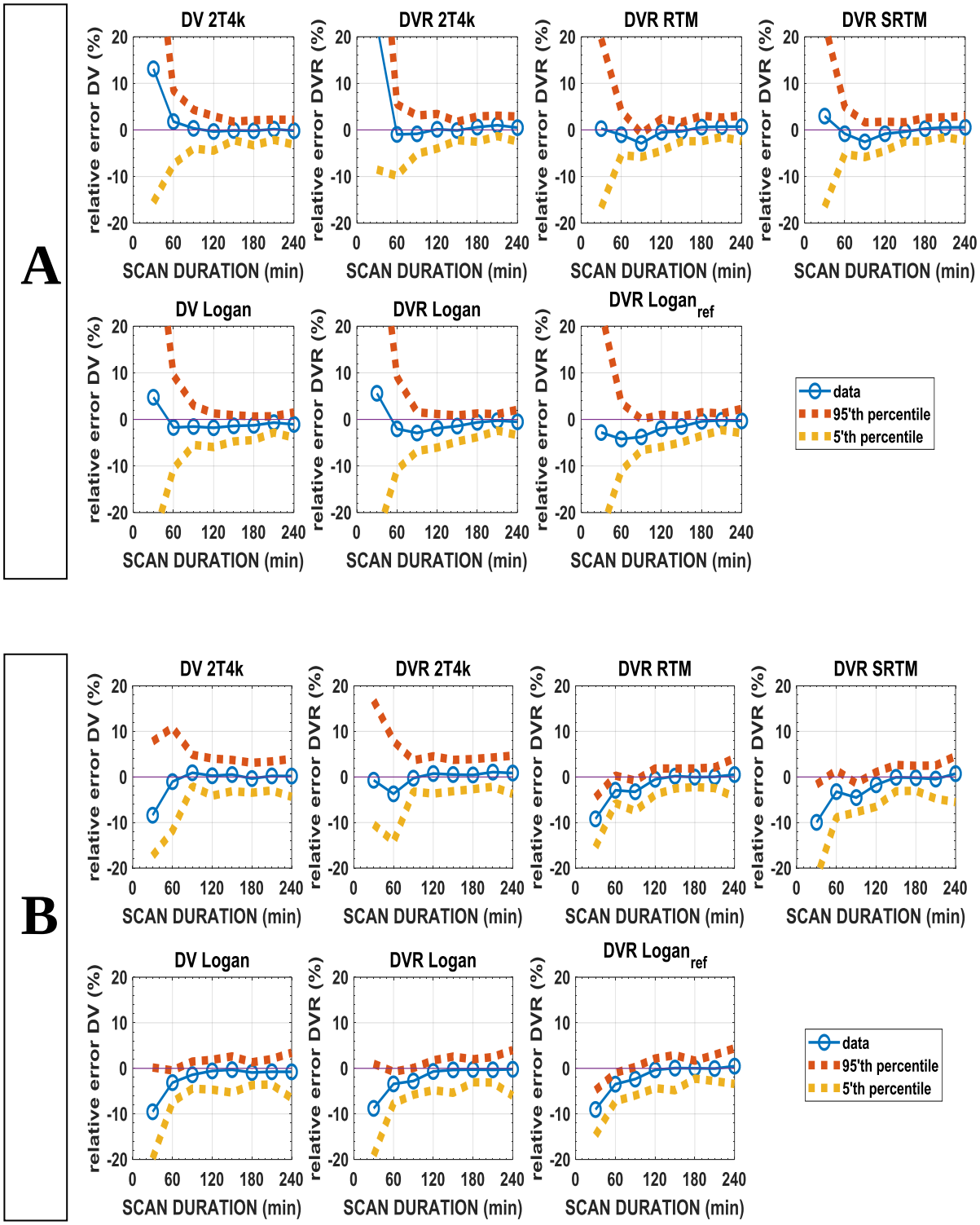


*Figure 4.8: The plots of the relative error (%) against the scan duration (continuous sampling scheme) for the distribution volume (DV) and the distribution volume ratio (DVR) in the brain region with moderate (A) and low (B) receptor density. The plots sh*

*ow invasive arterial blood sampling methods (2T4k and Logan) and reference region methods (RTM, SRTM and Logan$_{ref}$).*

From figure 4.8, all methods show almost no bias with the increasing scan duration. This is true for scan duration ≥ 120min.

In all cases, the relative error and variability were found to be within the range of ±10% for scan duration ≥ 120min. The non-invasive reference region methods can be use as the replacement of the invasive arterial blood sampling for scan duration ≥ 120min.

## 4.4 The effect of scan duration with breaks (interrupted sampling scheme) in brain regions with high, moderate, and low receptor density

### 4.3.3 Brain region with high receptor density (putamen)

The different interrupted sampling schemes are shown in table 3.2 and 3.3.

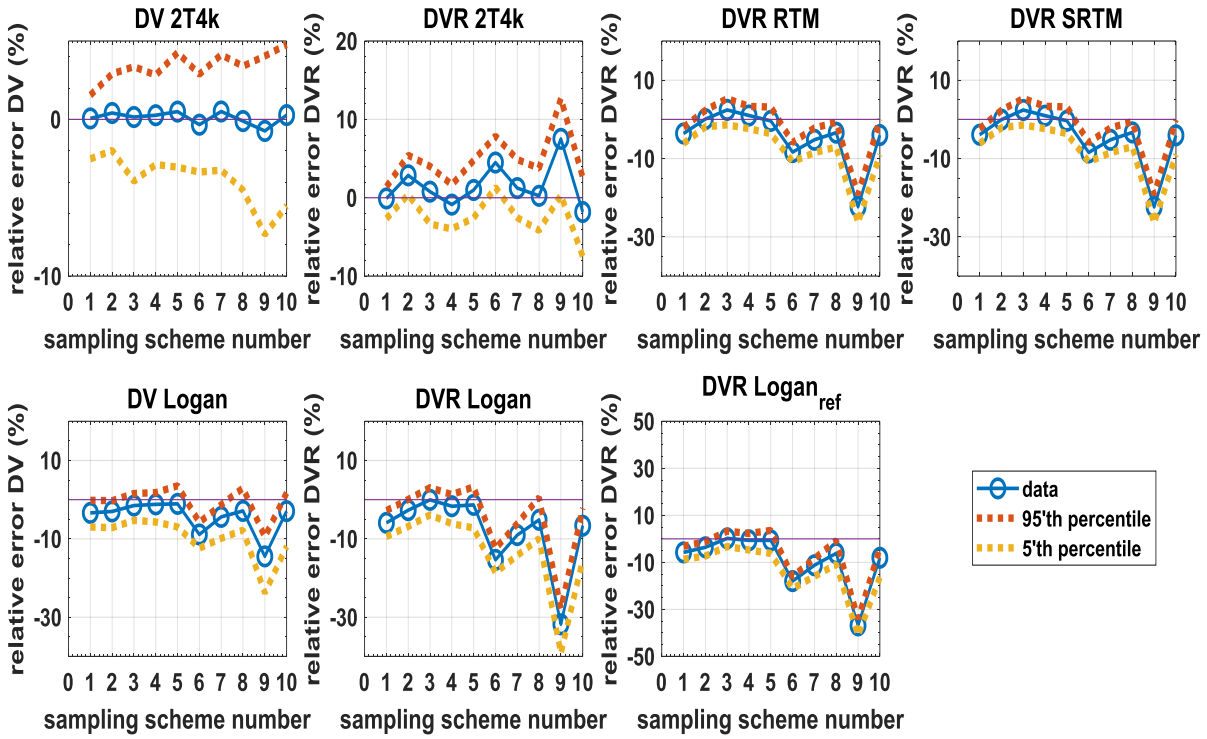


*Figure 4.9: The plots of the relative error (%) against the scan duration with breaks (interrupted sampling scheme) for the distribution volume (DV) and the distribution volume ratio (DVR) in the brain region with high receptor density (putamen). The plots show invasive arterial blood sampling methods (2T4k and Logan) and reference region methods (RTM, SRTM and Loganref).*

The change in the relative error and variability of the RTM, SRTM, Logan and $Logan_{ref}$ methods keeps similar trend in shape throughout different sampling schemes.

The interrupted sampling schemes (1-5) with breaks of 1 hour have a smaller relative error than interrupted sampling schemes (6 - 8) with breaks of 2 hours including the interrupted sampling scheme (10) with the break of 3 hours.

The interrupted sampling scheme (9) with the break of 3 hours has a larger bias than any other sampling scheme chosen for this study. In simple terms, the bias increases as the interrupted breaks between scans are prolonged.

### 4.3.4 Brain regions with moderate (thalamus) and low (temporal cortex) receptor density

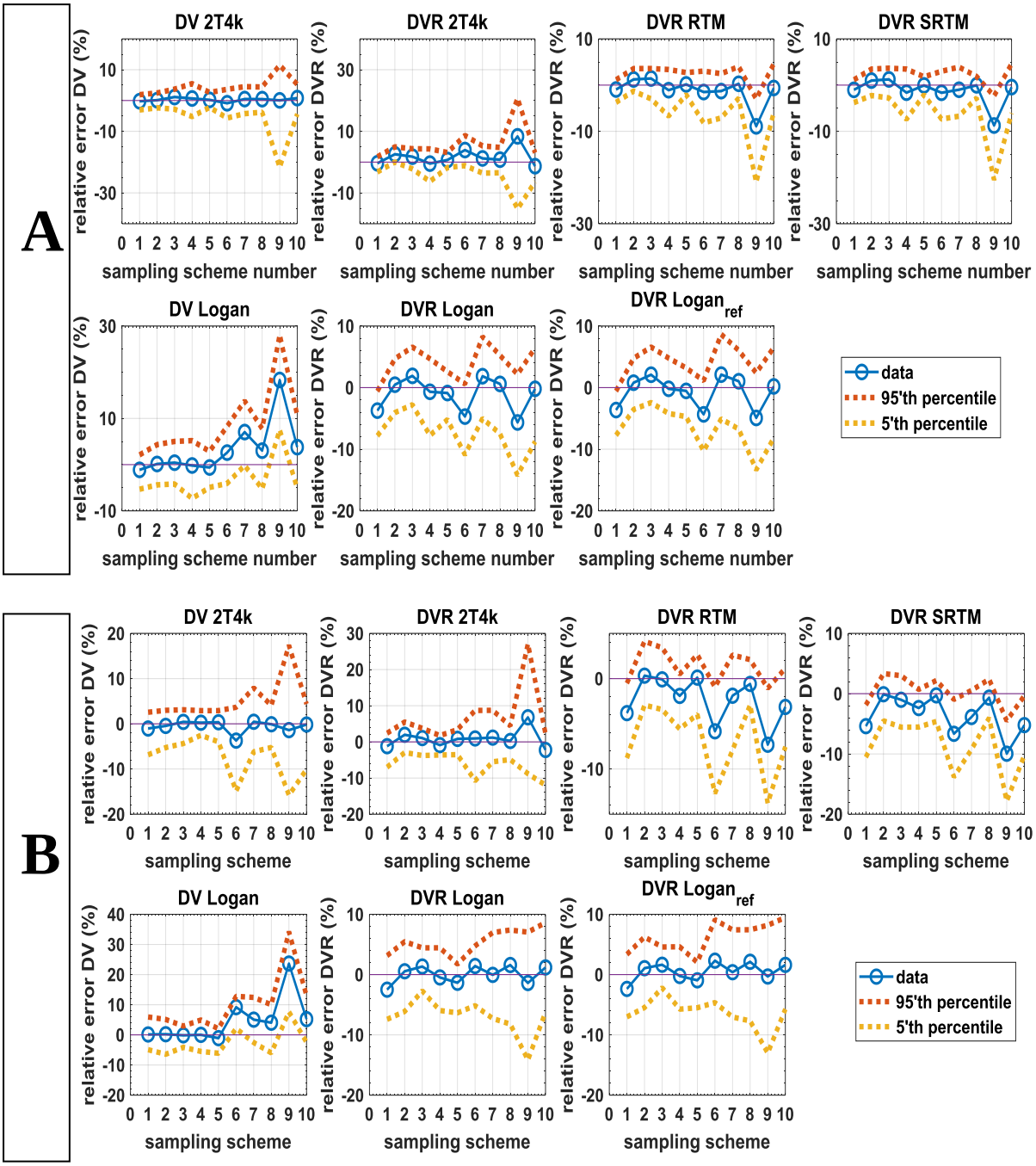


*Figure 4.10: The plots of the relative error (%) against the scan duration with breaks (interrupted sampling scheme) for the distribution volume (DV) and the distribution volume ratio (DVR) in the brain region with moderate (A) and low (B) receptor density. The plots show invasive arterial blood sampling methods (2T4k and Logan) and reference region methods (RTM, SRTM and Loganref).*

The change in the relative error and variability of the RTM, SRTM, Logan and Logan$_{ref}$ methods keeps similar trend in shape throughout different sampling schemes.

In figure 4.10 (A), moderate receptor density (thalamus), the change in the relative error and variability of the RTM, SRTM, Logan and $Logan_{ref}$ methods, keeps similar trend in shape throughout different sampling schemes. The same trend is also observed in low receptor density (temporal cortex), figure 4.10 (B).

All sampling schemes with interrupted breaks of 1 hour (sampling scheme 1-5), 2 hours (sampling scheme 6-8), and 2.5 hours (sampling scheme 10) have a small bias for RTM and SRTM except for 3 hours interrupted breaks (sampling scheme 9), which has a larger bias than any other acquisition chosen for this study. In simple terms, the bias increases as soon as the interrupted breaks between scans reach 3 hours.

The bias is also small for all sampling schemes with interrupted breaks of 1 hour (acquisition scheme 1-5), 2 hours (acquisition scheme 6-8), and 2.5 hours (acquisition scheme 10) for Logan and $Logan_{ref}$ in both figure 4.10 (A) and (B).

# Chapter 5: Discussion

This study explored the quantification of a simplified measurement protocol that omitted invasive arterial blood sampling. We studied the following graphical and/or simplified models: (1) LGA , (2) $Logan_{ref}$, (3) RTM, (4) SRTM (5) SUVR measured as the ratio of the activity in a region of interest, the activity in the cerebellum and (6) 2T4k as the ground truth model to analyze $^{18}$F-fallypride PET for visualization of $D_2/D_3$ receptors in the brain.

The three research questions (primary objectives) formulated in this study are discussed. For each of them, we first discuss the use of a graphical method (the Logan model), followed by the discussion of reference region models which do not require arterial blood sampling and finally the use of SUVR as a very simple method. In the discussions we have elaborated on applicability for high/moderate/low receptor density regions and formulated a conclusion based on the data we have presented per research topic.

The models were assessed in terms of their relative biases, variation, reproducibility and their reliability.

## 5.1 The accuracy/reliability of various methods in $^{18}$F-fallypride quantification

### 5.1.1 LGA

It was found that for $^{18}$F-fallypride, the DV and DVR for 2T4k and LGA gave high correlation and the results showed striking resemblance between the two methods. The results also showed relatively small inter-variation when two methods were compared to each other due to their small relative average biases and variability in both high and low receptor density regions.

LGA showed a slight underestimation of DV compared to 2T4k which is correlation to the study performed by Carson et al., (1993) and Slifstein and Laruelle et al., (2000)

In their study (Siessmeier et al., 2005), found that the $^{18}$F-fallypride estimates of DVR for the graphical methods were usually lower than estimates of DVR obtained with

the compartmental model in receptor-rich regions, which is in agreement with our study.

2T4k is theoretically the best model. If simplified models were to be used (e.g. Logan model) with blood sampling, it shows that Logan is still useful in a sense that it works almost equally well as the 2T4k model. Then parametric modeling on a voxel base for the estimation of DV, DVR can be used because it is quick (Logan et al., 2011; Logan (2003).

### 5.1.2 $Logan_{ref}$

It was found that the relative average bias and variation obtained $Logan_{ref}$ were large in the regions of high receptor density compared to the regions of low/moderate receptor density but within the limits of set criteria in both cases.

This means $Logan_{ref}$ can be used as a simplified measurement protocol that omitted arterial blood sampling in all regions but it is highly favoured in the regions of low/moderate receptor density.

### 5.1.3 RTM

RTM DVR showed larger relative bias of 4.9% in high receptor density region and smaller relative bias of -0.3% in low/moderate receptor density regions.
This method passed the set criteria and can be used as the replacement of the invasive arterial blood sampling methods in all the receptor density regions.

### 5.1.4 SRTM

The smallest relative average bias and variation were observed with the results in close proximity to the 2T4k method in low/moderate than in high receptor density region. It is clear that when the relative average biases are small, the estimation of DVR is well achieved. This method can be used to replace the invasive arterial blood sampling methods in all receptor density regions.

### 5.1.5 SUVR

The relative biases were larger with more variability in SUVR results in all receptor density regions, thus causing the results to produce a proportional bias. With SUVR,

much less true quantification is captured and the error produced also depends on the obtained values. This makes things tricky because the bias is not constant.

These findings reveal that using SUVR as a quantification for $^{18}$F-fallypride is not ideal. Our results suggest that SUVR calculations are probably not among the best ones, because they produce relatively large errors. We do not recommend it as the method of choice as a replacement for the invasive arterial blood sampling methods.

## 5.2 The effect of noise-level variation/signal to noise ratio (SNR) in brain regions with high, moderate, and low receptor density

### 5.2.1 LGA

Our study shows that in high, low/moderate receptor density region, the variability of Logan graphical analysis increases with increasing noise as expected.

At these higher noise levels, a corresponding bias becomes apparent and LGA tends towards negative bias with increasing noise in high receptor density region. This is in agreement with the paper documented by Slifstein and Laruelle et al., (2000), which states that the higher noise levels have been shown to introduce a negative bias estimated by the Logan graphical analysis.

The relative error and variability were well within tolerance in all receptor density regions based on the set criteria.

### 5.2.2 Logan$_{ref}$

The results here are almost similar to the LGA described in section 5.2.1 above.

The relative error and variability were well with in tolerance based on the set criteria in all receptor density regions. Logan$_{ref}$ can be used as the replacement of the invasive arterial blood sampling methods in all the receptor density regions.

### 5.2.3 RTM

The relative error and variability were well with in tolerance based on the set criteria in all receptor density regions. RTM can be used as the replacement of the invasive arterial blood sampling methods in all the receptor density regions.

### 5.2.4 SRTM

Increasing noise increases the variability of SRTM. A conclusion can be made that SRTM can be used as the replacement of the invasive arterial blood sampling methods in all the receptor density regions since it produces a small relative error.

## 5.3 The effect of total scan duration (continuous sampling scheme) in brain regions with high, moderate, and low receptor density.

For continuous scanning, kinetic modeling estimates for $^{18}$F-fallypride with LGA, $Logan_{ref}$, RTM and SRTM were found to be reasonably stable with less relative errors in DVR, but required long scan durations (> 150 min) in high receptor density regions and scan durations of > 120 min in low/moderate receptor density regions.

In their studies, Constantinescu et al., (2011) and Honer et al., (2004), used the maximum scan duration of up to 150 min for $^{18}$F-fallypride studies. It was found that at 150 min the kinetics of $^{18}$F-fallypride were stable.
Ishibashi et al., (2013) stated that $^{18}$F-fallypride has relatively slow kinetics, thus requiring a prolonged scanning time, at least 120 to 180 min scan duration. Similarly, Tantawy et al., (2009) used a total scan duration of 120 min.

## 5.4 The effect of the scan duration with breaks (interrupted sampling scheme) in brain regions with high, moderate, and low receptor density.

The acquisitions schemes are divided into the following groups (refer to table 3.2 and table 3.3):
The scan duration with 1 hour break are (interrupted sampling scheme 1-5), 2 hour break are (interrupted sampling scheme 6-9), 3 hour break is (interrupted sampling scheme 9) and 2.5 hour break is (interrupted sampling scheme 10)

The change in the relative error and variability of the RTM, SRTM, Logan and $Logan_{ref}$ methods keeps similar trend in shape throughout different sampling schemes in high receptor density region. The same trend is also observed in moderate and low receptor density regions.

The interrupted sampling schemes (1-5) with breaks of 1 hour have a smaller relative error than interrupted sampling schemes (6 - 8) with breaks of 2 hours including the interrupted sampling scheme (10) with the break of 3 hours.

The interrupted sampling scheme (9) with the break of 3 hours has a larger bias than any other sampling scheme chosen for this study. This might be due to a short scan at the beginning, followed by a long break. In simple terms, the bias increases as the interrupted breaks between scans are prolonged.

The most important factor in using interrupted sampling schemes is a clear understanding of the research population. What might seem reasonable in terms of interrupted sampling schemes with breaks for one patient group (older patients) might be totally inappropriate for another group (e.g. paediatric patients). Hence the recommendation on the interrupted sampling schemes with the break is required.

Our results suggest that when a scanning break is introduced, best quantitative results are achieved if a 30 min break is commenced immediately after 30 minutes of scanning.
This should be followed by the second break (120 min long) after 90 min of scanning (i.e. 30 min scan + 30 min break + 30 min scan).
The total duration of the scan was 90 min and the total length of the break was 150 min.

# Chapter 6: Conclusions and future research

The following conclusions can be drawn from the findings of this study.

When addressing the accuracy and reliability of various methods in $^{18}$F-fallypride quantification, parameter estimation is important. The LGA model allows parametric modelling on a voxel base for the estimation of DV, DVR and works almost as well as the 2T4k model.

All the various non-invasive reference region methods ($Logan_{ref}$, RTM and SRTM) were accurate and reliable in quantification of $^{18}$F-fallypride. They can all be used as the replacement of the invasive arterial blood sampling.

The $Logan_{ref}$ method was the most accurate, with the highest precision as the replacement of the invasive arterial blood sampling in low/moderate receptor density regions. While SRTM gave high precision in high receptor density region, SUVR calculations produce relatively large errors in all brain receptor density regions used in this study.

The effect of noise shows the relative error and variability increase with the increasing noise level variation in high, moderate and low receptor density regions. LGA, $Logan_{ref}$, RTM and SRTM produced results comparable to 2T4k method, therefore, all the non-invasive reference region methods used in this study are recommended to be used as the replacement of the invasive arterial blood sampling methods.

Addressing the issues of the scan duration, LGA, $Logan_{ref}$, RTM and SRTM can be used as the replacement of the invasive arterial blood sampling methods if the scan length (continuous sampling scheme) > 150 min in high receptor density region and > 120 min in low/moderate receptor density regions.

Addressing the issue of interrupted sampling scheme with breaks depends on the patient population group. The interrupted sampling schemes with breaks for one

patient group (older patients) might be totally inappropriate for another group (e.g. paediatric patients).

Our results suggest that when a scanning break is introduced, best quantitative results are achieved if a 30 minute break is commenced immediately after 30 minutes of scanning. This should be followed by a second break (120 minutes long) after 90 minutes of scanning (i.e. 30 minutes scan + 30 minutes break + 30 minutes scan).

In total, the duration of the two breaks together should not be longer than 150 minutes.

**Future clinical and research applications**

Since the tracer behaviour can be approximated by the ground truth model, the second line of research evolves around the idea of using a much more complex and accurate ground truth model, because the current study uses the 2T4k model of $^{18}$F-fallypride as the ground truth model for simulations. In reality the ground truth model is much more complex in a sense that the complexity is based on the parameters involving physiological and biological pathways of the tracer's molecule in the brain.

The complexity of the ground truth model will be improved to properly describe the complex dynamic processes and the behaviour of $^{18}$F-fallypride in the brain. However, the model will be reconstructed in such a way that it not too complicated to be used to analyze PET studies. This means fine tuning simulations to look at ideological aspects of $^{18}$F-fallypride, and how this tracer is behaving and what the dopamine receptors are doing in the brain.

Moreover, it would be interesting for future research to consider studying both the time-varying fluctuating levels of the dopamine concentration and its competition with the radiotracer for the available $D_2/D_3$ binding sites by exploring the activation studies.

Once $^{18}$F-fallypride becomes clinically available on the South African market, it would be an exciting project to compare actual clinical data with these and other kinetic models.

# Appendix

## A. Modelling the fraction of the intact tracer

```
function [intact_fractions] = LCN_calc_intact_tracer_hill(params,times)
%
% the function y(t) = b/(1+(a/t)^n) will be fitted with b set to 1
% b = asymptotic value, assumed 1 at time 0 (100% intact tracer)
% a = t where the function reaches half of its maximum (b/2)
% n determines the steepness of the slope
%
% FORMAT: intact_fractions = LCN_calc_intact_tracer_hill(params,times)
%
% params: [a, n]
% times: array of times in minutes
% intact_fractions: intact fraction of tracer (between 0 and 1)
%_____________________________________________________________________________
%
% author: Natalie Nelissen, Patrick Dupont
%_____________________________________________________________________________
% @(#)LCN_calc_intact_tracer_hill.m      1.0

intact_fractions = 1./(1+(params(1)./times).^params(2));
```

## B. Simulation/modelling of a representative input function

```
function [Ca] = LCNSIM_input_function(t,ts,tp,A,beta)
% this function calculates a theoretical input function defined by
% parameters ts, tp, A and beta at time points t (array of times in min).
% Ca = 0 if t < ts
% Ca = (t-ts).*(A1+A2+A3)/(tp-ts)
% Ca = A(1)*exp(-log(2)*(t-tp)/beta(1)) + A(2)*exp(-log(2)*(t-tp)/beta(2))
+ A(3)*exp(-log(2)*(t-tp)/beta(3))
% output = array of concentrations (kBq/ml) of the theoretical input
% function

index1 = (t<=ts);
index2 = (t<=tp);
index3 = (t>tp);

Ca(index3) = A(1)*exp(-log(2)*(t(index3)-tp)/beta(1))+A(2)*exp(-
log(2)*(t(index3)-tp)/beta(2))+A(3)*exp(-log(2)*(t(index3)-tp)/beta(3));
Ca(index2) = (t(index2)-ts).*sum(A)/(tp-ts);
Ca(index1) = 0;
 end
%+++++++++++++++ SETTINGS++++++++++++++++++++++++++++++++++++++++++++++++
 %% ideal input function
ts   = 0.35; % min
tp   = 0.7; % min
A    = [743.2432432432 202.7027027027 25.0]; % KBq/ml
beta = [0.1 1.2 100]; % min
MAX_TIME_INPUT = 200; % min

%% model for the intact fraction
param_hill = [70 -0.6];
STEP = 0.001; % step size for the calculation of integrals in min

FINETIMES = [0:STEP:MAX_TIME_INPUT]'; % min
% determine the input function
[Ca] = LCNSIM_input_function(FINETIMES',ts,tp,A,beta)'; % uncorrected input

% determine the model for intact fraction of tracer
intact_hill = LCN_calc_intact_tracer_hill(param_hill,FINETIMES);

% correct the input function for the intact fraction
Ca_corr = Ca.*intact_hill; % corrected input function
CA_FINETIMES = Ca_corr;

subplot(1,3,1)
   plot(FINETIMES,Ca)
   xlabel('Time (min)')
   ylabel('Arterial activity concentration, nCi/cc')
   title('Input function')
   subplot(1,3,2)
  plot(FINETIMES,intact_hill)
  xlabel('Time (min)')
   ylabel('Percent of 18F-fallypride(simulated intact fraction)')
   title('Fraction of the intact tracer')
   hold on

   subplot(1,3,3)
   plot(FINETIMES,Ca_corr)
   xlabel('Time (min)')
   ylabel('Arterial activity concentration, nCi/cc')
   title('Decay corrected input function')
```

### C. Analysis using different methods

```
% analysis using 2T4k
%-------------------------------------------------------------------------
ESTIMATED_K_PARAMS = tmp1_Kvalues(:,index_tmp_error(1));
DV_2T4k(i_voi,k)=
(ESTIMATED_K_PARAMS(1)./ESTIMATED_K_PARAMS(2)).*(1+ESTIMATED_K_PARAMS(3)./E
STIMATED_K_PARAMS(4));

% calculate SUVR
%-------------------------------------------------------------------------
SUVR(i_voi,j,k) = mean(C_MEASURED(end-4:end))./SUV_REF(j);

% analysis using Logan
%-----------------------------------------
[VD,error] =
LCN_LOGAN(MIDSCANTIMES,C_MEASURED,FINETIMES,CA_FINETIMES,logan_start_time,0
);
DV_Logan(i_voi,j,k) = VD;

% analysis using Logan_ref
%-------------------------------------------------------------------------
[slope,error] =
LCN_LOGAN_ref(MIDSCANTIMES,C_MEASURED,C_REF,logan_start_time,0);
DVR_Logan_ref(i_voi,j,k) = slope;

% analysis using RTM
%-------------------------------------------------------------------------
ESTIMATED_K_PARAMS = tmp1_Kvalues(:,index_tmp_error(1));
DVR_RTM(i_voi,j,k)    = ESTIMATED_K_PARAMS(4)+1;


% analysis using SRTM
%-------------------------------------------------------------------------
DVR_SRTM(i_voi,j,k)    = ESTIMATED_K_PARAMS(3)+1;

% True DV values
%-------------------------------------------------------------------------
DV_TRUE  =
(params_gold_standard(:,1)./params_gold_standard(:,2)).*(1+params_gold_stan
dard(:,3)./params_gold_standard(:,4));

% True DV values in reference region
%-------------------------------------------------------------------------
DV_TRUE_REF  =
(params_gold_standard_ref(:,1)./params_gold_standard_ref(:,2)).*(1+params_g
old_standard_ref(:,3)./params_gold_standard_ref(:,4));
DVR_TRUE = DV_TRUE./DV_TRUE_REF;
```

### D. The Correlation and Bland-Altman plots for 2T4k method

```
% generate plots
% plot correlations with true values as well as bland-altman plots for each
% method

% 2T4k
%--------------------------------------------------------------------------
figure
subplot(1,2,1)
x = DV_TRUE;
y = DV_2T4k;
[R, p] =corrcoef(x,y);
r = R(1,2);
dif = x-y;
average = (x+y)./2;
plot(x,y,'*')
xlabel('DV (true)')
ylabel('DV (2T4k)')
hold on
plot([0.9*min(x) 1.1*max(x)],[0.9*min(x) 1.1*max(x)],':')
P = polyfit(x,y,1);
xvalues = [0.9*min(x) 1.1*max(x)];
plot(xvalues,P(1).*xvalues+P(2),'-r')
title(['r = ' num2str(r)])

subplot(1,2,2)
plot(average,dif,'*')
xlabel('average DV')
ylabel('DV (true) - DV (2T4k)')
hold on
plot([0 1.1*max(average)],[mean(dif) mean(dif)])
% determine 5 and 95 percentiles
aa = sort(dif);
threshold_5p = aa(round(length(aa)*0.05));
threshold_95p = aa(round(length(aa)*0.95));
plot([0 1.1*max(average)],[threshold_5p  threshold_5p],':')
plot([0 1.1*max(average)],[threshold_95p  threshold_95p],':')
title(['bias = ' num2str(mean(dif))])
if min(aa) < 0
   lower_value = min(1.1*min(aa),-0.2*min(average));
else
   lower_value = min(0.9*min(aa),-0.2*min(average));
end
if max(aa) < 0
   upper_value = max(0.2*max(average));
else
   upper_value = max(1.1*max(aa),0.2*max(average));
end
axis([0.9*min(average) 1.1*max(average) lower_value upper_value])
```

## E. The relative error (%) and SNR/Scan duration for 2T4k method

```
%plot error = relative difference between calculated DV and DV_TRUE per VOI
%-------------------------------------------------------------------------
xvalues    = noise_levels(1:end);
nr_values = length(xvalues);
for i_voi = 1:nr_VOIS
    clear error tmp stdvalues meanvalues
    figure

% 2T4k
%-------------------------------------------------------------------------
    subplot(2,4,1)
    tmp = squeeze(DV_2T4k(i_voi,:,:));
    error = 100*(tmp-DV_TRUE(i_voi))./DV_TRUE(i_voi);
    meanvalues = zeros(nr_values,1);
    if nr_noise_realizations > 1
       for j = 1:nr_values
           clear datavalues
           datavalues = error(j,:);
           % remove NaN or Inf
           index_ok1 = (~isnan(datavalues)).*(~isinf(datavalues));
           datavalues = datavalues(index_ok1 > 0);
           % identify outliers
           [outlier_index]                                                  =
LCN_detect_outliers_univariate_data(datavalues,'classical');
           index_ok2 = setdiff([1:length(datavalues)]',outlier_index);
           meanvalues(j) = mean(datavalues(index_ok2));
           stdvalues(j)  = std(datavalues(index_ok2));
           minvalues(j)  = min(datavalues(index_ok2));
           maxvalues(j)  = max(datavalues(index_ok2));
       end
       plot(xvalues,meanvalues,'*')
       plot(xvalues,stdvalues,'*')

       hold on
        errorbar(xvalues,meanvalues,stdvalues,stdvalues)
       plot(xvalues,maxvalues,':')
       plot(xvalues,minvalues,':')
              hold on

    else
       plot(xvalues,error,'o')
       hold on
    end
    plot([0 xvalues(end)],[0 0])
    xlabel('SNR (min)')
    ylabel('relative error DV (%)')
    axis([0 xvalues(end) -20 20])
    title('DV 2T4k')
```

## F. Permissions and Licence Agreement

**JOHN WILEY AND SONS LICENSE TERMS AND CONDITIONS**

Jan 15, 2019

This Agreement between Mohlapoli S Mohlapholi ("You") and John Wiley and Sons ("John Wiley and Sons") consists of your license details and the terms and conditions provided by John Wiley and Sons and Copyright Clearance Center.

License Number 4510191045554
License date Jan 15, 2019
Licensed Content Publisher John Wiley and Sons
Licensed Content Publication Synapse
Licensed Content Title Brain imaging of 18F-fallypride in normal volunteers: Blood analysis, distribution, test-retest studies, and preliminary assessment of sensitivity to aging effects on dopamine D-2/D-3 receptors
Licensed Content Author Jogeshwar Mukherjee, Bradley T. Christian, Kelly A. Dunigan, et al
Licensed Content Date Sep 5, 2002
Licensed Content Volume 46
Licensed Content Issue 3
Licensed Content Pages 19
Type of use Dissertation/Thesis
Requestor type University/Academic
Format Electronic
Portion Figure/table
Number of figures/tables 2
Original Wiley figure/table number(s)
Figure 1
Will you be translating? No
Title of your thesis / dissertation
Quantification of positron emission tomography brain imaging using 18F-Fallypride: a simulation
Expected completion date Feb 2019
Expected size (number of pages)
100
Requestor Location P.O Box 19101 Tygerberg Hospital Post Office
Pine 28
Boston Place, Weelgemend street
Bellville
Cape Town, Western cape 7530
South Africa
Attn: P.O Bo x 19101 Tygerberg Hospital Post Office
Publisher Tax ID EU826007151
Total 0.00 USD
Terms and Conditions

NEITHER WILEY NOR ITS LICENSORS MAKES ANY WARRANTY OR REPRESENTATION OF ANY KIND TO YOU OR ANY THIRD PARTY, EXPRESS, IMPLIED OR STATUTORY, WITH RESPECT TO THE MATERIALS OR THE ACCURACY OF ANY INFORMATION CONTAINED IN THE MATERIALS, INCLUDING, WITHOUT LIMITATION, ANY IMPLIED WARRANTY OF MERCHANTABILITY, ACCURACY, SATISFACTORY QUALITY, FITNESS FOR A PARTICULAR PURPOSE, USABILITY, INTEGRATION OR NON-INFRINGEMENT AND ALL SUCH WARRANTIES ARE HEREBY EXCLUDED BY WILEY AND ITS LICENSORS AND WAIVED BY YOU.

WILEY shall have the right to terminate this Agreement immediately upon breach of this Agreement by you.

You shall indemnify, defend and hold harmless WILEY, its Licensors and their respective directors, officers, agents and employees, from and against any actual or threatened claims, demands, causes of action or proceedings arising from any breach of this Agreement by you.

IN NO EVENT SHALL WILEY OR ITS LICENSORS BE LIABLE TO YOU OR ANY OTHER PARTY OR ANY OTHER PERSON OR ENTITY FOR ANY SPECIAL, CONSEQUENTIAL, INCIDENTAL, INDIRECT, EXEMPLARY OR PUNITIVE DAMAGES, HOWEVER CAUSED, ARISING OUT OF OR IN CONNECTION WITH THE DOWNLOADING, PROVISIONING, VIEWING OR USE OF THE MATERIALS REGARDLESS OF THE FORM OF ACTION, WHETHER FOR BREACH OF CONTRACT, BREACH OF WARRANTY, TORT, NEGLIGENCE, INFRINGEMENT OR OTHERWISE (INCLUDING, WITHOUT LIMITATION, DAMAGES BASED ON LOSS OF PROFITS, DATA, FILES, USE, BUSINESS OPPORTUNITY OR CLAIMS OF THIRD PARTIES), AND WHETHER OR NOT THE PARTY HAS BEEN ADVISED OF THE POSSIBILITY OF SUCH DAMAGES. THIS LIMITATION SHALL APPLY NOTWITHSTANDING ANY FAILURE OF ESSENTIAL PURPOSE OF ANY LIMITED REMEDY PROVIDED HEREIN.

Should any provision of this Agreement be held by a court of competent jurisdiction to be illegal, invalid, or unenforceable, that provision shall be deemed amended to achieve as nearly as possible the same economic effect as the original provision, and the legality, validity and enforceability of the remaining provisions of this Agreement shall not be affected or impaired thereby.

The failure of either party to enforce any term or condition of this Agreement shall not constitute a waiver of either party's right to enforce each and every term and condition of this Agreement. No breach under this agreement shall be deemed waived or excused by either party unless such waiver or consent is in writing signed by the party granting such waiver or consent. The waiver by or consent of a party to a breach of any provision of this Agreement shall not operate or be construed as a waiver of or consent to any other or subsequent breach by such other party.

This Agreement may not be assigned (including by operation of law or otherwise) by you without WILEY's prior written consent.

Any fee required for this permission shall be non-refundable after thirty (30) days from receipt by the CCC.

These terms and conditions together with CCC's Billing and Payment terms and conditions (which are incorporated herein) form the entire agreement between you and WILEY concerning this licensing transaction and (in the absence of fraud) supersedes

all prior agreements and representations of the parties, oral or written. This Agreement may not be amended except in writing signed by both parties. This Agreement shall be binding upon and inure to the benefit of the parties' successors, legal representatives, and authorized assigns.

In the event of any conflict between your obligations established by these terms and conditions and those established by CCC's Billing and Payment terms and conditions, these terms and conditions shall prevail.

WILEY expressly reserves all rights not specifically granted in the combination of (i) the license details provided by you and accepted in the course of this licensing transaction, (ii) these terms and conditions and (iii) CCC's Billing and Payment terms and conditions.

This Agreement will be void if the Type of Use, Format, Circulation, or Requestor Type was misrepresented during the licensing process.

This Agreement shall be governed by and construed in accordance with the laws of the State of New York, USA, without regards to such state's conflict of law rules. Any legal action, suit or proceeding arising out of or relating to these Terms and Conditions or the breach thereof shall be instituted in a court of competent jurisdiction in New York County in the State of New York in the United States of America and each party hereby consents and submits to the personal jurisdiction of such court, waives any objection to venue in such court and consents to service of process by registered or certified mail, return receipt requested, at the last known address of such party.

**WILEY OPEN ACCESS TERMS AND CONDITIONS**

Wiley Publishes Open Access Articles in fully Open Access Journals and in Subscription journals offering Online Open. Although most of the fully Open Access journals publish open access articles under the terms of the Creative Commons Attribution (CC BY) License only, the subscription journals and a few of the Open Access Journals offer a choice of Creative Commons Licenses. The license type is clearly identified on the article.

**The Creative Commons Attribution License**

The Creative Commons Attribution License (CC-BY) allows users to copy, distribute and transmit an article, adapt the article and make commercial use of the article. The CC-BY license permits commercial and non-

**Creative Commons Attribution Non-Commercial License**

The Creative Commons Attribution Non-Commercial (CC-BY-NC)License permits use, distribution and reproduction in any medium, provided the original work is properly cited and is not used for commercial purposes.(see below)

**Creative Commons Attribution-Non-Commercial-NoDerivs License**

The Creative Commons Attribution Non-Commercial-NoDerivs License (CC-BY-NC-ND) permits use, distribution and reproduction in any medium, provided the original work is properly cited, is not used for commercial purposes and no modifications or adaptations are made. (see below)

**Use by commercial "for-profit" organizations**

Use of Wiley Open Access articles for commercial, promotional, or marketing purposes requires further explicit permission from Wiley and will be subject to a fee.

Further details can be found on Wiley Online Library

http://olabout.wiley.com/WileyCDA/Section/id-410895.html

**Other Terms and Conditions:**

**v1.10 Last updated September 2015**

**Questions? customercare@copyright.com or +1-855-239-3415 (toll free in the US) or +1-978-646-2777.**

# References

Blautzik, J., Brendel, M., Sauerbeck, J., Kotz, S., Scheiwein, F., Bartenstein, P., Rominger, A., Scheiwein, F., Bartenstein, P., Seibyl, J., Rominger, A. (2017). Reference region selection and the association between the rate of amyloid accumulation over time and the baseline amyloid burden. European Journal of Nuclear Medicine and Molecular Imaging, 44(8), 1364–1374.

Brier, M. R., Gordon, B., Friedrichsen, K., McCarthy, J., Stern, A., Christensen, J., Ances, B. M. (2016). Tau and A-beta imaging, CSF measures, and cognition in Alzheimer's disease. Science Translational Medicine, 11(338), 1–10.

Buchert, R., Thiele, F., Thomasius, R., Wilke, F., Petersen, K., Brenner, W., Mester, J., Spies, l., Clausen, M. (2007). Ecstasy-induced reduction of the availability of the brain serotonin transporter as revealed by [$^{11}$C](+)McN5652-PET and the multi-linear reference tissue model: loss of transporters or artifact of tracer kinetic modelling? Journal of Psychopharmacology, 21(6), 628–634.

Carson R.E. (2005). Tracer Kinetic Modeling in PET, in Bailey D.L., Townsend D.W., Valk P.E., Maisey M.N. (eds). Positron Emission Tomography: Basic Science and Clinical Practice. Springer, London

Ceccarini, J., Vrieze, E., Koole, M., Muylle, T., Bormans, G., Claes, S., & Van Laere, K. (2012). Optimized In Vivo Detection of Dopamine Release Using $^{18}$F-fallypride PET. Journal of Nuclear Medicine, 53(10), 1565–1572.

Christian, B. T., Lehrer, D. S., Shi, B., Narayanan, T. K., Strohmeyer, P. S., Buchsbaum, M. S., & Mantil, J. C. (2006). Measuring dopamine neuromodulation in the thalamus: Using [F-18]fallypride PET to study dopamine release during a spatial attention task. NeuroImage, 31(1), 139–152.

Christian, B. T., Narayanan, T., Shi, B., Morris, E. D., Mantil, J., & Mukherjee, J. (2004). Measuring the in vivo binding parameters of [18F]-fallypride in monkeys using a PET multiple-injection protocol. Journal of Cerebral Blood Flow and Metabolism, 24(3), 309–322.

Christian, B. T., Vandehey, N. T., Fox, A. S., Murali, D., Oakes, T. R., Converse, A. K., Nickles, R. J., Shelton, S. E., Davidson, R. J., Kalin, N. H. (2009). The distribution of D2/D3 receptor binding in the adolescent rhesus monkey using small animal PET imaging. NeuroImage, 44(4), 1334–1344.

Constantinescu, C. C., Coleman, R. a., Pan, M. L., & Mukherjee, J. (2011). Striatal and extrastriatal microPET imaging of D2/D3 dopamine receptors in rat brain with [18F]fallypride and [18F]desmethoxyfallypride. Synapse, 65(8), 778–787.

Cropley, V. L., Innis, R. B., Nathan, P. J., Brown, A. K., Sangare, J. L., Lerner, A., Ryu, Y. H., Sprague, K. E., Pike, V. W., Fujita, M. (2008). Small effect of dopamine release and no effect of dopamine depletion on [18F]fallypride binding in healthy humans. Synapse, 62(6), 399–408.

Crossley, N. A., Scott, J., Ellison-Wright, I., Mechelli, A. (2015) Neuroimaging distinction between neurological and psychiatric disorders. The British Journal of Psychiatry, 207(5): 429–434.

Cumming, P., Xiong, G., Fougère, C. La, Rominger, A., Bartenstein, P., Buchholz, H. G., Piel, M., Rosch, F., Grunder, G., Vernaleken, I. (2013). Surrogate markers for cerebral blood flow correlate with [$^{18}$F]-fallypride binding potential at dopamine D2/3 receptors in human striatum. Synapse, 67(4), 199–203.

Davenport, R. (1983). The Derivation of the Gamma-Variate Relationship for Tracer Dilution Curves. Journal of Nuclear Medicine, 24, 945–948.

D'Souza, U. M. (2010). Gene and Promoter Structures of the Dopamine Receptors, in Neve, K.A. (eds), The dopamine receptors. Humana Press, New York

Dunn, J. T., Clark-Papasavas, C., Marsden, P., Baker, S., Cleij, M., Kapur, S., Reeves, S. J. (2013). Establishing test-retest reliability of an adapted [(18)F]fallypride imaging protocol in older people. Journal of Cerebral Blood Flow and Metabolism, 33(7), 1098–103.

Golish, S. R., Hove, J. D., Schelbert, H. R., & Gambhir, S. S. (2001). A fast nonlinear method for parametric imaging of myocardial perfusion by dynamic (13)N-ammonia PET. Journal of Nuclear Medicine, 42(6), 924–31.

Gründer, G., Fellows, C., Janouschek, H., Veselinovic, T., Boy, C., Bröcheler, A., Kirschbaum, K. M., Hellmann, S., Spreckelmeyer, K. M., Hiemke, C., Rösch, F., Schaefer, W. M. (2008). Brain and Plasma Pharmacokinetics of Aripiprazole in Patients With Schizophrenia: An [$^{18}$F] fallypride PET Study. American Journal of Psychiatry, 165(8), 988–995.

Gunn, R. N., Gunn, S. R., Turkheimer, F. E., Aston, J. A. D., & Cunningham, V. J. (2002). Positron emission tomography compartmental models: a basis pursuit strategy for kinetic modeling. Journal of Cerebral Blood Flow and Metabolism, 22(12), 1425–1439.

Gunn, R. N., Lammertsma, A. A., Hume, S. P., & Cunningham, V. J. (1997). Parametric imaging of ligand-receptor binding in PET using a simplified reference region model. NeuroImage, 6(4), 279–287.

Gunn, R. N., Slifstein, M., Searle, G. E., Price, J. C. (2015). Quantitative imaging of protein targets in the human brain with PET Quantitative imaging of protein targets in the human brain with PET. Physics in Medicine & Biology, 60 R363

Heiss, W. D., & Herholz, K. (2006). Brain receptor imaging. Journal of Nuclear Medicine, 47(2), 302–312.

Heurling, K., Leuzy, A., Jonasson, M., Frick, A., Zimmer, E. R., Nordberg, A., & Lubberink, M. (2017). Quantitative positron emission tomography in brain research. Brain Research, 1670, 220–234.

Honer, M., Brühlmeier, M., Missimer, J., Schubiger, A. P., & Ametamey, S. M. (2004). Dynamic imaging of striatal D2 receptors in mice using quad-HIDAC PET. Journal of Nuclear Medicine, 45(3), 464–470.

Hurd YL & Hall H (2005). Chapter IX Human forebrain dopamine systems: Characterization of the normal brain and in relation to psychiatric disorders, in Dunnett, SB, Bentivoglio MA, Björklund A, Hökfelt T (eds), Handbook of Chemical Neuroanatomy, Elsevier, Amsterdam

Ichise, M., Toyama, H., Innis, R., & Carson, R. (2002). Strategies to improve neuroreceptor parameter estimation by linear regression analysis. Journal of Cerebral Blood Flow and Metabolism, 22, 1271–1281.

Innis, R. B., Cunningham, V. J., Delforge, J., Fujita, M., Gjedde, A., Gunn, R. N., Carson, R. E. (2007). Consensus nomenclature for in vivo imaging of reversibly binding radioligands. Journal of Cerebral Blood Flow and Metabolism, 27(9), 1533–1539.

Ishibashi, K., Robertson, C. L., Mandelkern, M. A., Morgan, A. T., & London, E. D. (2013). The simplified reference tissue model with 18F-Fallypride positron emission tomography: Choice of reference region. Molecular Imaging, 12(8), 1–9.

Ishiki, A., Okamura, N., Furukawa, K., Furumoto, S., Harada, R., Tomita, N., Hiraoka, K., Watanuki, S., Ishikawa, Y., Tago, T., Funaki, Y., Iwata, R., Tashiro, M., Yanai, k., Kudo, Y., Arai, H. (2015). Longitudinal assessment of Tau pathology in patients with Alzheimer's disease using [$^{18}$F] THK-5117 positron emission tomography. PLoS ONE, 10(10), 1–9.

Ito, H., Hietala, J., Blomqvist, G., Halldin, C., & Farde, L. (1998). Comparison of the Transient Equilibrium and Continuous Infusion Method for Quantitative PET Analysis of [$^{11}$C] Raclopride Binding. Journal of Cerebral Blood Flow and Metabolism, 18(9), 941–950.

Joshi, A., Fessler, J. A, & Koeppe, R. A. (2008). Improving PET receptor binding estimates from Logan plots using principal component analysis. Journal of Cerebral Blood Flow and Metabolism, 28(4), 852–865.

Kimura, Y., Naganawa, M., Shidahara, M., Ikoma, Y., & Watabe, H. (2007). PET kinetic analysis -- pitfalls and a solution for the Logan plot. Annals of Nuclear Medicine, 21(1), 1–8.

Kinahan, P. E., & Fletcher, J. W. (2010). PET/CT Standardized Uptake Values (SUVs) in Clinical Practice and Assessing Response to Therapy. Seminars in Ultrasound, CT and MRI, 31(6), 496–505.

Lammertsma, A. A., Bench, C. J., Hume, S. P., Osman, S., Gunn, K., Brooks, D. J., & Frackowiak, R. S. J. (1996). Comparison of Methods for Analysis of Clinical [$^{11}$C]raclopride Studies. Journal of Cerebral Blood Flow & Metabolism, 16(1), 42–52.

Lammertsma, A.A., Hume, S. P. (1996). Simplified Reference Tissue Model for PET Receptor Studies, NeuroImage, 4(3), 153-158

Logan, J. (2003). A review of graphical methods for tracer studies and strategies to reduce bias. Nuclear Medicine and Biology, 30(8), 833–844.

Logan, J., Alexoff, D., & Fowler, J. S. (2011). The use of alternative forms of graphical analysis to balance bias and precision in PET images. Journal of Cerebral Blood Flow and Metabolism, 31(2), 535–546.

Logan, J., Fowler, J. S., Volkow, N. D., Ding, Y. S., Wang, G. J., & Alexoff, D. L. (2001). A strategy for removing the bias in the graphical analysis method. Journal of Cerebral Blood Flow and Metabolism, 21(3), 307–320.

Logan, J., Fowler, J. S., Volkow, N. D., Wang, G. J., Ding, Y. S., & Alexoff, D. L. (1996). Distribution volume ratios without blood sampling from graphical analysis of PET data. Journal of Cerebral Blood Flow and Metabolism, 16(5), 834–840.

Logan, J., Fowler, J. S., Volkow, N. D., Wolf, A. P., Dewey, S. L., Schlyer, D. J., Gatley, S. J. (1990). Graphical analysis of reversible radioligand binding from time-activity measurements applied to [N-11C-methyl]-(-)-cocaine PET studies in human subjects. Journal of Cerebral Blood Flow and Metabolism, 10(5), 740–747.

Lystad, R. P., Pollard, H. (2009). Functional neuroimaging: a brief overview and feasibility for use in chiropractic research. Journal of the Canadian Chiropractic Association, 53(1):59–72

Madsen, M. T. (1992). A simplified formulation of the gamma variate function. Physics in Medicine and Biology, 37(7), 1597–1600.

Masdeu, J. C. (2011). Neuroimaging in Psychiatric Disorders. Neurotherapeutics, 8(1), 93-102.

Matsubara, K., Watabe, H., Kumakura, Y., Hayashi, T., Endres, C. J., Minato, K., & Iida, H. (2011). Sensitivity of kinetic macro parameters to changes in dopamine synthesis, storage, and metabolism:

A simulation study for [18F] FDOPA PET by a model with detailed dopamine pathway. Synapse, 65(8), 751–762.

McNamee, R. L., Yee, S.-H., Price, J. C., Klunk, W. E., Rosario, B., Weissfeld, L., Ziolko, S., Berginc, M., lopresti, B., Dekosky, S., Mathis, C. A. (2009). Consideration of optimal time window for Pittsburgh compound B PET summed uptake measurements. Journal of Nuclear Medicine, 50(3), 348–355.

Meier, J., Tewarie, P., Hillebrand, A., Douw, L., van Dijk, B. W., Stufflebeam, S. M., van Mieghem, P. (2016). A mapping between structural and functional brain networks. Brain Connect, 6(4): 298-311.

Morita, T., Asada, M., Naito, E. (2016). Contribution of neuroimaging studies to understanding development of human cognitive brain functions. Frontiers in Human Neuroscience, 10: 464

Morris, E. D., & Yoder, K. K. (2007). Positron emission tomography displacement sensitivity: predicting binding potential change for positron emission tomography tracers based on their kinetic characteristics. Journal of Cerebral Blood Flow and Metabolism, 27(3), 606–617.

Mukherjee, J., Christian, B. T., Dunigan, K. A., Shi, B., Narayanan, T. K., Satter, M., & Mantil, J. (2002). Brain imaging of $^{18}$F-fallypride in normal volunteers: Blood analysis, distribution, test-retest studies, and preliminary assessment of sensitivity to aging effects on dopamine D-2/D-3 receptors. Synapse, 46(3), 170–188.

Mukherjee, J., Christian, B. T., Narayanan, T. K., Shi, B., & Mantil, J. (2001). Evaluation of dopamine D-2 receptor occupancy by clozapine, risperidone, and haloperidol in vivo in the rodent and nonhuman primate brain using 18F-fallypride. Neuropsychopharmacology, 25(4), 476–488.

Nelissen N, Warwick J & Dupont P (2012). Kinetic Modelling in Human Brain Imaging, in Hsieh C-H (eds), Positron Emission Tomography - Current Clinical and Research Aspects, Intech, New York.

Patel, N. H., Vyas, N. S., Puri, B. K., Nijran, K. S., & Al-nahhas, A. (2010). Positron Emission Tomography in Schizophrenia: Journal of Nuclear Medicine, 51(4), 511–520.

Pavlopoulos, S., Thireou, T., Kontaxakis, G., & Santos, A. (2007). Analysis and interpretation of dynamic FDG PET oncological studies using data reduction techniques. Biomedical Engineering Online, 6, 36.

Resat, H., Petzold, L., Pettigrew, M. F. (2009). Kinetic Modeling of Biological Systems. Methods Molecular Biology, 541, 311–335.

Riccardi, P., Li, R., Ansari, M. S., Zald, D., Park, S., Dawant, B., Anderson. S., Doop. M., Woodward, N., Schoenberg, E., Schmidt, D.,Baldwin, R., Kessler, R. (2006). Amphetamine-induced displacement of

[$^{18}$F] fallypride in striatum and extrastriatal regions in humans. Neuropsychopharmacology, 31(5), 1016–1026.

Riccardi, P., Park, S., Anderson, S., Doop, M., Ansari, M. S., Schmidt, D., & Baldwin, R. (2011). Sex differences in the relationship of regional dopamine release to affect and cognitive function in striatal and extrastriatal regions using positron emission tomography and [18F]fallypride. Synapse, 65(2), 99–102.

Salinas, C. A., Searle, G. E., & Gunn, R. N. (2015). The simplified reference tissue model: model assumption violations and their impact on binding potential. Journal of Cerebral Blood Flow and Metabolism, 35(2), 304–311.

Siessmeier, T., Zhou, Y., Buchholz, H.-G., Landvogt, C., Vernaleken, I., Piel, M., Schirrmacher, R., Rosch, F., Schreckenberger, M., Wong, D. F., Cumming, P., Gründer, G., Bartenstein, P. (2005). Parametric Mapping of Binding in Human Brain of D2 Receptor Ligands of Different Affinities. Journal of Nuclear Medicine, 46(6), 964–972.

Sijbesma, J. W. A., Zhou, X., García, D. V., Houwertjes, M. C., Doorduin, J., Kwizera, C., Mass, B., Meerlo, P., Dierckx, R. A., Slart, R. H. J. A, Elsing, P. H., Van Waarde, A. (2016). Novel Approach to Repeated Arterial Blood Sampling in Small Animal PET: Application in a Test-Retest Study with the Adenosine A1 Receptor Ligand [$^{11}$C] MPDX. Molecular Imaging and Biology, 18, 715–723.

Slifstein, M., Hwang, D. R., Huang, Y., Guo, N., Sudo, Y., Narendran, R.,Talbot, P., Laruele, M. (2004). In vivo affinity of [18F] fallypride for striatal and extrastriatal dopamine D2 receptors in nonhuman primates. Psychopharmacology, 175(3), 274–286.

Slifstein, M., Kegeles, L. S., Xu, X., Thompson, J. L., Urban, N., Castrillon, J., Hackett, E., Bae, S. -A., Laruelle, M., Abi-Dargham, A. (2010). Striatal and extrastriatal dopamine release measured with PET and [ $^{18}$F] fallypride. Synapse, 64(5), 350–362.

Slifstein, M., & Laruelle, M. (2000). Effects of statistical noise on graphic analysis of PET neuroreceptor studies. Journal of Nuclear Medicine, 41(12), 2083–2088.

Slifstein, M., Narendran, R., Hwang, D. R., Sudo, Y., Talbot, P. S., Huang, Y., & Laruelle, M. (2004). Effect of amphetamine on [18F]fallypride in vivo binding to D2 receptors in striatal and extrastriatal regions of the primate brain: Single bolus and bolus plus constant infusion studies. Synapse, 54(1), 46–63.

Sossi, V. (2003). Positron emission tomography (PET) advances in neurological applications. Nuclear Instruments and Methods in Physics Research, Section (A), 510, 107–115.

Sullivan, J. M., Kim, S. J., Cosgrove, K. P., & Morris, E. D. (2013). Limitations of SRTM, Logan graphical method, and equilibrium analysis for measuring transient dopamine release with [$^{11}$C]raclopride PET. American Journal of Nuclear Medicine and Molecular Imaging, 3(3), 247–260.

Tai, Y-C., Laforest, R. (2005). Instrumentation Aspects of Animal PET. Annual Review of Biomedical Engineering, 7:255–85.

Tantawy, M. N., Jones, C. K., Baldwin, R. M., Ansari, M. S., Conn, P. J., Kessler, R. M., & Peterson, T. E. (2009). [$^{18}$F]-fallypride dopamine D2 receptor studies using delayed microPET scans and a modified Logan plot. Nuclear Medicine and Biology, 36(8), 931–940.

Thompson, H. K., Starmer, C. F., Whalen, R. E., & Mcintosh, H. D. (1964). Indicator Transit Time Considered as a Gamma Variate. Circulation Research, 14(6), 502–515.

van den Hoff, J., Oehme, L., Schramm, G., Maus, J., Lougovski, A, Petr, J., Beuttina-Baumann, B., Hofheinz, F. (2013). The PET-derived tumor-to-blood standard uptake ratio (SUR) is superior to tumor SUV as a surrogate parameter of the metabolic rate of FDG. European Journal of Nuclear Medicine and Molecular Imaging Research, 3(1), 77.

Vandehey, N. T., Moirano, J. M., Converse, A. K., Holden, J. E., Mukherjee, J., Murali, D., Christian, B. T. (2010). High-affinity dopamine D2/D3 PET radioligands 18F-fallypride and 11C-FLB457: a comparison of kinetics in extrastriatal regions using a multiple-injection protocol. Journal of Cerebral Blood Flow and Metabolism, 30(5), 994–1007.

Varga, J., Szabo, Z. (2002). Modified Regression Model for the Logan Plot. Journal of Cerebral Blood Flow and Metabolism, 22(2), 240–244.

Vernaleken, I., Peters, L., Raptis, M., Lin, R., Buchholz, H.-G., Zhou, Y., Winz, O., Rösch, F., Bartenstein, P., Wong, D. F., Schäfer, W. M., Gründer, G. (2011). The applicability of SRTM in [$^{18}$F]fallypride PET investigations: impact of scan durations. Journal of Cerebral Blood Flow and Metabolism: Journal of Cerebral Blood Flow and Metabolism, 31(9), 1958–1966.

Volkow, N. D., Fowler, J. S., Gatley, S. J., Logan, J., Wang, G. J., Ding, Y. S., & Dewey, S. (1996). PET evaluation of the dopamine system of the human brain. Journal of Nuclear Medicine, 37(7), 1242–1256.

Watabe, H., Ikoma, Y., Kimura, Y., Naganawa, M., & Shidahara, M. (2006). PET kinetic analysis--compartmental model. Annals of Nuclear Medicine, 20(9), 583–588.

Werhahn, K. J., Landvogt, C., Klimpe, S., Buchholz, H. G., Yakushev, I., Siessmeier, T., Müller-Forell, W., Piel, M., Rösch, F., Glaser, M., Shreckenberger, M., Bartenstein, P. (2006). Decreased dopamine

D2/D3-receptor binding in temporal lobe epilepsy: An [$^{18}$F]-fallypride PET study. Epilepsia, 47(8), 1392–1396.

Zald, D. H., Woodward, N. D., Cowan, R. L., Riccardi, P., Ansari, M. S., Baldwin, R. M., Smith, C. E., Hakyemez, H., Li, R., Kessler, R. M. (2010). Midbrain dopamine receptor availability is inversely associated with novelty-seeking traits in humans. The Journal of Neuroscience, 28(53), 14372–14378.

Zhou, Y., Resnick, S. M., Ye, W., Fan, H., Holt, D. P., Klunk, W. E., Mathis, C. A., Dannals, R., Wong, D. F. (2007). Using a reference tissue model with spatial constraint to quantify [$^{11}$C]Pittsburgh compound B PET for early diagnosis of Alzheimer's disease. NeuroImage, 36(2), 298–312.